

Testing Gravity on Cosmic Scales: A Case Study of Jordan-Brans-Dicke Theory

Shahab Joudaki,^{1,*} Pedro G. Ferreira,^{1,†} Nelson A. Lima,^{2,‡} and Hans A. Winther^{3,4,§}

¹*Astrophysics, University of Oxford, Denys Wilkinson Building, Keble Road, Oxford OX1 3RH, UK*

²*Institute for Theoretical Physics, University of Heidelberg, Philosophenweg 16, D-69120 Heidelberg, Germany*

³*Institute of Cosmology & Gravitation, Dennis Sciama Building, University of Portsmouth, Portsmouth PO1 3FX, UK*

⁴*Institute of Theoretical Astrophysics, University of Oslo, 0315 Oslo, Norway*

(Dated: December 12, 2023)

We provide an end-to-end exploration of a distinct modified gravitational theory in Jordan-Brans-Dicke (JBD) gravity, from an analytical and numerical description of the background expansion and linear perturbations, to the nonlinear regime captured with a hybrid suite of N -body simulations, to the cosmological constraints from existing probes of the expansion history, the large-scale structure, and the cosmic microwave background (CMB). We have focused on JBD gravity as it both approximates a wider class of Horndeski scalar-tensor theories on cosmological scales and allows us to adequately model the nonlinear corrections to the matter power spectrum. In a combined analysis of the Planck 2018 CMB temperature, polarization, and lensing reconstruction, together with Pantheon supernova distances and the Baryon Oscillation Spectroscopic Survey (BOSS) measurements of baryon acoustic oscillation distances, the Alcock-Paczynski effect, and the growth rate, we constrain the JBD coupling constant to $\omega_{\text{BD}} > 970$ (95% confidence level; CL) in agreement with the General Relativistic expectation (given by $\omega_{\text{BD}} \rightarrow \infty$). In the unrestricted JBD model, where the effective gravitational constant at present, G_{matter}/G , is additionally varied, increased dataset concordance (e.g. within 1σ agreement in $S_8 = \sigma_8 \sqrt{\Omega_m/0.3}$) enables us to further include the combined (“ $3 \times 2\text{pt}$ ”) dataset of cosmic shear, galaxy-galaxy lensing, and overlapping redshift-space galaxy clustering from the Kilo Degree Survey and the 2-degree Field Lensing Survey (KiDS \times 2dFLenS). In analyzing the weak lensing measurements, the nonlinear corrections due to baryons, massive neutrinos, and modified gravity are simultaneously modeled and propagated in the cosmological analysis for the first time. In the joint analysis of all datasets, we constrain $\omega_{\text{BD}} > 1540$ (95% CL), $G_{\text{matter}}/G = 0.997 \pm 0.029$, the sum of neutrino masses, $\sum m_\nu < 0.12$ eV (95% CL), and the baryonic feedback amplitude, $B < 2.8$ (95% CL), all in agreement with the standard model expectation. In fixing the sum of neutrino masses, the lower bound on the coupling constant strengthens to $\omega_{\text{BD}} > 1460$ and $\omega_{\text{BD}} > 2230$ (both at 95% CL) in the restricted and unrestricted JBD models, respectively. We explore the impact of the JBD modeling choices, and show that a more restrictive parameterization of the coupling constant degrades the neutrino mass bound by up to a factor of three. In addition to the improved concordance between KiDS \times 2dFLenS and Planck, the tension in the Hubble constant between Planck and the direct measurement of Riess et al. (2019) is reduced to $\sim 3\sigma$; however, we find no substantial model selection preference for JBD gravity relative to Λ CDM. We further show that a positive shift in the effective gravitational constant suppresses the CMB damping tail, which might complicate future inferences of small-scale physics, given its degeneracy with the primordial helium abundance, the effective number of neutrinos, and the running of the spectral index.

I. INTRODUCTION

As the quantity and quality of data from ground and space-based telescopes increase, cosmological tests of Einstein’s theory of General Relativity (GR) have become increasingly robust (e.g. [1–5]). These tests can take a “model-independent” form, for instance through the measurement of possible deviations of the gravitational potentials Ψ and Φ (denoting temporal and spatial perturbations to the spacetime metric, respectively, e.g. [6–10]), the index γ_G (parameterizing the linear growth rate [11, 12]), the E_G parameter (encapsulating the ratio of galaxy-galaxy lensing and galaxy-velocity cross-correlations [13, 14]), or the Bellini-Sawicki α_i parameters (encompassing a subset of effective field theories given by stable scalar-tensor theories universally coupled to gravity with at most second order equations of motion [15–18]). These

model-independent approaches are immensely useful for tests of GR on cosmic scales, where large classes of modified gravity (MG) models are simultaneously constrained (e.g. [1–6, 14, 19–33]).

A common limitation of model-independent approaches, however, is the need to avoid or suppress nonlinear scales in the matter density and galaxy density fields. This is due to the inability to adequately simulate the model-independent parameterizations. The screening mechanism responsible for the suppression of power is highly model dependent, and models that have similar signatures on linear scales can differ substantially in the nonlinear regime [34]. However, these nonlinear scales are necessary to include to fully utilize the expected constraining power of probes of the large-scale structure with next-generation telescopes such as Euclid [35], the Vera C. Rubin Observatory [36], the Dark Energy Spectroscopic Instrument (DESI) [37], and the Nancy Grace Roman Space Telescope [38].

As a result, in this paper, we will consider a specific extension of GR in the form of Jordan-Brans-Dicke (JBD) gravity, where Newton’s constant is promoted to a dynamical field [39]. We take a comprehensive approach by providing the underlying

* shahab.joudaki@physics.ox.ac.uk

† pedro.ferreira@physics.ox.ac.uk

‡ nelson.lima15@gmail.com

§ h.a.winther@astro.uio.no

ing theory, nonlinear description with numerical simulations, and constraints using the latest cosmological data. We choose this specific gravitational theory as it is the most extensively studied extension of GR and a fertile sandbox to explore the power of different observations for constraining gravity. It allows for a comparison of highly different regimes, the astrophysical and the cosmological, and an assessment of how adequately different types of data can be used to determine non-standard parameters. Moreover, it is one of the scalar-tensor theories that has survived the recent observation of a binary neutron star merger that places extremely tight constraints (at the level of one part in 10^{15}) on the speed of gravitational waves [40–43].

To understand JBD theory (see e.g. [34, 39, 44]) it consists of a metric, $g_{\alpha\beta}$ (with determinant g), and a real scalar field, ϕ , that satisfy the following non-minimally coupled action,

$$S_{\text{BD}} = \int d^4x \sqrt{-g} \left[-\frac{\alpha}{12} \varphi^2 R + \frac{1}{2} g^{\mu\nu} \partial_\mu \varphi \partial_\nu \varphi - 2\mathcal{V} + \mathcal{L}_m \right]. \quad (1)$$

Here, R is the Ricci scalar, \mathcal{L}_m is the Lagrangian density of matter minimally coupled to the metric (which can include a cosmological constant, Λ), \mathcal{V} is the potential, and α is the single free coupling constant which vanishes in GR. It is customary to re-express this theory in terms of the scalar field $\frac{M_{\text{Pl}}^2}{2} \phi \equiv -\frac{\alpha}{12} \varphi^2$ and potential $\frac{M_{\text{Pl}}^2}{2} V \equiv \mathcal{V}$, where we have identified the reduced Planck mass $M_{\text{Pl}}^2 = (8\pi G)^{-1}$ (which includes the “bare” gravitational constant, G). The action can then be rewritten as

$$S_{\text{BD}} = \int d^4x \sqrt{-g} \left[\frac{M_{\text{Pl}}^2}{2} \left(\phi R - \frac{\omega_{\text{BD}}}{\phi} g^{\mu\nu} \partial_\mu \phi \partial_\nu \phi - 2V \right) + \mathcal{L}_m \right], \quad (2)$$

where the single free coupling constant in the theory is now $\omega_{\text{BD}} = -\frac{3}{2\alpha}$ and GR is recovered in the limit $\omega_{\text{BD}} \rightarrow \infty$. We restrict our analysis to the simplest case of a constant potential (which is *not* equivalent to replacing R by $R - 2\Lambda$ in Eq. 2). We note that it is possible to consider extensions of this model by, for instance, incorporating a self-interaction potential $V(\phi)$ in the action above (see e.g. Lima & Ferreira 2016 [44]).¹

The motivation behind JBD gravity was originally to implement Mach’s principle in GR [39], but its presence has become ubiquitous, arising as the scalar-tensor component of unified field theories, as the low energy phenomenology of higher-dimensional theories, and as the decoupling limit of extensions of GR with higher spin fields (e.g. [34]). Over the years, extensions and generalizations of JBD gravity have been proposed, culminating in a cluster of results on general scalar-tensor theories [47–54]. Yet, even in this extended realm, JBD gravity still encapsulates, to some extent, the main long wavelength features of generalized scalar-tensor theories

such as Horndeski gravity [15]. Indeed, for many scalar-tensor theories of gravity, both the kinetic and potential terms can be expanded as polynomials in derivatives of the scalar field which become subdominant on cosmological scales – a form of gradient expansion which naturally reverts to JBD gravity on cosmological scales [55].

There are a number of rich phenomenological properties of JBD gravity, from cosmological tracker solutions, to black hole no-hair theorems, and a host of observational effects that can be measured with astrophysical observations (e.g. [56]). The most stringent constraint on JBD gravity has been obtained from Shapiro time delay measurements by the Cassini satellite, where the parametrized post-Newtonian (PPN) parameter $\eta \equiv \Phi/\Psi = 1 + (2.1 \pm 2.3) \times 10^{-5}$ [57]. This translates into a bound on $\omega_{\text{BD}} > 4.0 \times 10^4$ at 95% confidence level (CL; discarding the negative ω_{BD} solution due to ghost instability; see Sec. II for the relation between η and ω_{BD}). A complementary strong bound is obtained from the analysis of the pulsar–white dwarf binary PSR J1738+0333, where $\omega_{\text{BD}} > 1.2 \times 10^4$ (95% CL) [58].

Recent attempts at constraining JBD gravity with cosmological observations are promising, but not competitive with the astrophysical constraints (e.g. [55, 59–69]). For instance, in Avilez & Skordis (2014) [55], a lower bound of $\omega_{\text{BD}} > 1.9 \times 10^3$ (95% CL) was obtained using cosmic microwave background (CMB) temperature and lensing measurements from Planck 2013 [70]. In Ballardini et al. (2016) [64], an extended JBD model with a potential in Eq. (1) of the form $V(\phi) \propto \phi^n$ was considered. For the case of a quadratic potential, the authors constrained $\omega_{\text{BD}} > 330$ (95% CL) using CMB temperature, polarization, and lensing data from Planck 2015 [71] combined with baryon acoustic oscillation (BAO) distance measurements from the 6dF Galaxy Survey [72], SDSS Main Galaxy Sample [73], and BOSS LOWZ/CMASS samples [74]. In Ballardini et al. (2020) [68], this analysis was then updated to include CMB and BAO distance measurements from Planck 2018 [75] and BOSS DR12 [76], along with the Riess et al. (2019) [77] direct measurement of the Hubble constant, such that $\omega_{\text{BD}} > 450$ (95% CL).

In Ooba et al. (2017) [66], a modified JBD model with a field-dependent $\omega_{\text{BD}}(\phi)$ was considered instead. Using the same dataset combination as in Ballardini et al. (2016) [64], the authors obtained a lower bound on $\omega_{\text{BD}}(\phi(a=1))$, where a is the scale factor, between 2.0×10^3 and 3.3×10^3 (95% CL) depending on the shape of their prior on the JBD parameter. Another setup consisting of a JBD model with a vanishing potential and a scalar field that is unrestricted at early times ($a = 10^{-14}$) was considered in Peracaula et al. (2019) [67], where CMB measurements from Planck 2015 combined with low-redshift cosmological datasets were used to constrain $|\omega_{\text{BD}}| \gtrsim 300$ (95% CL). Hence, recent constraints on the JBD coupling constant fluctuate not only due to the specific datasets used but also given the specific configuration of the JBD model considered.

Beyond the CMB and post-recombination epochs considered above, the gravitational constant can be constrained during Big Bang nucleosynthesis (BBN). The production of light elements is highly sensitive to the expansion of the universe

¹ The generalized JBD action, where $\omega_{\text{BD}} \rightarrow \omega_{\text{BD}}(\phi)$ and $V \rightarrow V(\phi)$, encapsulates other distinct theories such as coupled quintessence [45] and $f(R)$ gravity [46].

when its temperature is around an MeV; the JBD scalar field will affect the expansion rate ($H \propto \sqrt{G/\phi}$) and thus the theory can be constrained through measurements of light element abundances in distant quasars (e.g. [78–83]; also see the review in [84]). In the GR limit, the most recent constraint is $G_{\text{BBN}}/G = 0.98^{+0.06}_{-0.06}$ (95% CL), which by assuming a linear time-dependence can be translated into a constraint on the time variation of the gravitational constant, $\dot{G}/G = 1.4^{+4.4}_{-4.7} \times 10^{-12} \text{ yr}^{-1}$ (95% CL) [83]. Naturally, these constraints might degrade in the context of JBD theory (as the scalar field will also source the background dynamics, thereby affecting the expansion rate, as well as being responsible for the time variation of G). Earlier self-consistent analyses find $\omega_{\text{BD}} \gtrsim 300$ (95% CL) from BBN alone [78, 81].

While astrophysical constraints on the JBD coupling constant are more powerful than the constraints from existing cosmological datasets, one expects nonlinear corrections arising in *generalized* JBD gravity (e.g. Horndeski gravity) to come into play that might weaken these constraints. Indeed, if on cosmological scales, JBD gravity is merely the long wavelength limit of Horndeski gravity [55], then on smaller scales, screening mechanisms may completely shield astrophysical systems from fifth forces arising from the presence of scalar fields (for example, through the Vainshtein [85, 86], Chameleon [87, 88] or Symmetron [89] mechanisms). This provides additional motivation to constrain JBD gravity (and other gravitational theories) on cosmic scales across the history of the Universe.

As the amount and quality of data increases with the next generation of cosmological surveys (e.g. [35–38, 90]), we expect to significantly improve constraints on fundamental parameters, in particular as related to the gravitational Universe (e.g. [91–94]). To achieve this, it will be important to understand and control a range of observational and theoretical systematic uncertainties. Concretely, it will be important to accurately account for observational systematics such as baryonic feedback, intrinsic galaxy alignments (IA), photometric redshift uncertainties, shear calibration uncertainties, galaxy bias, and pairwise velocity dispersion (see for instance Joudaki et al. 2018 [3] and references therein); to accurately account for theoretical systematics arising from the modeling of new physics such as neutrino mass, dark matter, and dark energy/modified gravity; and to understand the role of degeneracies between the different parameters (cosmological, astrophysical, gravitational, and instrumental) affecting the observables. We will account for these systematic uncertainties and parameter degeneracies, and will consider the JBD model as a case study for constraining extensions to GR with current and future cosmological data.

In constraining the JBD model, we primarily consider the Planck CMB [75] and the combined data vector of weak gravitational lensing and overlapping redshift-space galaxy clustering from KiDS×{2dFLenS+BOSS} [3]. In order to improve the cosmological parameter constraints, we further include complementary information from measurements of baryon acoustic oscillations, Alcock-Paczynski (AP) effect, and the growth rate (final consensus BOSS DR12 [76]), distances to type IA supernovae (SNe; Pantheon compilation [95]), and

the small-scale CMB (ACT [96, 97]). We include the key systematic uncertainties that affect these measurements, and pay particular attention to the interplay between modified gravity, neutrino mass, and baryonic feedback. We also explore the ability of the extended model to improve the concordance between cosmological datasets, and assess the extent to which it might be favored in a model selection sense relative to Λ CDM.

We structure the paper as follows. In Section II, we describe the background expansion and linear perturbations in JBD gravity, highlighting its impact on probes of the expansion history, the large-scale structure, and the cosmic microwave background. In Section III, we capture the impact of JBD gravity on the nonlinear corrections to the matter power spectrum by performing a hybrid suite of N -body simulations (using modified versions of COLA [98, 99] and RAMSES [100]) and subsequently modifying the prescription for the HMCODE [101, 102] fitting function. In Section IV, we outline the analysis techniques, cosmological datasets, and treatment of systematic uncertainties. In Sections V, VI, VII, and VIII, we provide the cosmological constraints on JBD gravity, and discuss their dependence on the datasets considered, the complexity of the cosmological model, and the analysis choices. We highlight the parameter degeneracies (in particular with massive neutrinos and baryonic feedback), model selection preferences (mainly JBD gravity against GR), and changes in the concordance between datasets (between Planck and KiDS, and between Planck and Riess et al. 2019 [77]). In Section IX, we conclude with a summary of the findings.

II. THEORY: BACKGROUND COSMOLOGY AND THE LINEAR REGIME

A. Background equations

The line element in the Newtonian gauge for small scalar perturbations, as captured by the scalar potentials Ψ and Φ , is given by

$$ds^2 = -(1 + 2\Psi)dt^2 + a^2(t)(1 - 2\Phi)\delta_{ij}dx^i dx^j, \quad (3)$$

where δ_{ij} is the Kronecker delta function, x is the comoving position coordinate, t refers to physical time, and we have implicitly assumed the speed of light in vacuum $c = 1$. We perturb the stress-energy tensor to linear order so that, for instance, the matter density $\rho_{\text{m}}(\vec{x}, t) = \bar{\rho}_{\text{m}}(t)(1 + \delta_{\text{m}}(\vec{x}, t))$, where the overbar denotes the mean of the matter density, and δ_{m} encodes the perturbations about the mean. In the case of JBD theory, the perturbations in the scalar field are given by $\delta\phi$, such that $\phi(\vec{x}, t) = \bar{\phi}(t) + \delta\phi(\vec{x}, t)$.

Following the standard approach, the JBD equations of motion are obtained by varying the action (Eq. 2) with respect to the metric and scalar field (see e.g. [34, 39, 44]). The former gives the Einstein equations,

$$G_{\mu\nu} = \frac{1}{M_{\text{Pl}}^2} T_{\mu\nu} + \frac{\omega_{\text{BD}}}{\phi^2} \left[\nabla_\mu \phi \nabla_\nu \phi - \frac{1}{2} g_{\mu\nu} \nabla_\alpha \phi \nabla^\alpha \phi \right] + \frac{1}{\phi} \left[\nabla_\mu \nabla_\nu \phi - g_{\mu\nu} (\Box \phi + V) \right], \quad (4)$$

where $T_{\mu\nu}$ is the total matter stress-energy tensor and \square denotes the d'Alembertian. The latter gives the scalar field's equation of motion,

$$\square\phi = \frac{1}{M_{\text{Pl}}^2} \left(\frac{T}{3+2\omega_{\text{BD}}} \right) - \frac{4V-2\phi V_\phi}{3+2\omega_{\text{BD}}}, \quad (5)$$

where T is the trace of the stress-energy tensor and $V_\phi = dV/d\phi$ (which vanishes in the case of the constant potential that we consider).

We begin by considering the contribution from the homogeneous background (i.e. no perturbations). Eq. (4) gives the two modified Friedmann equations,

$$\begin{aligned} 3H^2 &= \frac{\rho}{M_{\text{Pl}}^2} - 3H\frac{\dot{\phi}}{\phi} + \frac{\omega_{\text{BD}}}{2} \frac{\dot{\phi}^2}{\phi^2} + \frac{V}{\phi} \\ 2\dot{H} + 3H^2 &= -\frac{P}{M_{\text{Pl}}^2} - \frac{\omega_{\text{BD}}}{2} \frac{\dot{\phi}^2}{\phi^2} - 2H\frac{\dot{\phi}}{\phi} - \frac{\ddot{\phi}}{\phi} + \frac{V}{\phi}, \end{aligned} \quad (6)$$

where ρ and P are the total energy density and pressure of all components except the scalar field, respectively, the Hubble parameter $H \equiv \dot{a}/a$, and the N raised dots represent N th-order time derivatives. We will consider a cosmology that incorporates the usual components of the stress-energy of the Universe (photons, baryons, neutrinos, dark matter) along with the scalar field (which includes the constant potential $V = \Lambda$). In this more general case, the density parameter of each component (X) includes ϕ through

$$\Omega_X^* = \frac{\Omega_X}{\phi} = \frac{\rho_X}{3H^2 M_{\text{Pl}}^2 \phi}, \quad (7)$$

such that $\sum \Omega_X^* = 1$ in a flat Universe (in other words, when defining the density parameter of each component using the critical density in GR, they do not add to unity in a flat Universe – we will further discuss the implication of the choice between Ω_X^* and Ω_X on the concordance between datasets in Sec. VIII B). Moreover, in a flat Universe, we have $\Lambda = 3H_0^2(1 - \Omega_{\text{m},0}^*)$, where the “0” subscripts refer to the present time. Reading off the first line in Eq. (6), the energy density of the scalar field is

$$\rho_\phi = M_{\text{Pl}}^2 \left(\frac{\omega_{\text{BD}}}{2} \frac{\dot{\phi}^2}{\phi} - 3H\dot{\phi} + V \right). \quad (8)$$

The pressure of the scalar field is similarly read off the second line in Eq. (6), such that the effective equation of state of the scalar field is given by

$$w_\phi \equiv P_\phi/\rho_\phi = \frac{\dot{\phi}^2 \omega_{\text{BD}} + 4H\dot{\phi}\phi + 2\ddot{\phi}\phi - 2V\phi}{\dot{\phi}^2 \omega_{\text{BD}} - 6H\dot{\phi}\phi + 2V\phi}. \quad (9)$$

Hence, the scalar field (including a constant potential) is responsible for the accelerated expansion of the Universe, and $w_\phi \rightarrow -1$ when $\phi \rightarrow \text{constant}$. The evolution of the scalar field is given by Eq. (5), which can be expressed as

$$\ddot{\phi} + 3H\dot{\phi} = \frac{1}{M_{\text{Pl}}^2} \left(\frac{\rho - 3P}{3+2\omega_{\text{BD}}} \right) + \frac{4V-2\phi V_\phi}{3+2\omega_{\text{BD}}}. \quad (10)$$

Here, the left-hand side of the equation can further be expressed as $a^{-3} \frac{d}{dt}(\dot{\phi}a^3)$. We immediately see that there are two effects at play: the scalar field will affect the way that the energy-momentum tensor of the rest of the Universe drives the expansion rate by modifying the effective gravitational constant (i.e. $M_{\text{Pl}}^2 \rightarrow M_{\text{Pl}}^2 \phi$), and it will also itself be a source of energy and pressure. As we shall further see below, GR is recovered in the limit $\omega_{\text{BD}} \rightarrow \infty$; the corresponding density parameter satisfies $\Omega_\phi = \Omega_\Lambda + \mathcal{O}(\omega_{\text{BD}}^{-1})$ and the effective equation of state satisfies $w_\phi = -1 + \mathcal{O}(\omega_{\text{BD}}^{-1})$ which for large ω_{BD} reduces to that of a cosmological constant in GR.

In Eq. (10), we find that the scalar field begins to evolve after the end of the radiation-dominated era (i.e. ϕ is constant and $a \propto \sqrt{t/\phi}$ during radiation domination). During the matter-dominated regime, where $\rho \propto a^{-3}$, the scalar field evolves as a power law of the scale factor [34, 103, 104],

$$\phi = \phi_0 a^{\frac{1}{1+\omega_{\text{BD}}}}. \quad (11)$$

Here, the subscript “0” refers to the present time, such that $\phi \leq \phi_0 \equiv \phi(a=1)$ as $a \leq 1$ (with non-negative ω_{BD}), and the scale factor is given by

$$a(t) = \left(\frac{t}{t_0} \right)^{\frac{2+2\omega_{\text{BD}}}{4+3\omega_{\text{BD}}}}. \quad (12)$$

In the limit $\omega_{\text{BD}} \rightarrow \infty$, one recovers $\phi \rightarrow \phi_0$ (a constant) and $a \propto t^{2/3}$, i.e. the standard GR result in the matter-dominated era. The effect of the JBD coupling constant itself is to slow down the expansion rate, i.e. the exponent in Eq. (12) is bounded from above by the GR value (2/3). Moreover, t_0 is related to the Hubble constant through $t_0 H_0 = (2+2\omega_{\text{BD}})/(4+3\omega_{\text{BD}})$.

In a “restricted” JBD cosmology, we fix ϕ_0 to be given by $\phi(a=1)|_{\text{restricted}} = \frac{4+2\omega_{\text{BD}}}{3+2\omega_{\text{BD}}}$ by requiring that the effective gravitational constant is the same on local and cosmological scales at present (e.g. [55]). We also consider an “unrestricted” JBD cosmology, where we allow the data to determine ϕ_0 independently. Further in this section, we will show that this corresponds to allowing for the effective gravitational constant at present, $(G_{\text{matter}}/G)|_{a=1} \propto \phi_0^{-1}$, to vary freely. At late times, the constant potential in the JBD action gives rise to the cosmic accelerating epoch, such that the effective equation of state of the scalar field at present is given by $w_\phi(a=1) \simeq -1$ (to increasing precision as ω_{BD} increases; evolving towards more negative values with decreasing scale factor [44]). In this epoch, $\phi \propto a^{\frac{4}{1+2\omega_{\text{BD}}}}$ [105, 106], such that the scalar field increases marginally more rapidly with time than in the earlier matter dominated regime (for instance, by $\lesssim 0.3\%$ at present for $\omega_{\text{BD}} = 100$ [44]).

B. Toy model: modifications to distances due to JBD gravity

In a matter-dominated Universe with zero curvature, given the impact of JBD gravity on its expansion (Eq. 12), the angular diameter distance is given by

$$D_A(z) = \frac{2+2\omega_{\text{BD}}}{2+\omega_{\text{BD}}} \frac{cH_0^{-1}}{1+z} \left[1 - (1+z)^{-\frac{2+\omega_{\text{BD}}}{2+2\omega_{\text{BD}}}} \right], \quad (13)$$

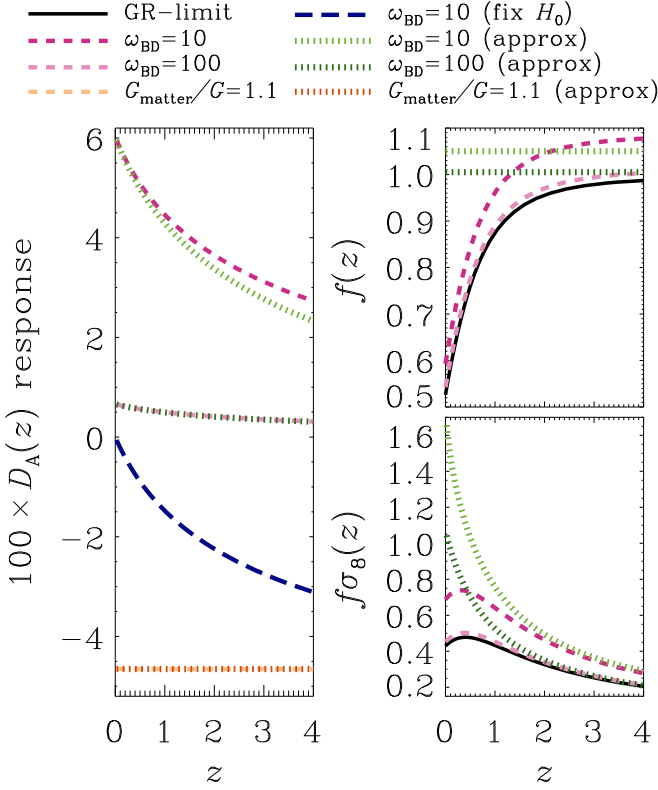


FIG. 1. The angular diameter distance response (left), quantified as $(D_A^{\text{JBD}} - D_A^{\text{GR}})/D_A^{\text{GR}}$, the growth rate $f(z)$ (upper right), and the product of the growth rate and the root-mean-square of the linear matter overdensity field on $8 h^{-1}$ Mpc scales, $f\sigma_8(z)$ (bottom right). We consider the GR-limit (solid black, corresponding to $\omega_{\text{BD}} \rightarrow \infty$) and cosmologies with $\omega_{\text{BD}} = \{10, 100\}$ from EFTCAMB (dashed pink and light dashed pink, respectively), to be compared with the corresponding analytical matter-domination approximations for $\Delta D_A(z)$, $f(z)$, and $f\sigma_8(z)$ in Eqs. (14, 21, 22) (light dotted green and dotted green for $\omega_{\text{BD}} = \{10, 100\}$, respectively). For the angular diameter distance, to assess the behavior of Eq. (14), we assume matter-domination for both the EFTCAMB and approximate analytical solutions, and we consider a setup where the Hubble constant is kept fixed between JBD and GR (long dashed blue; instead of fixing the matter density $\Omega_m h^2$). We also allow the present effective gravitational constant to deviate from the GR expectation, with $G_{\text{matter}}/G = 1.1$ (dashed orange and dotted red for the EFTCAMB and approximate analytical solutions, respectively). For visual clarity, we only show the impact of a deviation in G_{matter}/G for $D_A(z)$ as its impact on $f(z)$ and $f\sigma_8(z)$ is negligible. We note that our use of “ G_{matter}/G ” here is shorthand for $(G_{\text{matter}}/G)|_{a=1}$ (as defined in Eq. 18).

where $z = a^{-1} - 1$ is the redshift. For an improved qualitative understanding, for small ω_{BD}^{-1} , this differs from the GR angular diameter distance by

$$\Delta D_A(z) \simeq -\frac{2c}{\omega_{\text{BD}} H_0^{\text{JBD}} (1+z)} \left[\left(1 - \frac{1}{\sqrt{1+z}} \right) - \frac{\ln(1+z)}{2\sqrt{1+z}} \right] + \frac{2c}{1+z} \left(1 - \frac{1}{\sqrt{1+z}} \right) \left(\frac{1}{H_0^{\text{JBD}}} - \frac{1}{H_0^{\text{GR}}} \right). \quad (14)$$

We note that aside from the explicit ω_{BD} dependence in the angular diameter distance, there is also an implicit dependence

on both ω_{BD} and $(G_{\text{matter}}/G)|_{a=1}$ in the Hubble constant (when it is taken to be a derived parameter; seen in Eq. 6). In Fig. 1, keeping the densities $\Omega_X h^2$ fixed (for X given by baryons, cold dark matter, scalar field, and massive neutrinos), we find that the angular diameter distance is enhanced as we consider JBD instead of GR, to a decreasing extent towards higher redshifts.

This overall enhancement is driven by the second term in Eq. (14), as the Hubble constant in a JBD cosmology is suppressed relative to that in GR (as also seen in Fig. 2), while the first term in Eq. (14) drives the decrease in the enhancement towards higher redshifts. Indeed, for fixed H_0 across cosmologies, the second term in Eq. (14) vanishes, such that at the same redshift, objects instead appear closer than in the corresponding GR Universe. Instead of a decrease in the difference between the distances in JBD and GR cosmologies with redshift, here the difference between the distances increases with redshift. Hence, as is well known, in comparing observables between cosmologies, it is imperative to have clarity in the specific parameters kept fixed.

As expected, given the assumption of small ω_{BD}^{-1} in deriving Eq. (14), the analytical approximate solution for $\Delta D_A(z)$ improves as ω_{BD} increases, and the difference between the angular diameter distances in JBD and GR cosmologies decreases as ω_{BD} increases. Indeed, we recover $\Delta D_A \rightarrow 0$ as $\omega_{\text{BD}} \rightarrow \infty$ and $(G_{\text{matter}}/G)|_{a=1} \rightarrow 1$. Moreover, as expected from Eqs. (6) and (18) below, and shown in Fig. 1, the angular diameter distance scales inversely with the square root of the present effective gravitational constant (i.e. $D_A \propto 1/\sqrt{(G_{\text{matter}}/G)|_{a=1}}$).

C. Linear perturbations

We now turn to linear perturbations in JBD theory. While $\delta\phi$ can be thought of as the potential for a putative fifth force (see Sec. III), it is often useful to consider the Einstein field equations on sub-horizon scales, i.e. $k^2 \gg (aH)^2$ where k is the wavenumber. In this “quasistatic” regime (which is moreover characterized by the condition that time derivatives of the metric and scalar-field perturbations are negligible relative to their respective spatial derivatives), the field equations reduce to a modified Poisson equation² (e.g. [92, 107]),

$$\frac{k^2}{a^2} \Psi \simeq -4\pi G_{\text{matter}} \rho_m \delta_m, \quad (15)$$

and a gravitational slip equation that depends only on the JBD coupling constant,

$$\gamma \equiv \frac{\Psi}{\Phi} \simeq \frac{2 + \omega_{\text{BD}}}{1 + \omega_{\text{BD}}}, \quad (16)$$

where the time-varying gravitational constant is given by

$$\frac{G_{\text{matter}}}{G} \simeq \frac{1}{\phi} \frac{4 + 2\omega_{\text{BD}}}{3 + 2\omega_{\text{BD}}}. \quad (17)$$

² Here, we have defined our effective gravitational constant to be dimensionful. However, we note that it is also common to define the effective gravitational constant as dimensionless by normalizing with the bare gravitational constant, i.e. $G_{\text{matter}}/G \rightarrow G_{\text{matter}}$.

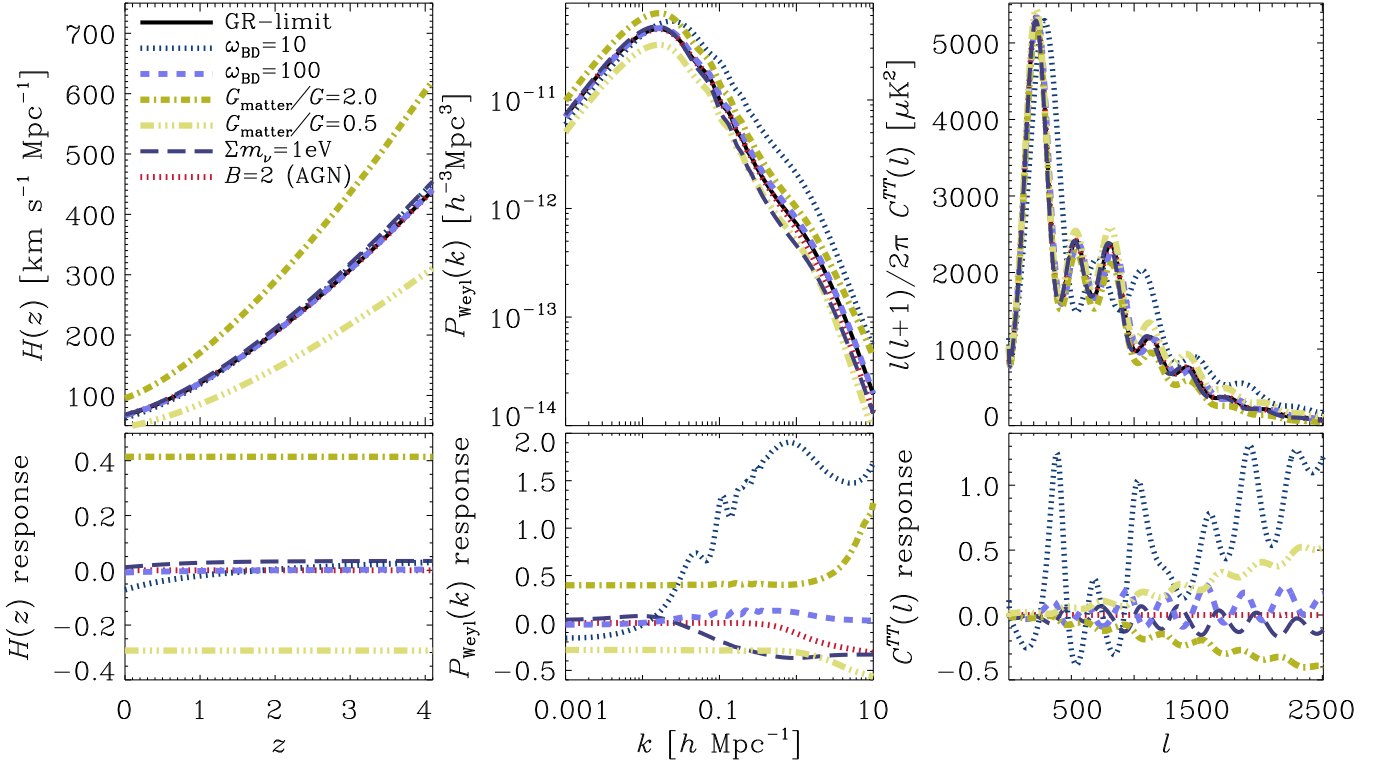


FIG. 2. The expansion history, $H(z)$, Weyl power spectrum, $P_{\text{Weyl}} \equiv P_{\Psi+\Phi}(k)$, and CMB temperature power spectrum, $C^{TT}(\ell)$, along with their respective responses, defined as $(A^{\text{JBD}} - A^{\text{GR}})/A^{\text{GR}}$, where $A \in \{H(z), P(k), C(\ell)\}$. Here, the Weyl power spectrum is considered at $z=0$. For our GR limit, we have effectively imposed $\omega_{\text{BD}} \rightarrow \infty$ and $G_{\text{matter}}/G = 1$. For the JBD model, we show the four cases $\omega_{\text{BD}} = 10$, $\omega_{\text{BD}} = 100$, $G_{\text{matter}}/G = 0.5$, and $G_{\text{matter}}/G = 2.0$ (such that $\omega_{\text{BD}} \rightarrow \infty$ when $G_{\text{matter}}/G \neq 1$, and $G_{\text{matter}}/G = 1$ when $\omega_{\text{BD}} \neq \infty$). We emphasize that our use of “ G_{matter}/G ” here is shorthand for $(G_{\text{matter}}/G)|_{a=1}$ (as defined in Eq. 18), and that we have kept the density parameters $\Omega_{\chi} h^2$ fixed rather than $\Omega_{\chi}^* h^2$, where “ χ ” denotes the matter components and the scalar field (see distinction in Eq. 7). For comparison, we show the impact of the sum of neutrino masses, fixed to $\Sigma m_{\nu} = 1$ eV, along with baryonic feedback corresponding to the “AGN” case of the OWL simulations (given by $B = 2$ in HMCODE). We moreover show the impact of JBD gravity on the polarization power spectra in Appendix A (Fig. 20).

The motion of non-relativistic particles is thereby dictated by the modified potential

$$\Psi = \frac{G_{\text{matter}}}{G} \Psi_{\text{GR}} \simeq \left[\frac{\tilde{\phi}(a=1)}{\tilde{\phi}} \left(\frac{G_{\text{matter}}}{G} \right) \right]_{a=1} \Psi_{\text{GR}}. \quad (18)$$

Hence, the effective gravitational constant evolves with time even when it is set to unity at present in the restricted JBD model. Given $\tilde{\phi}(a)$ increases with a this implies G_{matter}/G is larger in the past. A crucial point here is that we can in principle allow *both* ω_{BD} and the value of G_{matter}/G at the present time to be independent parameters of the theory (corresponding to an unrestricted JBD model as discussed earlier). We will consider such a setup in this paper to obtain general constraints on JBD gravity.³ In addition to the Poisson equation, G_{matter}/G enters the Friedmann equations via $\tilde{\phi}$.

³ We emphasize that the value of G_{matter}/G at the present time is determined by the choice of initial condition when solving Eq. (5) for $\tilde{\phi}$. Allowing this to be a free parameter is what Ref. [55] calls the *unrestricted* JBD model. This is to be contrasted to the *restricted* JBD model which corresponds to setting the initial conditions such that $\tilde{\phi}(a=1) = (4+2\omega_{\text{BD}})/(3+2\omega_{\text{BD}})$ implying $G_{\text{matter}}/G = 1$ at the present time.

As a result, the $(G_{\text{matter}}/G)|_{a=1}$ parameter that we vary in our analysis affects the expansion rate and any other physical process where the gravitational constant appears relative to other physical constants.

On sub-horizon scales, pressureless matter at late times obeys an evolution equation of the form (e.g. [107])

$$\delta_{\text{m}}'' + \left[1 + \frac{\mathcal{H}'}{\mathcal{H}} \right] \delta_{\text{m}}' - \frac{3}{2} \left(\frac{4+2\omega_{\text{BD}}}{3+2\omega_{\text{BD}}} \right) \Omega_{\text{m}}^*(a) \delta_{\text{m}} \simeq 0, \quad (19)$$

where $\mathcal{H} = aH$ and primes are derivatives with $\ln a$ (note that $\Omega_{\text{m}}^*(a)$ here includes a $1/\phi$ term given its definition in Eq. 7). This can be expressed in terms of the growth rate, $f \equiv \frac{d \ln \delta_{\text{m}}}{d \ln a}$, such that (e.g. [108])

$$f' + \left[1 + \frac{\mathcal{H}'}{\mathcal{H}} \right] f + f^2 = \frac{3}{2} \left(\frac{4+2\omega_{\text{BD}}}{3+2\omega_{\text{BD}}} \right) \Omega_{\text{m}}^*(a). \quad (20)$$

There are two distinct effects on the growth of structure: the expansion rate (which is lower compared to GR while the first derivative is more negative) enters the friction term and enhances growth, while the source term that sets the strength of the gravitational response also boosts growth. Unlike many proposals for scalar tensor theories, where deviations from

GR are synchronized with the onset of Λ -domination (and thus only kick in at late times), in JBD theory the scalar field has an effect throughout the full evolution of the Universe.

D. Toy model: modified growth rate in JBD gravity

Again, let us focus on a pure matter-dominated cosmology, where we know that $\delta_m \sim a$ and $f = 1$ in GR. If we consider the effects of the scalar field to be small, an analytic approximation to the growth rate is given by

$$f \simeq 1 + \frac{1}{2\omega_{\text{BD}}}. \quad (21)$$

The impact of ω_{BD} is enhanced when considering the density weighted growth rate, $f\sigma_8 \sim d\delta_m/d\ln a$, where σ_8 is the root-mean-square of the linear matter overdensity field on $8 h^{-1}$ Mpc scales, given its integrated effect over a long time scale (essentially since the beginning of matter domination). This can be seen via the approximate solution for f in the matter era, which when integrated gives

$$f\sigma_8 \simeq f\sigma_8|_{\text{GR}} \left[1 + \frac{1}{2\omega_{\text{BD}}} \left(1 + \ln \frac{z_{\text{eq}}}{z} \right) \right]. \quad (22)$$

In Fig. 1, we illustrate this enhancement in $f(z)$ and $f\sigma_8(z)$, along with the agreement between the EFTCAMB and approximate analytical solutions in the matter-dominated regime. The insensitivity of the growth rate to the present effective gravitational constant also agrees with that obtained from EFTCAMB.

E. Impact of JBD gravity on the propagation of light

Lastly, we consider the impact of JBD gravity on the propagation of light. The geodesic equation for relativistic particles (e.g. photons) is sensitive to the sum of the metric potentials ($\Psi + \Phi$). Given the quasistatic expressions (Eqs. 15–18),

$$\begin{aligned} \Psi + \Phi &= (1 + \gamma^{-1})\Psi = -\left(1 + \gamma^{-1}\right) G_{\text{matter}} \frac{4\pi a^2 \rho_m \delta_m}{k^2} \\ &= -\frac{2}{\bar{\phi}} \frac{4\pi G a^2 \rho_m \delta_m}{k^2} = \frac{2}{\bar{\phi}} \Psi_{\text{GR}}, \end{aligned} \quad (23)$$

which differs from the GR expectation by a factor of $1/\bar{\phi}$ (i.e. $G_{\text{light}} = ((1 + \gamma)/(2\gamma)) G_{\text{matter}} = G/\bar{\phi}$, where the first relation is general and the second relation is specific to JBD theory). We moreover consider the ratio of the metric potential Ψ (probed by e.g. redshift-space distortions) and the sum of the potentials $(\Psi + \Phi)/2$ (probed by e.g. weak lensing). This ratio of the potentials corresponds to the ratio of G_{matter} and G_{light} , and is targeted by measurements of the “ E_G parameter” (e.g. [5, 13, 14]). The ratio is only sensitive to the gravitational slip and thereby only to ω_{BD} in JBD theory (which holds in both the restricted and unrestricted JBD scenarios in the quasistatic regime):

$$2 \frac{\Psi}{\Psi + \Phi} = \frac{2\gamma}{1 + \gamma} \simeq \frac{4 + 2\omega_{\text{BD}}}{3 + 2\omega_{\text{BD}}}. \quad (24)$$

For a given ω_{BD} , this ratio does not evolve with time (such that any time variation observed would rule out JBD gravity in addition to GR and a range of other models entirely). As expected, the ratio approaches 1 in the GR limit ($\omega_{\text{BD}} \rightarrow \infty$), and the largest deviation is given by $4/3$ as $\omega_{\text{BD}} \rightarrow 0$. Since γ deviates from the GR expectation by less than a percent already for $\omega_{\text{BD}} \gtrsim 100$ (where such a small ω_{BD} is disfavored by current cosmological measurements, as discussed in Sec. I, but also see Sec. VIII C), we do not expect even future measurements of the gravitational slip alone (where $\sigma(\gamma) \sim 0.05$ at best for Stage-IV surveys [109–111]) to powerfully constrain the space of viable JBD models (noting that a similar argument holds for the E_G parameter). Instead, we need to measure the expansion history and both of the potentials distinctly in order to place the strongest constraints on the underlying cosmology, which is the approach taken here.

F. Connecting JBD theory to effective field theory

As a side note, we highlight that JBD theory can be connected to effective field theory via the α_i parameters defined in Bellini & Sawicki [15, 18] (which are all zero in GR), where the “Planck-mass run rate” $\alpha_M = d \ln \phi / d \ln a$, the “braiding” $\alpha_B = -\alpha_M$, the “kineticity” $\alpha_K = \omega_{\text{BD}} \alpha_M^2$, and the “tensor speed excess” $\alpha_T = 0$ [112]. Here, α_T encapsulates the zero deviations to the speed of gravitational waves relative to the speed of light in JBD theory, thereby satisfying the LIGO-Virgo bound [40]. In this language, JBD theory can be reduced to two independent α_i parameters (along with the expansion rate which can be expressed in terms of the same two α_i). These α_i parameters are in turn described in terms of only the coupling constant and the time-variation of the scalar field. Hence, it is straightforward to translate between constraints on $\{\omega_{\text{BD}}, (G_{\text{matter}}/G)|_{a=1}\}$ and $\{\alpha_M, \alpha_K\}$ (noting that α_M is directly related to the time derivative of G_{matter}/G).

G. Correlations between modified gravity, massive neutrinos, and baryonic feedback in cosmological observables

We now have the required ingredients for a qualitative understanding of the impact of JBD gravity on cosmological observables. The scalar field has an effect throughout the history of the Universe, decreasing the expansion rate (hence increasing BAO and SN distances) and largely increasing the Weyl power spectrum ($P_{\text{Weyl}} \equiv P_{\frac{\Psi+\Phi}{2}}(k)$), to which lensing is sensitive, as $\omega_{\text{BD}} \rightarrow 0$ (i.e. away from the GR limit). This is illustrated in Fig. 2, where the suppression in the expansion rate diminishes towards higher redshift (asymptoting to the GR rate), and where the Weyl power spectrum has a turnover from suppression to enhancement at $k \sim 10^{-2} h \text{Mpc}^{-1}$ (to within 10% for $\omega_{\text{BD}} \in [10, 100]$) with an amplitude that increases with the strength of JBD gravity. As a result, as ω_{BD} decreases, it will counter any degrees of freedom that might suppress the Weyl power spectrum on scales below this turnover (such as

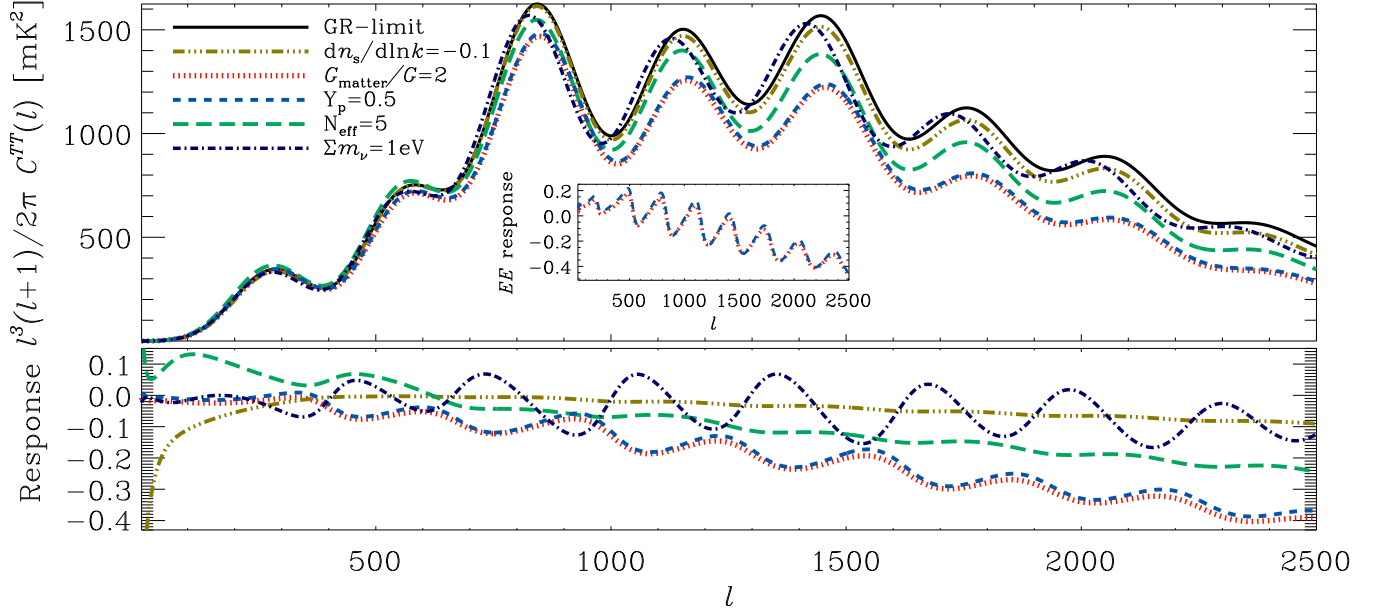


FIG. 3. CMB temperature power spectra in extended cosmological parameter spaces along with their respective responses, defined as $C^{\text{extended}}(\ell)/C^{\Lambda\text{CDM}}(\ell) - 1$. We consider deviations in the running of the spectral index, $dn_s/d\ln k$, the effective number of neutrinos, N_{eff} , the sum of neutrino masses, Σm_ν , the primordial helium abundance, Y_p , and the present effective gravitational constant, G_{matter}/G . We also highlight the E -mode polarization power spectrum response for Y_p and G_{matter}/G in the inset (for further polarization details, see Appendix A).

baryonic feedback⁴ and massive neutrinos⁵).

Meanwhile, as $\omega_{\text{BD}} \rightarrow 0$, the response of the CMB temperature power spectrum, $C^{TT}(\ell)$, is oscillatory along the multipoles ℓ (due to shifts in the locations of the peaks), and is both positive and negative below $\ell \sim 10^3$, above which it gradually increases relative to GR (further see Fig. 20 for the CMB polarization power spectrum and polarization-temperature cross-spectrum). Here, we note the largely opposing effects of ω_{BD} and the sum of neutrino masses, Σm_ν , on the CMB power spectra.

We further show the impact of changes in G_{matter}/G (note that as a primary parameter we always implicitly refer to its value at present), where a ratio below unity decreases the expansion rate, albeit at a constant level with redshift (given Eq. 6 where $H_{\text{JBD}}^2/H_{\text{GR}}^2 \approx 1/\phi$), such that there is an overall renormalization of the expansion history when $G_{\text{matter}}/G \neq 1$. Similarly, for the Weyl power spectrum, $G_{\text{matter}}/G < 1$ provides a constant suppression on linear and mildly nonlinear scales

(down to $k \sim 1 \text{ h Mpc}^{-1}$), where it is of the same magnitude as for the expansion rate (given Eq. 23 where $G_{\text{light}}/G = 1/\phi$ in the quasistatic regime). This suppression is enhanced on highly nonlinear scales, where we have modified `HMCODE` to match the numerical simulations in Sec. III. However, in contrast to $H(z)$ and $P_{\text{Weyl}}(k)$, the CMB temperature power spectrum is enhanced as $G_{\text{matter}}/G < 1$, such that the response increases with ℓ , making it a particularly suitable target for probes of the CMB damping tail (and correlated with other physics such as the running of the spectral index, neutrino mass, primordial helium abundance, and the effective number of neutrinos that affect the small-scale CMB).

As a result, there is a particular correlation between the effects of modified gravity, the sum of neutrino masses, and baryonic feedback on the Weyl power spectrum, along with distinct correlations between the effects of modified gravity and the sum of neutrino masses on the expansion rate and CMB power spectrum. A notable difference between the three is that the effective gravitational constant can in principle take on values on both ends of the fiducial expectation, where $G_{\text{matter}}/G < 1$ provides an enhancement of power (rather than suppression) and thereby allows for even greater neutrino masses and baryonic feedback. The fact that the effective gravitational constant allows for both suppression and enhancement of the cosmological quantities (depending on whether G_{matter}/G is greater or smaller than unity) gives it greater flexibility than ω_{BD} which only allows for “one-sided” modifications (i.e. either suppression or enhancement). This implies that G_{matter}/G is better suited to alleviating possible discordances between datasets, but also to be correlated with the other aforementioned physics.

We note that the responses to ω_{BD} are smaller for the expansion rate as compared to the Weyl and CMB power spectra.

⁴ Baryonic feedback is incorporated in `HMCODE` [101] through calibration to the Overwhelmingly Large (OWL) hydrodynamical simulations [113–115], as further discussed in Sec. III and Sec. IV B. In Fig. 2, we consider a feedback amplitude that corresponds to the “AGN” case of these simulations.

⁵ We note that the Weyl power spectrum response for the sum of neutrino masses (Fig. 2) is slightly positive for $k \sim 10^{-2} \text{ h Mpc}^{-1}$ because the fiducial GR cosmology here has the sum of neutrino masses fixed to $\Sigma m_\nu = 0.06 \text{ eV}$, which implies that the suppression in the Weyl power spectrum begins on larger scales, even though the strength of the suppression is smaller on increasingly nonlinear scales, relative to a cosmology with $\Sigma m_\nu = 1 \text{ eV}$. In other words, the free streaming length of each neutrino species is inversely proportional to its mass [116, 117] (which can in principle be used as a distinct feature with which to probe the neutrino mass hierarchy [118]).

While distinct physics might be correlated or even degenerate for a single physical observable, they often have different signatures for distinct observables, as seen in their impact on the responses for $\{H(z), P_{\text{Weyl}}(k), C^{TT}(\ell)\}$. For instance, the baryonic feedback suppresses the Weyl power spectrum but has no impact on the expansion history and CMB power spectra, while the sum of neutrino masses affects both the Weyl power spectrum and CMB power spectra but only negligibly the expansion history, and by contrast JBD gravity has a non-negligible impact on all three of these cosmological quantities. Hence, we expect that a combination of multiple complementary probes is required to robustly constrain the underlying cosmology of the Universe.

H. Degeneracies with the effective gravitational constant in the CMB damping tail

In Fig. 3, we continue to highlight the impact of the effective gravitational constant in the CMB damping tail, and its possible degeneracies with other physics, such as the primordial helium abundance, Y_P (i.e. the mass fraction of baryons in ^4He), the running of the spectral index, $dn_s/d\ln k$, and the effective number of neutrinos, N_{eff} (along with the sum of neutrino masses again for comparison). As discussed in Sec. II G, we obtain a suppression in the damping tail for positive perturbations in G_{matter}/G , which is correlated with the expected suppression due to {positive, negative, positive} perturbations in $\{Y_P, dn_s/d\ln k, N_{\text{eff}}\}$, respectively. In Ref. [119], the ratio of the angular scales of the diffusion length and sound horizon, θ_d/θ_s , is shown to be the primary quantity that governs modifications to the damping tail and is responsible for the correlations between Y_P and N_{eff} .

In detail, $\theta_d = r_d/D_A$ and $\theta_s = r_s/D_A$, where r_d is the comoving diffusion length at recombination, r_s is the comoving size of the sound horizon at recombination, and D_A is the angular diameter distance to recombination, such that the D_A terms cancel in the ratio $\theta_d/\theta_s = r_d/r_s$. We define

$$r_s(a_*) = \int_0^{a_*} \frac{c_s(a) da}{a^2 H(a)}, \quad (25)$$

where $c_s(a) = c/\sqrt{3(1+R(a))}$, $R(a) = 3\rho_b(a)/(4\rho_\gamma(a))$, ρ_b and ρ_γ are the energy densities of baryons and photons, respectively, and a_* is the recombination scale factor for which the optical depth equals unity [119, 120]. Moreover,

$$r_d(a_*) = \frac{\pi}{6} \left(\int_0^{a_*} \frac{g(a) da}{a^3 \sigma_T n_e H(a)} \right)^{1/2}, \quad (26)$$

where $g(a) = c [R^2(a) + \frac{16}{15}(1+R(a))]/(1+R^2(a))$, σ_T is the Thomson cross-section, and n_e is the number density of free electrons [119, 120]. As a result, $\theta_d/\theta_s \propto \sqrt{H(a)/n_e} \propto (1 + CN_{\text{eff}})^{1/4}/\sqrt{1-Y_P}$ [119]. The first term in the second proportionality follows for fixed matter-radiation equality redshift as $H \propto \rho_r \propto 1 + \rho_\nu/\rho_\gamma$, where ρ_r is the energy density of radiation which includes a contribution from the neutrino energy density $\rho_\nu = CN_{\text{eff}}\rho_\gamma$, given the constant $C = (7/8)(4/11)^{4/3}$ [121].

The second term follows from $n_e = (1 - Y_P)\rho_b/m_p$, where m_p is the proton mass, and reflects the fact that helium recombines earlier than hydrogen which changes the free electron density at last scattering [122].

Turning to the effective gravitational constant, we realize that its impact through the expansion rate is $H^2 \propto G_{\text{matter}}/G$, such that $\theta_d/\theta_s \propto (G_{\text{matter}}/G)^{1/4}(1 + CN_{\text{eff}})^{1/4}/\sqrt{1-Y_P}$. As pointed out in Ref. [119], increasing the expansion rate decreases a_* and increases $n_e(a)$ [123], which together slightly modify the power of $1/4$ in $(1 + CN_{\text{eff}})^{1/4}$, and the same applies in the case of G_{matter}/G . We note that the correlation between the helium abundance and baryon density is broken through the measurement of the latter on larger scales in the CMB (specifically by the first-to-second peak ratio relative to the first-to-third peak ratio in the temperature power spectrum) [124]. Meanwhile, the degeneracy between Y_P and N_{eff} (and between G_{matter}/G and N_{eff}) is partly broken by the early integrated Sachs-Wolfe (ISW) effect, the potential high baryon fraction as N_{eff} increases, and the phase shift in the acoustic oscillations due to neutrino perturbations [119] (for the neutrino phase shift, also see Ref. [125]). However, these and other physical effects do not help to break the degeneracy between Y_P and G_{matter}/G , which persists as shown in Fig. 3.

We note that for $\omega_{\text{BD}} \rightarrow \infty$, which is the limit taken as we vary G_{matter}/G in Fig. 3, the effective gravitational constant does not evolve with time (hence, does not directly contribute to the ISW effect). Even as we consider an unrestricted JBD model where ω_{BD} and G_{matter}/G are simultaneously constrained, in forthcoming sections we find that our constraints are sufficiently strong that the evolution is $\lesssim 1\%$ (from the present to the BBN epoch), in agreement with the BBN constraint in Ref. [83] (see Sec. VIII B 3). Focusing on the degeneracy between G_{matter}/G and Y_P , we have also explicitly checked that the CMB temperature and polarization power spectra remain invariant to sub-percent level as we modify these two parameters (here, up to a factor of two) but keep θ_d/θ_s fixed according to the relation we provide above.

We further note that G_{matter}/G will in principle also modify Y_P itself, as $G_{\text{matter}}/G > 1$ enhances the expansion rate, which leads to an earlier freeze out of the weak and nuclear interactions in the early Universe, and thereby an over-production of ^4He [81, 126]. In Ref. [127], this dependence of the helium abundance on the effective gravitational constant is shown to take on the form $Y_P \propto (G_{\text{matter}}/G)^{0.36}$ (also see Ref. [128]). We do not account for this effect in Fig. 3, but note that this would further enhance the impact of G_{matter}/G on the CMB ($\sim 1\%$ change in Y_P for the strongest constraint, approximately 0.03, that we obtain on G_{matter}/G in forthcoming sections).⁶

While the CMB polarization is useful in constraining G_{matter}/G (given the qualitatively different signature of the ef-

⁶ As similar-factor changes in G_{matter}/G and Y_P have comparable effects on the CMB, this implies that the impact of G_{matter}/G on the CMB would be enhanced by $\sim 30\%$. Put differently, our constraints on G_{matter}/G in forthcoming sections can either be viewed as somewhat conservative (i.e. $\lesssim 30\%$ weaker), or alternatively in the context of a Universe where GR is enforced during BBN.

effective gravitational constant on the polarization power spectrum, as pointed out in Ref. [123] and explicitly shown in Sec. V and Appendix A), it exhibits a similar degeneracy between Y_P and G_{matter}/G (shown in Fig. 3). This level of degeneracy also applies to the temperature-polarization cross-spectrum as shown in Appendix A. We therefore note that the uncertainty in the underlying gravitational theory (or the expansion rate more generally) has the potential to complicate inferences of small-scale physics targeted by CMB surveys such as AdvACT [129], SPT-3G [130], and the Simons Observatory [131]. While the direct measurement of Y_P from observations of low-metallicity extragalactic HII regions [132, 133] is able to break its degeneracies with other parameters, the correlation of G_{matter}/G with parameters such as N_{eff} and $dn_s/d\ln k$ would still remain to be disentangled (and for the CMB would be similar in nature to the correlations of a freely-varying Y_P with N_{eff} and $dn_s/d\ln k$ in GR).

In summary, the JBD scalar field will have an impact on a multitude of cosmological observables that we will consider in our analysis, such as the cosmic microwave background temperature and polarization, along with lower-redshift probes of the expansion history and the growth of structure, such as supernova distances, the weak lensing of galaxies, the weak lensing of the CMB, and the clustering of galaxies in redshift space. In testing JBD gravity with the latest cosmological observations, we have implemented this theory in the Einstein-Boltzmann solver EFTCAMB [134], and have performed an extensive comparison with four distinct codes [112]. The level of agreement between the codes is found to be at the sub-percent level for both the matter power spectrum and CMB temperature, polarization, and lensing power spectra, well within the precision required for current observations.

III. THEORY: NONLINEAR REGIME AND N -BODY IMPLEMENTATION

A. Background: numerical simulations with JBD gravity

In order to more fully utilize current cosmological data, we proceed to model the density perturbations in the nonlinear regime. We revisit the equations of motion, and now consider the effect of the scalar field as that of a fifth force. Given $\phi = \bar{\phi} + \delta\phi$ in the quasistatic regime (such that $\delta\phi/\nabla\delta\phi \ll 1$ and $k^2/(aH)^2 \gg 1$), and considering a constant potential, the scalar field equation of motion (Eq. 5) is well approximated by

$$\frac{1}{a^2} \nabla^2 \delta\phi \simeq -\frac{1}{M_{\text{Pl}}^2} \left(\frac{\delta\rho_m}{3 + 2\omega_{\text{BD}}} \right). \quad (27)$$

As $\delta\rho_m = \bar{\rho}_m \delta_m$, this implies $\delta\phi/\bar{\phi} = \Psi/(2 + \omega_{\text{BD}})$. We note that $\Psi \lesssim 10^{-4}$ in a cosmological simulation and given that we are interested in the $\omega_{\text{BD}} \gg 1$ regime, we can neglect terms of order $(\nabla\phi)^2/\bar{\phi}^2$ in the Einstein equations. In other words, the standard contribution of the energy density of the scalar field is insignificant as compared to the clustering component of the overall energy density.

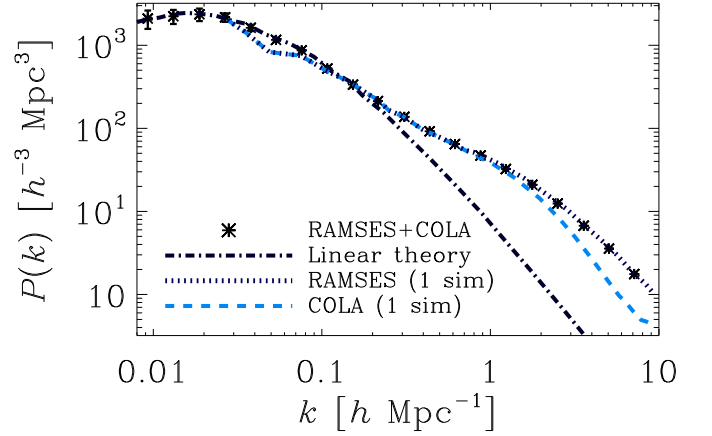


FIG. 4. Matter power spectrum $P(k, z=0)$ for $\omega_{\text{BD}} = 100$. Here, “1 sim” refers to a single realization of the initial conditions for which we run a high-resolution RAMSES simulation (dotted line) in addition to the COLA simulations (dashed line). As a result, the dip at $k \sim 0.05 h \text{ Mpc}^{-1}$ is due to cosmic variance (for both RAMSES and COLA given the same initial conditions). Here, RAMSES+COLA incorporates all of the simulations (some with a larger box size and thereby a smaller minimum k) and the error bars denote the 68% confidence level. For comparison, we also show the linear theory prediction (dot-dashed line) which expectedly agrees with the simulations on large scales but visibly deviates for $k \gtrsim 10^{-1} h \text{ Mpc}^{-1}$.

As a result, in the N -body simulations we evolve the non-relativistic geodesic equation (e.g. [135]),

$$\ddot{\mathbf{x}} + 2H\dot{\mathbf{x}} = -\frac{1}{a^2} \nabla\Psi, \quad (28)$$

where \mathbf{x} is the position of each particle and the raised dots are, as before, derivatives with physical time. The geodesic equation is evolved along with the modified Poisson equation, re-expressed here in the form

$$\nabla^2\Psi = \frac{3}{2} \Omega_{\text{m},0} H_0^2 a^{-1} \frac{G_{\text{matter}}}{G} \delta_m, \quad (29)$$

where we emphasize that the effective gravitational constant, G_{matter} , is time-dependent (Eq. 17). The initial conditions for the particles were generated with the MG-PICOLA code [99, 136] using second-order Lagrangian perturbation theory (2LPT) given a power-spectrum $P(k, z=0)$ from EFTCAMB [134]. The first and second order growth factors of the density contrast in 2LPT, denoted D_1 and D_2 , are determined by the equations [99]

$$\begin{aligned} \ddot{D}_1 + 2H\dot{D}_1 &= \frac{3}{2} \frac{\Omega_{\text{m},0}}{a^3} \frac{G_{\text{matter}}}{G} H_0^2 D_1, \\ \ddot{D}_2 + 2H\dot{D}_2 &= \frac{3}{2} \frac{\Omega_{\text{m},0}}{a^3} \frac{G_{\text{matter}}}{G} H_0^2 (D_2 - D_1^2), \end{aligned} \quad (30)$$

which are of the same form as in Λ CDM [137] aside from the G_{matter}/G factor.

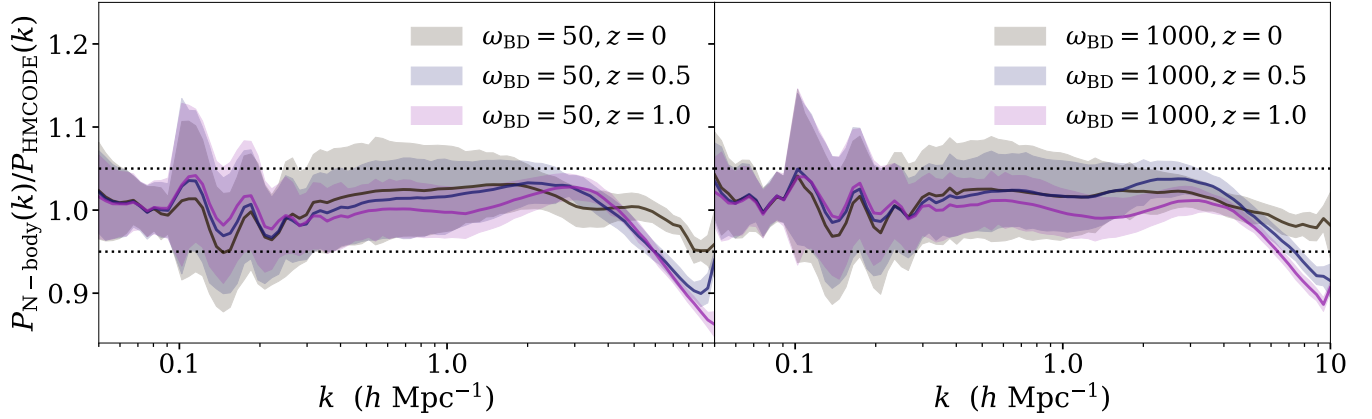


FIG. 5. The ratio of matter power spectra between the N -body simulations and HMCODE , $P_{N\text{-body}}(k)/P_{\text{HMCODE}}(k)$, for $\omega_{\text{BD}} = 50$ (left) and $\omega_{\text{BD}} = 1000$ (right) illustrating the accuracy of our modifications to HMCODE . The shaded bands encapsulate the 68% confidence intervals given the variations within the simulations (for each of the considered redshifts, $z = 0$ in grey, $z = 0.5$ in light blue, and $z = 1.0$ in light violet), the thin colored lines inside the bands correspond to the ratio with HMCODE given the mean of the simulations, and the dotted (black) horizontal lines mark $\pm 5\%$ deviations from unity. The agreement between HMCODE and the simulations improves towards lower redshift by our construction.

B. Hybrid suite of N -body simulations: COLA and RAMSES

We have modified two N -body codes to obtain an accurate measurement of $P(k)$ beyond the linear regime.⁷ For $k < 0.5 \, h \, \text{Mpc}^{-1}$, we use a modified version of the Comoving Lagrangian Acceleration (COLA) code [98, 99], which solves for perturbations around paths predicted from 2LPT, and has been shown to be accurate and fast on large scales. This enables the generation of a large enough ensemble of realizations to substantially reduce sample variance on large scales: we generate 50 realizations with $N = 1024^3$ particles in a box of size $L = 1000 \, h^{-1} \, \text{Mpc}$ (to cover large scales) and 100 realizations with $N = 512^3$ particles in a box of size $L = 250 \, h^{-1} \, \text{Mpc}$ (to cover small scales). We also use a large number of steps to increase the accuracy on smaller scales (~ 100 steps, an order of magnitude more than typical COLA simulations). On very small scales, to probe wavenumbers out to $k = 10 \, h \, \text{Mpc}^{-1}$, we use the RAMSES grid-based hydrodynamical solver with adaptive mesh refinement [100], modified to include JBD gravity. For each ω_{BD} , we have generated a higher resolution RAMSES simulation with $N = 512^3$ particles in a box of size $L = 250 \, h^{-1} \, \text{Mpc}$.

The RAMSES simulation is run with the same seed as one of the COLA simulations, chosen by the requirement that it has a $P(k, z)$ as close as possible to the mean of the ensemble of COLA simulations, which ensures that it is not an outlier realization. The COLA simulations are found to agree to 1% with the RAMSES simulation for $k < 0.5 \, h \, \text{Mpc}^{-1}$ at $z = 0$, and with an improved accuracy towards higher redshifts. For the largest wavenumbers considered here ($k_{\text{max}} = 10 \, h \, \text{Mpc}^{-1}$), with our simulation setup, the RAMSES simulation is accu-

rate to $\sim 5\text{--}10\%$.⁸ The ratio of the RAMSES and the COLA $P(k, z)$ for the same seed are then used to correct the COLA simulations $P(k, z)$ out to its maximum wavenumber. These simulations are carried out for $\omega_{\text{BD}} = \{50, 100, 500, 1000\}$, and we use outputs at $z = \{0, 0.5, 1.0\}$ as the basis for producing our modifications to the nonlinear matter power spectrum (see Fig. 4).

C. JBD gravity modifications to HMCODE

We include these modifications to the matter power spectrum in HMCODE [101, 102] (also see Refs. [139, 140]), which is a fitting function for the nonlinear matter power spectrum based on the halo model (reviewed in e.g. [141]). For the dark matter power spectrum, HMCODE has been calibrated to the Coyote N -body simulations [142] and is accurate at the level of 5–10% for $z \leq 2$ and $k \leq 10 \, h \, \text{Mpc}^{-1}$ (improving towards lower neutrino mass, where massive neutrinos suppress the clustering of matter below the neutrino free-streaming scale). A benefit of HMCODE over other fitting functions such as HALOFIT [143, 144] is that it has also been calibrated to the Overwhelmingly Large (OWL) hydrodynamical simulations [113–115]. As a result, it is able to capture the impact of baryonic feedback in the nonlinear $P(k, z)$ (at $\simeq 5\%$ level precision for the same redshifts and scales) and to marginalize over the uncertainty in the modeling. HMCODE moreover improves its modeling of the impact of massive neutrinos in the nonlinear $P(k, z)$ by calibrating to the massive neutrino simulations of Massara et al. (2014) [145] (agreement achieved at the few percent level for $m_\nu \leq 0.6 \, \text{eV}$, $z \leq 1$, $k \leq 10 \, h \, \text{Mpc}^{-1}$ [102]).

To account for JBD gravity within the HMCODE framework, in addition to modifying the expansion rate, density param-

⁷ A patch with the modifications to RAMSES can be found in <https://github.com/HAWinther/RamsesPatchApproxMGSolver> and the COLA code used can be found in <https://github.com/HAWinther/MG-PICOLA-PUBLIC>.

⁸ For a study of the accuracy of RAMSES compared to other N -body codes, see e.g. Schneider et al. (2016) [138].

ters, and growth function, we follow the approach in Mead et al. (2016) [102] and adjust the virialized halo overdensity, Δ_V , defined through

$$r_V = \left(\frac{3M}{4\pi\Delta_V\bar{\rho}_m} \right)^{\frac{1}{3}}, \quad (31)$$

where r_V is the corresponding virial radius and M is the halo mass. We find that a good fit that accounts for JBD gravity is given by

$$\Delta_V = \Omega_m(z)^{-0.352} \times \left(d_0 + (418.0 - d_0) \arctan \left((0.001|\omega_{BD} - 50.0|)^{0.2} \right) \frac{2}{\pi} \right), \quad (32)$$

where $d_0 = 320.0 + 40.0z^{0.26}$. Our fitting function has the desired property that as $\omega_{BD} \rightarrow \infty$ we recover the usual GR prescription in `HMCODE`.⁹ We note that baryonic feedback does not modify the fitting function for the virialized halo overdensity in `HMCODE`; instead it modifies the halo concentration-mass relation and the amount of halo “bloating” [101]. However, to account for the impact of massive neutrinos, the fitting function is further multiplied by a factor of $1 + 0.916f_V$ [102], where $f_V = \Omega_V/\Omega_m$.¹⁰

D. JBD matter power spectrum

In Fig. 5, we show the ratio of $P(k)$ measured from our simulations to the modified `HMCODE` for ω_{BD} of 50 and 1000 considering $z \in \{0, 0.5, 1.0\}$ and $k \leq 10 h \text{ Mpc}^{-1}$. We find that the agreement is within $\sim 10\%$ for the full range of nonlinear scales and redshifts, and across the wide range of coupling strengths, which is sufficient for our purposes given the precision of current data. The agreement is achieved through the `HMCODE` modifications, and would substantially degrade in their absence (for instance, by up to a factor of three for $\omega_{BD} = 100$ over the range of scales and redshifts considered).

As $P_{\omega_{BD}=1000}(k, z)/P_{GR}(k, z) \approx 1$ (at the sub-percent level across scales and redshifts, as also indicated in Fig. 2), together the $\omega_{BD} = 50$ and $\omega_{BD} = 1000$ cases effectively show that our `HMCODE` implementation has the same level of accuracy in JBD gravity as in GR (which is the optimal outcome). We also employed simulations with $(G_{\text{matter}}/G)|_{a=1} \in [0.5, 1.5]$; as `HMCODE` includes the effects of this degree of freedom via the linear matter power spectrum (through an overall rescaling of the amplitude, as seen in Fig. 2), we found that no further `HMCODE` modifications were needed to fit the simulations on nonlinear scales (with agreement due to changing $(G_{\text{matter}}/G)|_{a=1}$ to within 5% for $k \leq 10 h \text{ Mpc}^{-1}$).

⁹ We also considered ω_{BD} -dependent modifications to the linear collapse threshold, δ_c , and the linear spectrum damping factor, f_{damp} , and found that they only marginally improve the `HMCODE` fit to the JBD simulations.

¹⁰ In accounting for the impact of massive neutrinos on the nonlinear matter power spectrum, we note that `HMCODE` further modifies the linear collapse threshold, δ_c , by a factor of $1 + 0.262f_V$ [102].

E. Alternative approaches to capturing nonlinear corrections

For the precision needs of future surveys, this approach to capturing the nonlinear corrections can be improved through both a greater number of simulations and higher-resolution simulations taking into account the full cosmology dependence (instead of fitting for a fixed cosmology, and in the `HMCODE` context modifying parameters in addition to Δ_V entering the halo model). We note that an alternative approach consists of creating a full simulation-based emulator as has been achieved in Λ CDM (e.g. [146–148]). Given the simplicity of the JBD model (where a JBD simulation has the same computational cost as a standard GR simulation), an emulator accounting for JBD gravity is feasible but computationally expensive.

In this regard, the “reaction approach” of Cataneo et al. (2019) [149] (also see Bose et al. (2020) [150]) is promising, as it only requires a computation of halo model and 1-loop perturbation theory power spectra in the modified gravity cosmology together with an emulator for Λ CDM, and has already demonstrated percent-level accuracy on highly nonlinear scales for more complicated modified gravity models. Ultimately, an emulator needs to be able to *simultaneously* account for a wide range of physics, such as cold dark matter, massive neutrinos, modified gravity, and baryonic feedback, which is increasingly within reach.¹¹

F. Including physical effects: independently versus combined

While we have considered changes to `HMCODE` by calibrating to simulations that only include a single extension to Λ CDM (i.e. simulations that either account for baryonic feedback, neutrino mass, or modified gravity, but not simultaneously), we note that their effects are propagated in a coherent way in `HMCODE` through changes to the expansion rate, density parameters, growth function, virialized halo overdensity, the linear collapse threshold, concentration-mass relation, and halo bloating. In a sense, therefore, `HMCODE` is simultaneously accounting for the impact of baryonic feedback, neutrino mass, and modified gravity (also see the discussion in Ref. [102]).

We note that the differences are small ($\lesssim 5\%$ even for $k = 10 h \text{ Mpc}^{-1}$) compared to the case where the effects of baryonic feedback, neutrino mass, and modified gravity are separately propagated in the nonlinear matter power spectrum [102]. This is in agreement with a range of simulations where baryons and modified gravity [154–156], baryons and massive neutrinos [157, 158], and modified gravity and massive neutrinos [159–161] have been simultaneously considered. Lastly, we note that the question of separability of the physical effects is distinct from the question of degeneracies between the effects; as shown in Fig. 2 it might indeed be a challenge to distinguish the physical imprints of baryonic feedback, massive neutrinos, and modified gravity from one another, which we further explore in this analysis.

¹¹ We note that a separate emulator for baryonic feedback based on the ‘baryonic correction model’ [151] has been considered in Refs. [152, 153].

IV. ANALYSIS: DATASETS, SYSTEMATIC UNCERTAINTIES, PRIORS, MODEL SELECTION

In our cosmological analysis, we perform Markov Chain Monte Carlo (MCMC) calculations with a modified version of CosmoLSS [3, 162], which is based on CAMB [163] and CosmoMC [164]. We use a convergence criterion that obeys $R - 1 < 2 \times 10^{-2}$, where the Gelman-Rubin R -statistic [165] is the variance of chain means divided by the mean of chain variances. Here, we describe the cosmological datasets used, systematic uncertainties included, parameter priors enforced, and the approaches for performing model selection and assessing dataset concordances.

A. Cosmological datasets

We consider the following datasets in our cosmological analysis, either separately or in combination.

1. Cosmic microwave background

We consider the CMB temperature, polarization, and lensing reconstruction angular power spectra from the Planck satellite. We consider the 2018 dataset of Planck [75], and in some cases also contrast the differences in the parameter constraints with the 2015 dataset of Planck [71]. In addition to Planck, we consider the improvements in the parameter constraints from a combined analysis with the small-scale CMB temperature and polarization measurements from the 2008–2018 observing seasons of the Atacama Cosmology Telescope (ACT; primarily DR4 [97] but also contrasting against DR3 [96]).

We distinguish between two setups for Planck 2018, one that we denote “Planck18” which includes the CMB temperature and polarization data (TT,TE,EE+lowE; where the low-multipole polarization is obtained from the High Frequency Instrument, HFI), and another that we denote “All-Planck18” which additionally includes the lensing reconstruction (TT,TE,EE+lowE+lensing). The corresponding two cases for Planck 2015 are “Planck15” which includes the CMB temperature and low- ℓ polarization data (TT+lowP; where the low-multipole polarization is obtained from the Low Frequency Instrument, LFI), along with “All-Planck15” which additionally includes the TE and EE spectra at high multipoles together with lensing reconstruction (TT,TE,EE+lowP+lensing).

For the primary CMB anisotropies, JBD gravity provides a shift in the locations of the peaks due to the change in the expansion history (as seen in Fig. 2 and Fig. 20; where the JBD expansion history directly modifies quantities such as the epoch of matter-radiation equality and angular size of the sound horizon at recombination [34, 59, 166]). By modifying the time-variation in the gravitational potentials, $\frac{d}{dt}(\Psi + \Phi)$, JBD gravity in principle also affects the lowest multipoles in the CMB temperature power spectrum (and cross-correlations) via the integrated Sachs-Wolfe (ISW) effect [167]. The impact of JBD gravity on the CMB due to the ISW effect, however, is statistically diminished due to cosmic variance (along with the

generally mild evolution of the scalar field). The CMB lensing potential power spectrum [168, 169], $C_\ell^{\phi\phi}(\theta)$, is affected by JBD gravity through modifications to the sum of the metric potentials ($\Psi + \Phi$) and the expansion history, and to lesser extent through the growth function, as described in Sec. II (also see Ref. [21] on the impact of modified gravity on the CMB).

2. Weak gravitational lensing tomography and overlapping redshift-space galaxy clustering

Following the analysis of Joudaki et al. (2018) [3], we consider measurements of cosmic shear, galaxy-galaxy lensing, and redshift-space galaxy clustering from the Kilo Degree Survey (KiDS-450) [170, 171] overlapping with the 2-degree Field Lensing Survey [172] (2dFLenS) and the Baryon Oscillation Spectroscopic Survey (BOSS DR10¹²) [174]. The measurements are given by $\{\xi_+^{ij}, \xi_-^{ij}, \gamma_i^j, P_0, P_2\}$, where $\xi_\pm^{ij}(\theta)$ are the tomographic two-point shear correlation functions (for bins i and j , and angular scales θ), $\gamma_i^j(\theta)$ is the tomographic galaxy-galaxy lensing angular cross-correlation function, and $P_{0/2}(k)$ are the monopole and quadrupole power spectra [3]. We emphasize that the galaxy-galaxy lensing and multipole power spectrum measurements are only considered in the overlapping areas with KiDS.

This data vector is constructed from four tomographic bins of source galaxies in the redshift range $0.1 < z_B < 0.9$, where $\Delta z_B = 0.2$ and z_B is the best-fit redshift by the Bayesian photometric redshift code BPZ [175]. Moreover, there are four samples of lens galaxies: {2dFLOZ, BOSS LOWZ} which cover the redshift range $0.5 < z < 0.43$ and {2dFHIZ, BOSS CMASS} which cover the redshift range $0.43 < z < 0.7$. We include the full covariance between these observables using numerical simulations, as detailed in Ref. [3]. This covariance assumes a fixed Λ CDM cosmology, which is a sufficient approximation to current data [176].

KiDS-450 [171] encompasses 360 deg² on the sky, contains an effective number density $n_{\text{eff}} = 8.5$ galaxies arcmin⁻², possesses a median source redshift $z_m = 0.53$, and yields similar cosmological constraints to the subsequent analysis of the KiDS+VIKING-450 cosmic shear dataset [177]. We consider both KiDS×2dFLenS and KiDS×{2dFLenS+BOSS} [3] as described here, in order to explore the capabilities of a “3×2pt” dataset where the galaxy clustering is restricted to the overlapping regions with KiDS, as compared to a combined analysis of KiDS with the full spectroscopic datasets (where the impact of galaxy-galaxy lensing becomes negligible given the substantial difference in current imaging and spectroscopic observing areas). We do not consider the recent KiDS-1000 cosmic shear dataset [178] as it was not available during the course of this work, and we do not consider the combined cosmic shear dataset of KiDS+VIKING-450 and DES-Y1 [179], with similar constraining power to KiDS-1000.

¹² We note that subsequent BOSS and eBOSS data releases [173] do not contain additional observations in the KiDS footprint.

The wide spectroscopic surveys of {BOSS, 2dFlenS} contain $\{1 \times 10^6, 4 \times 10^4\}$ galaxies over $\{1 \times 10^4, 7 \times 10^2\}$ deg² on the sky, respectively [172, 174]. We restrict both of these surveys to the overlapping regions with KiDS-450, such that in these regions LOWZ contains 5044 lens galaxies over 125.0 deg², CMASS contains 20476 lens galaxies over 221.7 deg², 2dFLOZ contains 2214 lens galaxies over 122.4 deg², and 2dFHIZ contains 3676 lens galaxies over 122.4 deg² (also see below for use of the full BOSS dataset) [3].

To avoid nonlinearities in the galaxy bias, we restrict the galaxy-galaxy lensing and redshift-space galaxy clustering measurements to linear scales, such that $\theta_{\min} = 12$ arcmin for galaxy-galaxy lensing and $k_{\max} = 0.125 h \text{ Mpc}^{-1}$ for the multipole power spectra in accordance with the “fiducial” analysis in Ref. [3] (see Table 2 therein). The cosmic shear measurements are allowed to extend into the nonlinear regime, and correspond to the same scale cuts as in the fiducial KiDS-450 analyses [3, 171].

Analogous to CMB lensing, the galaxy lensing $\xi_{\pm}^{ij}(\theta)$ and galaxy-galaxy lensing $\gamma_{\pm}^i(\theta)$ measurements are mainly sensitive to JBD gravity via the modifications to the expansion history and the auto and cross-spectrum of $\Psi + \Phi$ (i.e. we integrate over the Weyl power spectrum rather than the matter power spectrum for the weak lensing and galaxy-galaxy lensing calculations; there is also a minor contribution to the intrinsic galaxy alignments through the growth function). In turn, the multipole power spectra $P_{0/2}$ are sensitive to JBD gravity via the expansion history, matter power spectrum, and the growth rate (and thereby the potential Ψ), discussed in Sec. II.

3. Growth rate, baryon acoustic oscillations, and Alcock-Paczynski effect

In order to more fully utilize the statistical power of BOSS, we also consider the “final BAO+FS consensus” constraints on $\{f\sigma_8, D_V/r_d, F_{\text{AP}}\}$ from the BOSS DR12 dataset [76] (i.e. not restricted to the overlapping regions with KiDS-450).¹³ Here, we use the distance scale, $D_V(z) = \left[D_M^2(z) \frac{cz}{H(z)} \right]^{1/3}$, where $D_M(z)$ is the comoving angular diameter distance, along with the comoving size of the sound horizon, $r_d = \int_{z_d}^{\infty} c_s(z)/H(z) dz$, at the end of the baryon-drag epoch, z_d , where $c_s(z)$ is the sound speed, and the Alcock-Paczynski parameter $F_{\text{AP}}(z) = D_M(z)H(z)/c$.

In combining these measurements with the weak lensing, galaxy-galaxy lensing, and overlapping redshift-space galaxy clustering measurements of Sec. IV A 2, we avoid double-counting BOSS by only including the KiDS×2dFlenS measurements (i.e. excluding the KiDS×BOSS galaxy-galaxy lensing and multipole power spectrum measurements). Given the

significantly larger amount of BOSS data outside of the overlapping regions with KiDS (in our case by more than a factor of 50), we expect this trade-off to increase the cosmological constraining power. We do not include a covariance between the BOSS $\{f\sigma_8, D_V/r_d, F_{\text{AP}}\}$ measurements with the galaxy-galaxy lensing and galaxy clustering measurements involving 2dFlenS as the two datasets encompass distinct areas on the sky. To distinguish these BOSS measurements from those restricted to the overlapping regions with KiDS, we will refer to these as “All-BOSS” (given their use of the full BOSS dataset).

As discussed in Sec II, JBD gravity directly modifies these observables through its impact on the growth rate and expansion history (and thereby distances and sound horizon).

4. Supernovae

To further improve the cosmological constraining power, we consider Type Ia supernova (SN) distance measurements from the Pantheon compilation [95] in some of our calculations. This compilation contains a total of 1048 SNe between $0.01 < z < 2.3$ from Pan-STARRS1, SDSS, SNLS, various low- z and HST samples, and constitutes the largest combined sample of SN Ia. We use these SN distances to constrain JBD gravity through the impact of the expansion history (described in Sec. II).

B. Systematic uncertainties

1. Cosmic microwave background (temperature, polarization, lensing reconstruction)

In obtaining unbiased cosmological results, we account for the systematic uncertainties affecting the measurements. For the Planck {2018, 2015} CMB temperature and polarization power spectra, this includes marginalizing over {21, 27} astrophysical foreground and instrumental modeling parameters in the MCMC analysis, respectively (15 nuisance parameters for TT alone and {6, 12} additional parameters when further including TE+EE; in particular due to galactic dust emission, the cosmic infrared background, the thermal and kinetic Sunyaev-Zel’dovich effects, radio and infrared point sources, and power spectrum calibration uncertainties) [181, 182]. The difference in the number of nuisance parameters between the 2018 and 2015 datasets of Planck is that the dust amplitudes in EE are fixed from the cross-correlations with the 353-GHz maps in the 2018 analysis [181]. When including the Planck CMB lensing power spectrum, the map-based calibration parameter is varied in the analysis, which already belongs to the above set of CMB nuisance parameters [168, 169].

Moreover, in combining Planck with ACT, one additional calibration parameter is varied in the analysis, which linearly scales the estimated ACT temperature-polarization cross-spectrum and quadratically scales the polarization auto-spectrum [96, 97].

¹³ We do not use the eBOSS DR16 dataset [173, 180] as the likelihood has not yet become publicly available. This dataset will allow for higher redshifts to be probed than considered here (i.e. $z > 0.7$), in particular through the higher-redshift growth rate measurements (as the impact of JBD gravity on BAO distances diminishes with redshift).

2. $3\times 2pt$ (cosmic shear, galaxy-galaxy lensing, multipole power spectra)

For the KiDS \times {2dFLenS+BOSS} cosmic shear, galaxy-galaxy lensing, and redshift-space galaxy clustering observables, we include uncertainties due to the intrinsic galaxy alignments, baryonic feedback, photometric redshift distributions, multiplicative shear calibration, galaxy bias, pairwise velocity dispersion, and non-Poissonian shot noise in our analysis in accordance with the treatment in Joudaki et al. (2018) [3]. This introduces 14 additional parameters that are varied in the MCMC calculations (1 from intrinsic galaxy alignments, 1 from baryonic feedback, 4 from galaxy bias, 4 from velocity dispersion, 4 from non-Poissonian shot noise).

The intrinsic galaxy alignments encapsulate correlations of the intrinsic ellipticities of galaxies with themselves and with the shear of background sources (i.e. the lensing two-point functions are constructed from correlations of the sum of shear and intrinsic ellipticity). We modify the strength of the intrinsic alignment signal by allowing for the amplitude A_{IA} in the “nonlinear linear alignment (NLA) model” [183, 184] to vary freely (noting that the results are robust to the redshift dependence [3]), which affects the theoretical estimates for cosmic shear and galaxy-galaxy lensing. We note that the modeling of the intrinsic alignments is assumed to be the same as in GR (i.e. we have not modified the NLA model), and further work is required to understand how separable the modeling of this systematic uncertainty is from physics such as modified gravity and massive neutrinos. However, as our parameter constraints tend to be consistent with GR (and zero neutrino mass; shown in Secs. VI, VII, VIII), any correction to the NLA model is expected to be small (as in a sense it is a “correction to a correction”).

We propagate the uncertainties in the photometric redshift distributions of the source samples by performing each MCMC calculation over 1000 bootstrap realizations of the redshift distributions (until convergence) [171], which does not introduce additional parameters and affects only the cosmic shear and galaxy-galaxy lensing estimates (we do not allow for uncertainties in the spectroscopic redshift distributions used for the lens samples). We assume a linear galaxy bias for each lens sample (2dFLOZ, 2dFHI, LOWZ, CMASS), motivated by our linear scale cuts for galaxy-galaxy lensing and redshift-space galaxy clustering (described in Sec. IV A 2), which introduces 4 additional parameters that are varied. The same holds for the velocity dispersion and non-Poissonian shot noise, where a parameter is introduced for each lens sample, leading to 8 additional parameters that modify the theoretical estimates for the multipole power spectra. The uncertainties in the multiplicative shear calibration are propagated via the covariance matrix as in Hildebrandt et al. (2017) [171] and does not introduce additional degrees of freedom.

Lastly, we allow for the baryonic feedback amplitude, B , to vary via *HMcode* (as discussed in Sec. III), which modifies the halo concentration-mass relation (and further modifies the halo bloating parameter η_0 through the relationship given in Ref. [3]). We place particular emphasis on baryon feedback given the degeneracy with modified gravity and neutrino

mass through their impact on the nonlinear matter power spectrum (as shown in Fig. 2; also see Refs. [102, 185]). Here, we have assumed that calibrating *HMcode* to simulations that separately include baryonic physics, massive neutrinos, and modified gravity provides a close approximation to one where it is calibrated to simulations that simultaneously include these effects (see Sec. III for a discussion). As different approaches to simulating baryonic feedback lead to quantitatively different predictions for the nonlinear matter power spectrum [186], we aim to capture this uncertainty by our wide prior on the feedback amplitude ($1 < B < 4$) in accordance with Ref. [3] (effectively “washing out” some of the information in the nonlinear regime). Here, $B = 3.13$ corresponds to “dark matter only” (i.e. no feedback), while $B = 2.0$ corresponds to the AGN case of the OWL simulations [101, 114].¹⁴

3. BAO distances, Alcock-Paczynski effect, and growth rate

For the BOSS growth rate and BAO measurements ($f\sigma_8, D_V/r_d, F_{AP}$), survey-related systematics are propagated into the galaxy weights (e.g. due to redshift failures, fibre collisions, and dependencies between the number density of observed galaxies and stellar density and seeing) and modeling systematics are propagated into the covariance matrix (e.g. due to differences between different pre-reconstruction and post-reconstruction measurement approaches, modeling of redshift space distortions and galaxy bias, and differences in covariance matrix approaches) [74, 76, 187]. As a result, no additional parameters are varied in the MCMC analysis when these BOSS measurements are considered.

We emphasize that the KiDS \times BOSS galaxy-galaxy lensing and multipole power spectrum measurements are not used together with these BOSS growth rate and BAO measurements to avoid double-counting the BOSS data (i.e. we restrict to combining KiDS \times 2dFLenS with only either of the two, as described in Sec. IV A 3). We also note that our Jordan-Brans-Dicke gravity analysis brings about secondary systematic uncertainties, as for instance the redshift-space distortion and galaxy bias modeling and reconstruction methods have not been adequately tested in the context of modified gravity, but we expect that these uncertainties are subdominant to the present statistical uncertainties.

4. Supernova distances

For the Pantheon supernova distances, uncertainties due to e.g. calibration, distance bias corrections, coherent flow corrections, and Milky Way extinction corrections are included in the analysis [95]. These uncertainties are not propagated via additional parameters in the MCMC, but instead through a

¹⁴ We note that the AGN case of the OWL simulations is quoted as corresponding to $B = 2.3$ in Mead et al. (2015) [101], but it is given by $B = 2.0$ following the updated η_0 - B parameterization in Ref. [3].

TABLE I. Priors on the cosmological and astrophysical parameters varied in the MCMC runs (excluding the CMB nuisance parameters). Here, “JBD potential density” refers to the density parameter of the scalar potential (see e.g. Eq. 8), and the Hubble constant is a derived parameter. While varied independently, we impose the same prior ranges on the galaxy bias, pairwise velocity dispersion, and shot noise for all four lens samples (2dFLOZ, 2dFHIZ, LOWZ, CMASS) in the overlapping regions with KiDS. Here, our Λ CDM limit corresponds to $\ln \omega_{\text{BD}}^{-1} = -17$ and $G_{\text{matter}}/G = 1.0$ (we have confirmed the agreement in our results between this choice and pure Λ CDM). We note that the effective gravitational constant parameter is defined at present and “ G_{matter}/G ” is here shorthand for $(G_{\text{matter}}/G)|_{a=1}$ (see Eq. 18).

Parameter	Symbol	Prior
Cold dark matter density	$\Omega_c h^2$	[0.001, 0.99]
Baryon density	$\Omega_b h^2$	[0.013, 0.033]
JBD potential density	$\Omega_V h^2$	[0.01, 0.99]
Amplitude of scalar spectrum	$\ln(10^{10} A_s)$	[1.7, 5.0]
Scalar spectral index	n_s	[0.7, 1.3]
Optical depth	τ	[0.01, 0.8]
Dimensionless Hubble constant	h	[0.4, 1.0]
Pivot scale [Mpc $^{-1}$]	k_{pivot}	0.05
Intrinsic alignment amplitude	A_{IA}	[-6, 6]
Baryonic feedback amplitude	B	[1, 4]
Linear galaxy bias	b_x	[0, 4]
Velocity dispersion [h^{-1} Mpc]	$\sigma_{v,x}$	[0, 10]
Non-Poissonian shot noise [h^{-1} Mpc] 3	$N_{\text{shot},x}$	[0, 2300]
Sum of neutrino masses [eV]	$\sum m_\nu$	[0.06, 10]
JBD coupling constant	$\ln \omega_{\text{BD}}^{-1}$	[-17, -2.3]
Effective gravitational constant	G_{matter}/G	[0.5, 2.0]

correction to the covariance matrix (i.e. by adding a systematic covariance matrix to the statistical covariance matrix).

C. Parameter priors

We consider uniform priors on the standard cosmological parameters, with ranges given in Table I (similar to Ref. [3]). Concretely, this model includes the 6 standard, or “vanilla”, cosmological parameters: the present cold dark matter density parameter, $\Omega_c h^2 \in [0.001, 0.99]$, the present baryon density parameter, $\Omega_b h^2 \in [0.013, 0.033]$, the present density parameter of the flat JBD potential which constitutes a component of the full JBD density in Eq. (8), $\Omega_V h^2 \in [0.01, 0.99]$ (varied in lieu of the approximation to the angular size of the sound horizon, θ_{MC}), the amplitude of the scalar spectrum, $\ln(10^{10} A_s) \in [1.7, 5.0]$, the scalar spectral index, $n_s \in [0.7, 1.3]$, and the optical depth to reionization, $\tau \in [0.01, 0.8]$. Here, the informative uniform prior on the baryon density is motivated by measurements of the primordial deuterium abundance [188, 189], where our prior range encapsulates the 10σ uncertainties.

In our fiducial model, we fix the neutrinos to be massless. We note that this massless neutrino setup yields similar results to one where the sum of neutrino masses is fixed to $\sum m_\nu = 0.06$ eV (for existing datasets) and is chosen for increased computational speed. However, we also consider a

setup where the sum of neutrino masses is varied, where we impose a uniform prior on $\sum m_\nu \in [0, 2.0]$ eV. We use the pivot scale $k_{\text{pivot}} = 0.05$ Mpc $^{-1}$, and note that the Hubble constant $H_0 = 100 h$ km s $^{-1}$ Mpc $^{-1}$ is a derived parameter, for which we impose the implicit bound $h \in [0.4, 1.0]$. We will also consider constraints on the derived parameter $S_8 = \sigma_8 \sqrt{\Omega_m/0.3}$, where σ_8 is the present root-mean-square of the linear matter density contrast on $8 h^{-1}$ Mpc scales and Ω_m is the present matter density parameter.

For the KiDS $\times\{2\text{dFLenS}+\text{BOSS}\}$ nuisance parameters, we impose the same fiducial priors as given in Ref. [3], and for the CMB nuisance parameters, we impose the same priors as used by Planck [75]. Notably, as discussed in Sec. IV B, we allow for a wide uniform prior on the baryonic feedback amplitude $B \in [1, 4]$. We moreover impose a uniform prior on $\ln \omega_{\text{BD}}^{-1}$ in agreement with the approach in Avilez & Skordis (2014) [55]. As the GR-limit is obtained for $\omega_{\text{BD}} \rightarrow \infty$, we have taken $\ln \omega_{\text{BD}}^{-1} \in [-17, -2.3]$ such that we obtain the upper bound $\omega_{\text{BD}} \lesssim 2.4 \times 10^7$ (noting that this limit yields close to identical MCMC results to a pure Λ CDM run) while the lower bound is given by $\omega_{\text{BD}} \geq 10$. When allowing for variations in the present effective gravitational constant, G_{matter}/G (written as shorthand for $(G_{\text{matter}}/G)|_{a=1}$), we impose a uniform prior in the range [0.5, 2.0], designed to be non-informative (i.e. constraints restricted to a narrower region within the range) and motivated by our numerical simulations (Sec. III).

D. Model selection and data concordance assessment

There has been a substantial amount of recent activity in devising the optimal approach for performing model selection and assessing dataset concordances (e.g. [162, 190–206]). Here, we consider the Deviance Information Criterion (DIC) [190] to assess the relative preference of two distinct cosmological models. The DIC is given by $\chi_{\text{eff}}^2 + 2p_D$, where the first term is the best-fit effective χ^2 (here defined as the effective χ^2 at the posterior maximum point, equivalent to the maximum likelihood point for uniform priors) and the second term is the Bayesian complexity (given by the difference of the mean of the χ^2 over the posterior and the best-fit effective χ^2). The Bayesian complexity encapsulates the effective number of parameters of a model, such that more complex models are penalized. For reference, we take a difference of $\Delta\text{DIC} = \text{DIC}_{\text{extended}} - \text{DIC}_{\Lambda\text{CDM}} = \{5, 10\}$ to correspond to {moderate, strong} preference in favor of the standard cosmological model (given odds of 1/12 and 1/148, respectively).

In assessing the concordance between distinct cosmological datasets, we consider the $\log \mathcal{I}$ statistic [162], where “log” denotes the common logarithm. This concordance statistic is obtained from the DIC estimates, such that

$$\log \mathcal{I}(D_1, D_2) = \mathcal{A} [\text{DIC}(D_1 \cup D_2) - \text{DIC}(D_1) - \text{DIC}(D_2)], \quad (33)$$

where $\mathcal{A} = -[2\ln(10)]^{-1}$, while D_1 and D_2 denote two distinct datasets and $\text{DIC}(D_1 \cup D_2)$ is the joint DIC of the two datasets. This allows us to estimate the probability of the combined data with respect to the individual data probabilities (in

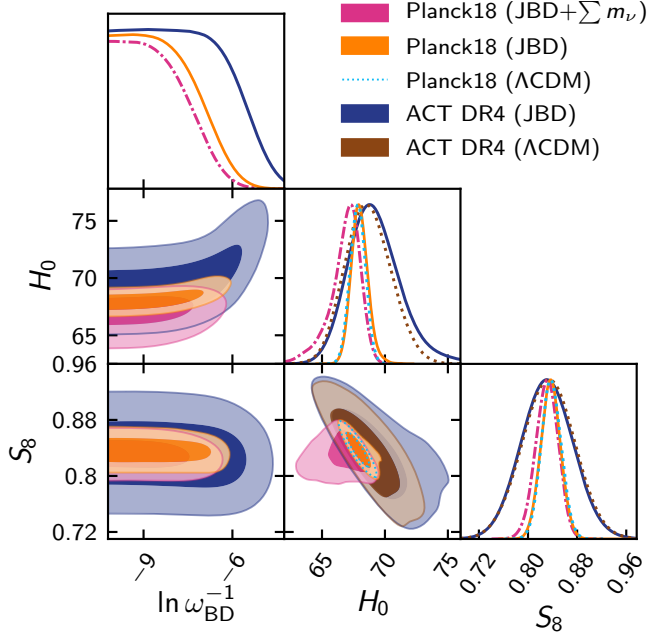


FIG. 6. Marginalized posterior distributions (inner 68% CL, outer 95% CL) of the JBD parameter $\ln \omega_{\text{BD}}^{-1}$, the Hubble constant H_0 (in units of $\text{km s}^{-1} \text{Mpc}^{-1}$), and $S_8 = \sigma_8 \sqrt{\Omega_m/0.3}$ from the CMB temperature and polarization measurements of Planck 2018 and ACT DR4. All other standard cosmological parameters are simultaneously varied. For visual clarity, we have zoomed in on the $\ln \omega_{\text{BD}}^{-1}$ axis where the contours begin to flatten in the plane with H_0 , as they stay flat and unbounded to the negative end of our prior (at $\ln \omega_{\text{BD}}^{-1} = -17$).

a similar form to the Bayes factor). The DIC has the advantages that it is symmetric (neither dataset is considered to be more fundamental than the other), it is simple to compute (in particular compared to the full evidence), and it can be used to assess possible discordances between constraints from the same dataset (allowing for improvements in the treatment of systematic uncertainties). Turning to the drawbacks, among others, its use of a point estimate can be stochastically affected by the data, and beyond brute force, no accurate and efficient method exists for computing the uncertainties in the DIC (for further details, see e.g. Ref. [162]).

For reference, we follow Jeffreys’ scale [207, 208] and take $|\log \mathcal{I}| \gtrsim \{1/2, 1, 2\}$ to reflect {substantial, strong, decisive} concordance between the datasets (given probability ratios in excess of 3.2, 10, and 100, respectively). Similar negative values correspond to discordance, or “tension”, between datasets. We also consider the tension between datasets for distinct cosmological parameters, such as H_0 and S_8 , by evaluating

$$T(p) = \left| \overline{p^{D_1}} - \overline{p^{D_2}} \right| / \sqrt{\sigma^2(p^{D_1}) + \sigma^2(p^{D_2})} \quad (34)$$

for a given parameter p , where overbar denotes the posterior mean, the vertical bars denote absolute value, and σ refers to the symmetric 68% confidence interval about the posterior mean (we note that the posterior maximum is another popular choice, with similar results for current data; e.g. [179, 209]).

Given the computational simplicity, we restrict the model

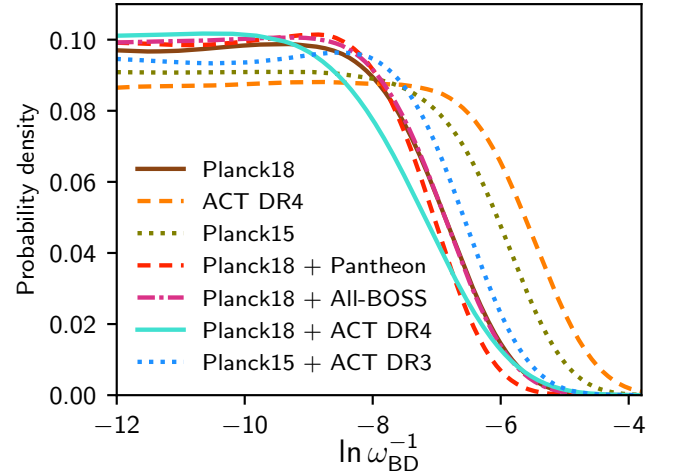


FIG. 7. Marginalized posterior distributions for the JBD parameter $\ln \omega_{\text{BD}}^{-1}$. We simultaneously vary all standard cosmological parameters (but keep $\sum m_\nu$ and G_{matter}/G fixed). For visual clarity, we have zoomed in on the $\ln \omega_{\text{BD}}^{-1}$ axis, as the distributions continue to stay flat towards the GR limit at $\ln \omega_{\text{BD}}^{-1} = -\infty$ (in practice to the negative end of our prior range at $\ln \omega_{\text{BD}}^{-1} = -17$).

selection and dataset concordance assessments to the DIC and $\log \mathcal{I}$ statistic, respectively. However, we note that similar results are expected for analogous computations with the Bayesian evidence and Bayes factor [194], respectively (see for example the agreement between the approaches in Ref. [162]). Further alternative approaches for data concordance assessments include, among others, the “surprise” [197, 198], the “index of inconsistency” [199], the “debiased evidence ratio” [200], the Q_{DMAP} statistic [200], the Q_{UDM} statistic [200], the “suspiciousness” [201, 202], and posterior predictive distributions (e.g. [203, 204]). As noted in Refs. [200, 209], these concordance statistics can often be directly related; of particular relevance here

$$\log \mathcal{I} = [2 \ln(10)]^{-1} [Q_{\text{DMAP}} + 4 \ln S], \quad (35)$$

where S is the suspiciousness.

V. RESULTS: COSMIC MICROWAVE BACKGROUND

We now methodically present the cosmological results of the JBD model, with a particular focus on the impact of different data combinations, modeling choices, and possible degeneracies between modified gravity, massive neutrinos, and astrophysics (especially baryonic feedback). Henceforth, we interchangeably refer to “ G_{matter} ” and “ G_{matter}/G ” when considering the normalized effective gravitational constant at present, $(G_{\text{matter}}/G)|_{a=1}$, as a free parameter in our analysis. In the assessment of the concordance between datasets, this is self-consistently performed under the same cosmological model.

We consider the following six distinct cosmologies: a) “ ΛCDM ” which refers to our ΛCDM limit of the JBD model (see Table I), b) “ $\Lambda\text{CDM} + \sum m_\nu$ ” where we allow the sum of neutrino masses to be further varied, c) “JBD” where the

TABLE II. Marginalized posterior means and 68% confidence intervals for a subset of the cosmological parameters. For the JBD parameter ω_{BD} and the sum of neutrino masses $\sum m_\nu$, we quote the 95% confidence lower and upper bounds, respectively. The Hubble constant H_0 is in units of $\text{km s}^{-1} \text{Mpc}^{-1}$, $\sum m_\nu$ is in units of eV, and $S_8 = \sigma_8 \sqrt{\Omega_m}/0.3$. A table element with “...” implies that the parameter is not varied in the analysis. Here, “ Λ CDM” includes massless neutrinos and is taken as the limiting case of the JBD model, in principle as $\omega_{\text{BD}} \rightarrow \infty$, and in practice as $\ln \omega_{\text{BD}}^{-1} = -17$ (along with $G_{\text{matter}}/G = 1$). We note that minor deviations in the Λ CDM results from those reported by Planck [71, 75] and ACT [96, 97] are due to this limit and the specific priors used (e.g. we do not add an external Gaussian prior on τ as in ACT, and all three neutrinos are massless in our fiducial model). The tensions $T(H_0)$ and $T(S_8)$ are against Riess et al. 2019 [77] and KiDS×{2dFLenS+BOSS}, respectively (in the latter case only against KiDS×2dFLenS when Planck is combined with BOSS), and are evaluated in a consistent manner where the datasets are considered in the same cosmology relative to one another (in practice only applies for S_8).

Probe setup	ω_{BD}	G_{matter}/G	$\sum m_\nu$	H_0	S_8	$T(H_0)$	$T(S_8)$
Planck18 (Λ CDM)	$67.84^{+0.61}_{-0.60}$	$0.838^{+0.016}_{-0.016}$	4.0	2.4
Planck18 (Λ CDM + $\sum m_\nu$)	0.38	$66.73^{+1.48}_{-0.69}$	$0.830^{+0.018}_{-0.018}$	4.1	2.5
Planck18 (JBD)	1150	$68.00^{+0.60}_{-0.71}$	$0.837^{+0.016}_{-0.016}$	3.9	2.4
Planck18 (JBD + $\sum m_\nu$)	1710	...	0.37	$66.79^{+1.44}_{-0.76}$	$0.831^{+0.018}_{-0.018}$	4.0	2.4
Planck18 (JBD + G_{matter} + $\sum m_\nu$)	1120	$0.993^{+0.026}_{-0.038}$	0.43	$66.40^{+1.99}_{-1.97}$	$0.835^{+0.023}_{-0.023}$	3.1	1.5
Planck18 + ACT DR4 (Λ CDM)	$68.00^{+0.55}_{-0.56}$	$0.841^{+0.015}_{-0.015}$	4.0	2.5
Planck18 + ACT DR4 (JBD)	1380	$67.88^{+0.55}_{-0.65}$	$0.840^{+0.015}_{-0.015}$	3.9	2.5
ACT DR4 (Λ CDM)	$68.68^{+1.69}_{-1.92}$	$0.833^{+0.042}_{-0.042}$	2.3	1.6
ACT DR4 (JBD)	330	$69.25^{+2.35}_{-1.67}$	$0.831^{+0.042}_{-0.042}$	1.9	1.6
All-Planck18 (Λ CDM)	$67.97^{+0.55}_{-0.54}$	$0.834^{+0.012}_{-0.013}$	4.0	2.4
All-Planck18 (JBD)	810	$68.15^{+0.50}_{-0.75}$	$0.833^{+0.013}_{-0.013}$	3.8	2.3
Planck18 + Pantheon (JBD)	1440	$68.05^{+0.57}_{-0.64}$	$0.835^{+0.015}_{-0.015}$	3.9	2.3
Planck18 + All-BOSS (JBD)	1170	$68.18^{+0.45}_{-0.54}$	$0.832^{+0.013}_{-0.013}$	3.9	2.3
Planck15 (Λ CDM)	$67.94^{+1.00}_{-0.98}$	$0.853^{+0.025}_{-0.025}$	3.5	2.5
Planck15 (JBD)	530	$68.27^{+0.93}_{-1.29}$	$0.850^{+0.025}_{-0.025}$	3.2	2.4
Planck15 (JBD + G_{matter})	850	$1.024^{+0.046}_{-0.053}$...	$69.86^{+2.57}_{-2.88}$	$0.842^{+0.034}_{-0.034}$	1.6	1.6
Planck15 + ACT DR3 (JBD)	900	$67.97^{+0.92}_{-1.10}$	$0.851^{+0.023}_{-0.024}$	3.5	2.5

modified gravity parameter $\ln \omega_{\text{BD}}^{-1}$ is varied in addition to the Λ CDM parameters (referred to as the standard, or restricted, JBD model), *d*) “JBD + $\sum m_\nu$ ” where the sum of neutrino masses is varied in the restricted JBD model, *e*) “JBD + G_{matter} ” where the present effective gravitational constant, $(G_{\text{matter}}/G)|_{a=1}$, is varied together with $\ln \omega_{\text{BD}}^{-1}$ in addition to the Λ CDM parameters (referred to as the unrestricted JBD model), and *f*) “JBD + G_{matter} + $\sum m_\nu$ ” where the sum of neutrino masses is varied together with the two modified gravity parameters in the unrestricted JBD model.

A. Planck and ACT

It is well established that the CMB currently constrains the standard cosmological model more powerfully than any other cosmological probe (e.g. [75]). Here, we find the strongest independent constraints on the JBD model from the Planck CMB, in particular through the impact of JBD gravity on the location of the CMB peaks and the damping tail (as discussed in Secs. II and IV A 1).

1. Constraining the JBD coupling constant

As shown in Table II and Figs. 6 and 7, our constraints are sensitive to the specific details of the CMB data and cosmological model, but are generally at the $\omega_{\text{BD}} \gtrsim 10^3$ level (at 95% CL, where the inequality symbol is here taken to denote “greater

than approximately”). Concretely, $\omega_{\text{BD}} > \{1150, 1710, 1120\}$ at 95% CL from the Planck 2018 CMB temperature and polarization measurements when considering the restricted JBD model, the restricted JBD model where the sum of neutrino masses is allowed to vary, and the unrestricted JBD model where the sum of neutrino masses is allowed to vary, respectively. For comparison, by further including the Planck CMB lensing reconstruction in our “All-Planck18” setup, the lower bound in the restricted JBD model with fixed neutrino masses weakens to $\omega_{\text{BD}} > 810$ (95% CL).

We emphasize that larger values of ω_{BD} imply greater consistency with GR. Moreover, while the uncertainty on ω_{BD} improves as we add more data, the one-sided bound will either weaken or strengthen depending on how much JBD gravity is favored by the additional data (i.e. it reflects a shift in the posterior rather than a narrowing of the posterior, similar to the one-sided bound for the sum of neutrino masses). Our results can be contrasted with the Planck constraints on ω_{BD} in Refs. [55, 64, 66–68, 210], where the upper bound fluctuates between approximately 10^2 to 10^3 at 95% CL depending on the specific datasets and details of the JBD modeling. We will return to this comparison in Secs. VIII B and VIII C.

We moreover consider the high-multipole CMB temperature and polarization measurements from ACT DR4, which on its own constrains $\omega_{\text{BD}} > 330$ (95% CL) in the restricted JBD model with fixed neutrino masses. By combining Planck 2018 (temperature and polarization) and ACT DR4 in this model, we find a strengthening in the lower bound on ω_{BD} from 1150 to 1380 (see Table II). We again note that this does not imply

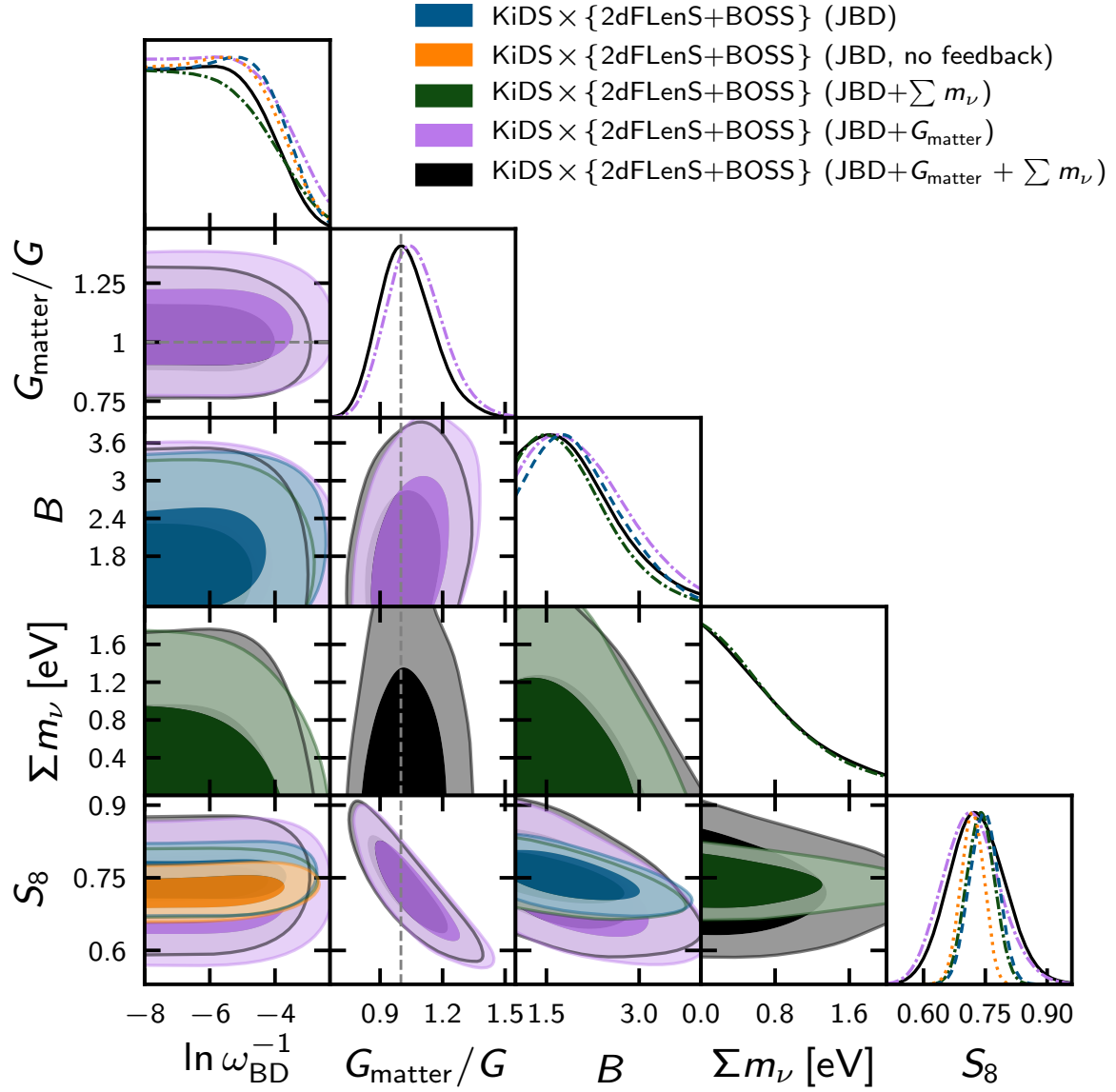


FIG. 8. Marginalized posterior distributions (inner 68% CL, outer 95% CL) of the JBD parameter $\ln \omega_{\text{BD}}^{-1}$, the present effective gravitational constant, G_{matter}/G , the baryonic feedback amplitude, B , the sum of neutrino masses, Σm_ν , and $S_8 = \sigma_8 \sqrt{\Omega_m}/0.3$ from $\text{KiDS} \times \{2\text{dFLenS}+\text{BOSS}\}$. All other standard cosmological and systematics parameters are simultaneously varied. For visual clarity, we have zoomed in on the $\ln \omega_{\text{BD}}^{-1}$ axis where the distributions begin to flatten, as they stay flat and unbounded in the direction of the GR limit (i.e. towards the negative end of our prior range at $\ln \omega_{\text{BD}}^{-1} = -17$). We do not include the ΛCDM case for visual clarity, given the similar constraints on $\{B, S_8\}$ to the JBD case.

a correspondingly significant improvement in the uncertainty on ω_{BD} , but rather a shift in the amount of modified gravity favored by the data (given the one-sided bound). In Fig. 7, we show the marginalized posteriors for the coupling constant for Planck and ACT, along with other datasets such as BOSS and Pantheon, where the lower bound on ω_{BD} is largely unchanged for Planck combined with BOSS and it strengthens to 1440 for Planck combined with Pantheon.

2. Impact of restricted JBD gravity on H_0 and S_8

In Fig. 6, we show the Planck and ACT constraints for the restricted JBD model in the subspace $\{\ln \omega_{\text{BD}}^{-1}, H_0, S_8\}$, where the Hubble constant increases as ω_{BD} decreases (i.e. as the strength of JBD gravity increases). The upturn in H_0 is stronger for ACT because its constraint on the coupling constant is weaker, and it is less pronounced for Planck when the sum of neutrino masses is varied (as compared to fixed neutrino masses; given the stronger constraint on the coupling constant). As expected, the contours in the plane of $\ln \omega_{\text{BD}}^{-1}$ and H_0 flatten as we approach the GR limit, here in practice as $\ln \omega_{\text{BD}}^{-1} \lesssim -9$. Meanwhile, the contour in the plane of S_8 and

TABLE III. Marginalized posterior means and 68% confidence intervals for a subset of the cosmological parameters. For the JBD parameter, ω_{BD} , and the sum of neutrino masses, $\sum m_\nu$ (in units of eV), we quote the 95% confidence lower and upper bounds, respectively. We also quote the 95% confidence upper bound for the feedback amplitude, B . The Hubble constant H_0 , is in units of $\text{km s}^{-1} \text{Mpc}^{-1}$ and we define $S_8 = \sigma_8 \sqrt{\Omega_m/0.3}$. The tensions $T(H_0)$ and $T(S_8)$ are against Riess et al. (2019) [77] and Planck 18, respectively. See Table II for further details.

Probe setup	ω_{BD}	G_{matter}/G	B	A_{IA}	$\sum m_\nu$	H_0	S_8	$T(H_0)$	$T(S_8)$
KiDS \times 2dFLenS (ΛCDM)	3.5	$1.23^{+0.69}_{-0.55}$...	\diamond	$0.736^{+0.039}_{-0.038}$	\circ	2.4
KiDS \times {2dFLenS + BOSS} (ΛCDM)	3.2	$1.71^{+0.48}_{-0.47}$...	\diamond	$0.746^{+0.034}_{-0.035}$	\circ	2.4
KiDS \times 2dFLenS + All-BOSS (ΛCDM)	3.3	$1.12^{+0.52}_{-0.46}$...	$70.6^{+5.8}_{-4.4}$	$0.745^{+0.029}_{-0.028}$	0.65	2.8
KiDS \times {2dFLenS + BOSS} ($\Lambda\text{CDM} + \sum m_\nu$)	3.1	$1.65^{+0.48}_{-0.44}$	1.7	\diamond	$0.736^{+0.033}_{-0.033}$	\circ	2.5
KiDS \times {2dFLenS + BOSS} (JBD)	56	...	3.3	$1.64^{+0.49}_{-0.48}$...	\diamond	$0.747^{+0.035}_{-0.035}$	\circ	2.4
KiDS \times {2dFLenS + BOSS} (JBD, no feedback)	63	$1.78^{+0.49}_{-0.49}$...	\diamond	$0.718^{+0.028}_{-0.028}$	\circ	3.7
KiDS \times {2dFLenS + BOSS} (JBD + $\sum m_\nu$)	80	...	3.2	$1.67^{+0.46}_{-0.46}$	1.7	\diamond	$0.739^{+0.034}_{-0.034}$	\circ	2.4
KiDS \times {2dFLenS + BOSS} (JBD + $\sum m_\nu$, no feedback)	71	$1.76^{+0.48}_{-0.48}$	1.6	\diamond	$0.707^{+0.028}_{-0.028}$	\circ	3.7
KiDS \times {2dFLenS + BOSS} (JBD + G_{matter})	50	$1.07^{+0.12}_{-0.15}$	3.4	$1.54^{+0.47}_{-0.47}$...	\diamond	$0.717^{+0.064}_{-0.073}$	\circ	1.7
KiDS \times {2dFLenS + BOSS} (JBD + $G_{\text{matter}} + \sum m_\nu$)	78	$1.03^{+0.11}_{-0.15}$	3.3	$1.67^{+0.47}_{-0.47}$	1.7	\diamond	$0.731^{+0.064}_{-0.070}$	\circ	1.6
KiDS \times 2dFLenS + All-BOSS (JBD + $G_{\text{matter}} + \sum m_\nu$)	83	$1.05^{+0.18}_{-0.20}$	3.2	$1.36^{+0.49}_{-0.44}$	1.4	$73.9^{+8.1}_{-8.2}$	$0.737^{+0.064}_{-0.085}$	0.02	1.3

In ω_{BD}^{-1} has a negligible downturn in S_8 as JBD gravity increases, and appears largely flat.

The Hubble constant is $H_0 = 67.88^{+0.55}_{-0.65} \text{ km s}^{-1} \text{Mpc}^{-1}$ and $H_0 = 69.25^{+2.35}_{-1.67} \text{ km s}^{-1} \text{Mpc}^{-1}$ in the restricted JBD model for Planck and ACT, respectively. These constraints are both approximately 10% weaker and positively shifted by 0.3σ relative to the corresponding constraints in ΛCDM . As compared to the direct measurement of the Hubble constant by Riess et al. 2019 [77], where $H_0 = 74.03 \pm 1.42 \text{ km s}^{-1} \text{Mpc}^{-1}$, this implies $\{0.1\sigma, 0.4\sigma\}$ decreases in the tension for {Planck, ACT}, respectively. The combined Planck+ACT constraint on the Hubble constant is $H_0 = 67.88^{+0.55}_{-0.65} \text{ km s}^{-1} \text{Mpc}^{-1}$, which corresponds to a marginal increase in the uncertainty and decrease of the tension (by 8% and 0.1σ , respectively) compared to ΛCDM . Turning to the S_8 parameter, the marginalized constraints are effectively unchanged relative to ΛCDM for these datasets.

3. The effective gravitational constant and its impact on tensions

Focusing on Planck 2018 alone, in addition to the coupling constant, in the unrestricted JBD model with massive neutrinos, we constrain the present effective gravitational constant at few-percent level precision, such that $G_{\text{matter}}/G = 0.993^{+0.026}_{-0.038}$, in full agreement with GR. As shown in Table II (and illustrated in the forthcoming sections), when the present effective gravitational constant is varied, the uncertainties in the Hubble constant and S_8 increase substantially. Concretely, $H_0 = 66.40^{+1.99}_{-1.97} \text{ km s}^{-1} \text{Mpc}^{-1}$ and $S_8 = 0.835^{+0.023}_{-0.023}$. As compared to the restricted JBD model with massive neutrinos (i.e. where $G_{\text{matter}}/G = 1$), the posterior means are marginally shifted (by $0.2\text{--}0.3\sigma$), while the uncertainties on H_0 and S_8 increase by 80% and 25%, respectively. As a result, the discordance with the Riess et al. (2019) measurement of H_0 alleviates to 3.1σ in this model, while the difference in S_8 with low-redshift probes such as KiDS \times {2dFLenS + BOSS} (discussed further in Sec. VI) narrows down to 1.5σ . As compared to the ΛCDM model with massive neutrinos, this implies a 1.0σ decrease in both tensions.

We can understand these results in the context of Fig. 2, where G_{matter}/G has a greater flexibility in its modification of the CMB power spectra (i.e. both suppression and enhancement of the responses depending on whether $G_{\text{matter}}/G < 1$ or $G_{\text{matter}}/G > 1$, while $\omega_{\text{BD}} \rightarrow 0$ largely enhances the fluctuations). Indeed, larger H_0 is favored by $G_{\text{matter}}/G > 1$. For a given response in the CMB temperature power spectrum by either ω_{BD} or G_{matter}/G , the corresponding response in the expansion rate is moreover substantially larger for the effective gravitational constant. We note that this is qualitatively similar in the case of S_8 . In forthcoming sections, we will revisit the unrestricted JBD model as additional datasets are considered and will explicitly show the positive correlation between G_{matter}/G and H_0 , and the negative correlation between G_{matter}/G and S_8 (and, correspondingly, the negative correlation between H_0 and S_8).

4. The sum of neutrino masses

The constraint on the sum of neutrino masses is robust, changing from 0.38 eV in ΛCDM to 0.37 eV in the restricted JBD model and to 0.43 eV in the unrestricted JBD model. However, we note that the marginalized constraints (on the sum of neutrino masses, along with other parameters such as the present effective gravitational constant) possess some dependence on the choice of parameterization of the coupling constant, which we explore further for the full combination of datasets in Sec. VIII C.

5. Planck 2018 + ACT DR4 versus Planck 2015 + ACT DR3

We can further contrast the Planck 2018 constraints to those obtained with the baseline 2015 dataset (in other words, we are here comparing Planck 2018 “TT,TE,EE+lowE” with Planck 2015 “TT+lowP”). As shown in Table II and Fig. 7, in the restricted JBD model, the lower bound on ω_{BD} for Planck 2018 is more than a factor of two stronger than Planck 2015, while the lower bound for Planck 2018 + ACT DR4 is 50% stronger than

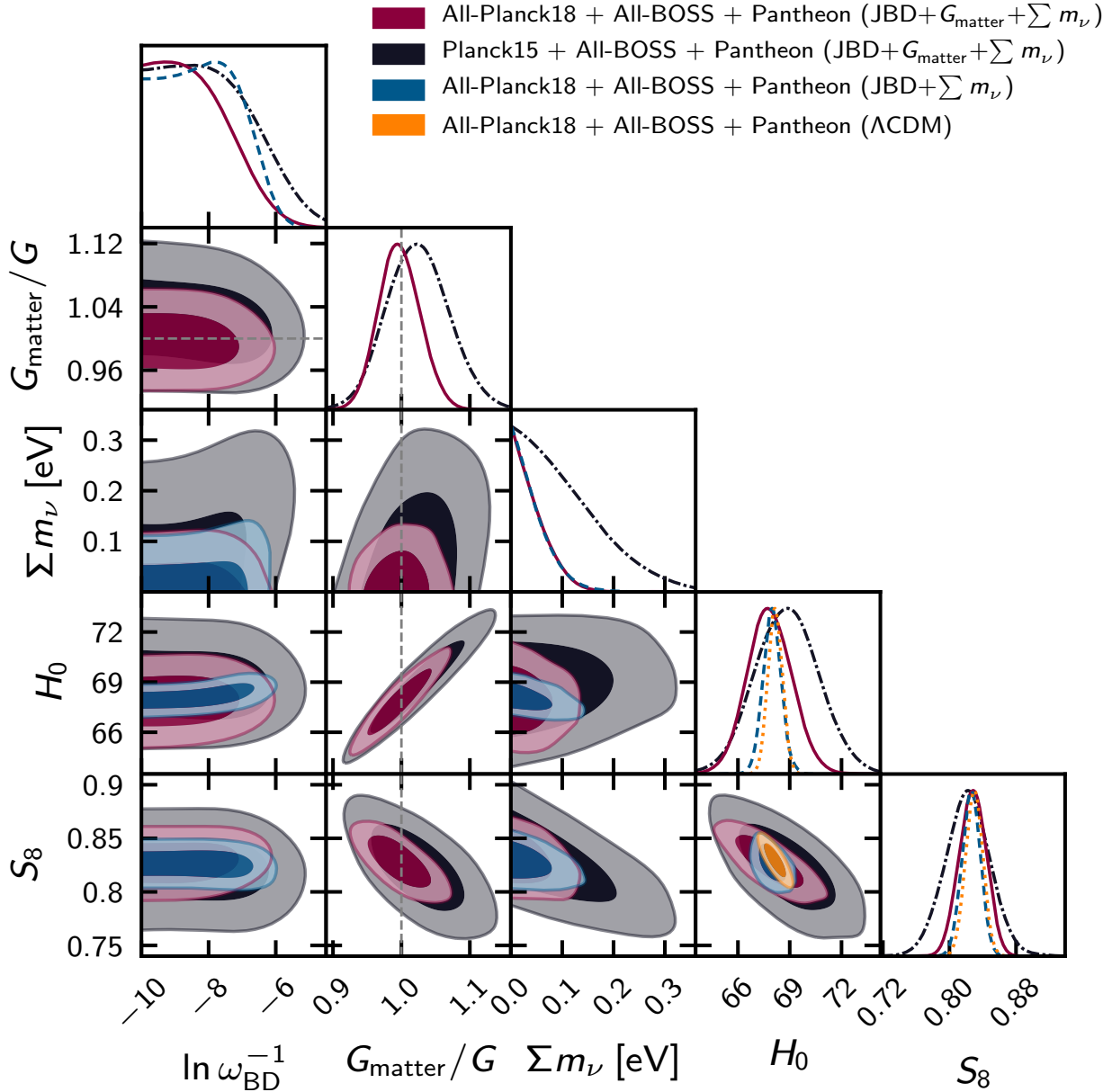


FIG. 9. Marginalized posterior distributions (inner 68% CL, outer 95% CL) of the JBD parameter, $\ln \omega_{\text{BD}}^{-1}$, the present effective gravitational constant, G_{matter}/G , the sum of neutrino masses, Σm_ν , the Hubble constant, H_0 (in units of $\text{km s}^{-1} \text{Mpc}^{-1}$), and $S_8 = \sigma_8 \sqrt{\Omega_m/0.3}$ from the Planck, BOSS, and Pantheon datasets. All other standard cosmological and systematics parameters are simultaneously varied. For visual clarity, we have zoomed in on the $\ln \omega_{\text{BD}}^{-1}$ axis where the distributions flatten towards the GR limit at $-\infty$ (in practice towards $\ln \omega_{\text{BD}}^{-1} = -17$).

the bound from Planck 2015 + ACT DR3. As our Planck 2018 baseline setup includes both the CMB temperature and polarization, while the Planck 2015 setup only includes the CMB temperature (and low- ℓ LFI polarization), this highlights the impact of including the high-multipole CMB polarization in the analysis (along with the new HFI low-multipole polarization likelihood in lieu of the LFI likelihood).

Moreover, by allowing for the effective gravitational constant to vary, the tension in the Hubble constant is ameliorated by 2σ for Planck 2015 (instead of 1σ for Planck 2018, where high-multipole polarization is notably included). In Appendix D, we will further contrast the constraints from these two datasets when including the CMB temperature, polariza-

tion, and lensing reconstruction in both cases.

6. Model selection

We quantify the model selection preference for the JBD gravity model relative to the standard model by the deviance information criterion (discussed in Sec. IV D), where the additional degrees of freedom impose a penalty on the extended model through the Bayesian complexity. As shown in Appendix C (specifically Table VII), for all of the models considered here, $\Delta\text{DIC} \gtrsim 0$, indicating no model selection preference for JBD gravity relative to ΛCDM .

TABLE IV. Marginalized posterior means and 68% confidence intervals for a subset of the cosmological parameters. For the JBD parameter, ω_{BD} , and the sum of neutrino masses, $\sum m_\nu$, we quote the 95% confidence lower and upper bounds, respectively. The sum of neutrino masses is in units of eV, the Hubble constant H_0 is in $\text{km s}^{-1} \text{Mpc}^{-1}$, $S_8 = \sigma_8 \sqrt{\Omega_m/0.3}$, and “...” implies that the parameter is not varied in the analysis. The tensions $T(H_0)$ and $T(S_8)$ are against Riess et al. (2019) [77] and KiDS×2dFLenS, respectively. See Table II for further details.

Probe setup	ω_{BD}	G_{matter}/G	$\sum m_\nu$	H_0	S_8	$T(H_0)$	$T(S_8)$
All-Planck18 + All-BOSS + Pantheon (ΛCDM)	$68.15^{+0.42}_{-0.41}$	$0.830^{+0.010}_{-0.010}$	4.0	2.3
All-Planck18 + All-BOSS + Pantheon ($\Lambda\text{CDM} + \sum m_\nu$)	0.11	$67.86^{+0.51}_{-0.44}$	$0.826^{+0.011}_{-0.011}$	4.1	2.7
All-Planck18 + All-BOSS + Pantheon (JBD)	1460	$68.22^{+0.42}_{-0.48}$	$0.830^{+0.010}_{-0.010}$	3.9	2.3
All-Planck18 + All-BOSS + Pantheon (JBD + $\sum m_\nu$)	970	...	0.11	$67.97^{+0.44}_{-0.52}$	$0.826^{+0.011}_{-0.011}$	4.0	2.6
All-Planck18 + All-BOSS + Pantheon (JBD + G_{matter})	2040	$0.989^{+0.030}_{-0.030}$...	$67.80^{+1.28}_{-1.32}$	$0.835^{+0.015}_{-0.015}$	3.2	0.7
All-Planck18 + All-BOSS + Pantheon (JBD + $G_{\text{matter}} + \sum m_\nu$)	1420	$0.997^{+0.028}_{-0.032}$	0.11	$67.83^{+1.28}_{-1.27}$	$0.828^{+0.016}_{-0.016}$	3.2	0.6

VI. RESULTS: COSMIC SHEAR AND OVERLAPPING REDSHIFT-SPACE GALAXY CLUSTERING

We next consider the combined analysis of KiDS overlapping with 2dFLenS and BOSS, where JBD has an impact on both the expansion history and the growth of structure (see Sec. IV A 2). We do not consider KiDS cosmic shear on its own but always in conjunction with the spectroscopic surveys to leverage the ability to constrain modified gravity.

A. KiDS×{2dFLenS+BOSS}

1. Correlations of modified gravity, neutrino mass, baryonic feedback, and intrinsic alignments

In the analysis of KiDS×{2dFLenS+BOSS}, we constrain $\omega_{\text{BD}} \gtrsim 100$ (shown in Table III) for all of the different cosmological models considered (where we include or exclude the baryonic feedback amplitude, B , the sum of neutrino masses, $\sum m_\nu$, and the present effective gravitational constant, G_{matter}/G , as free parameters in the model). As shown in Fig. 8, this consistency in the bounds is explained by the lack of correlation between ω_{BD} and $\{B, \sum m_\nu, G_{\text{matter}}/G\}$. The effective gravitational constant is further marginally correlated with the baryonic feedback amplitude and uncorrelated with the sum of neutrino masses, while the latter two are anti-correlated with one another.

The 95% upper bound on the sum of neutrino masses is within 1.6 eV to 1.7 eV for the different cases, and the upper bound on the baryonic feedback amplitude varies between 3.1 to 3.4 (near the border of the no-feedback, or “dark matter only,” value of $B = 3.13$ [101]). We find, however, that the posterior for the baryonic feedback amplitude peaks at $B \lesssim 2$ suggesting a preference for strong feedback (as noted in Ref. [3]). Moreover, we do not find a significant correlation between the intrinsic alignment amplitude and $\{B, \sum m_\nu, \omega_{\text{BD}}, G_{\text{matter}}/G\}$, such that the posterior mean for A_{IA} varies between 1.54 to 1.78 for the different cosmological setups while the uncertainty changes by less than 5% (from 0.47 to 0.49).

Beyond ω_{BD} , in the unrestricted JBD model, we constrain $G_{\text{matter}}/G = 1.07^{+0.12}_{-0.15}$ when the neutrinos are assumed massless and $G_{\text{matter}}/G = 1.03^{+0.11}_{-0.15}$ when the sum of neutrino masses is allowed to vary (the marginally tighter constraint

on G_{matter}/G is due to the one-sided nature of the neutrino mass bounds), both in full agreement with the GR expectation and nearly a factor of four weaker than the constraint from the Planck CMB.

2. Impact on the S_8 tension

KiDS×{2dFLenS+BOSS} is not sufficiently powerful to meaningfully constrain the Hubble constant. However, this dataset does constrain S_8 in a way that is sensitive to the cosmological modeling. In the ΛCDM limit, $S_8 = 0.746^{+0.034}_{-0.035}$, which is only marginally affected (at the sub-percent level) by a restricted coupling to the JBD scalar field (i.e. to ω_{BD} ; see Table III). We find a 20% decrease in the uncertainty in S_8 and $\sim 1\sigma$ shift towards lower values when neglecting baryonic feedback, in agreement with earlier KiDS analyses (e.g. Refs. [3, 171]; also see Refs. [177, 178]). Moreover, as found in earlier analyses (e.g. Refs. [3, 20]), varying the sum of neutrino masses decreases the posterior mean of S_8 , here by approximately $\Delta S_8 \sim -0.01$ corresponding to a 0.3σ negative shift (with marginal change in the uncertainty).

As we consider an unrestricted JBD model (where G_{matter} is varied alongside ω_{BD}), the additional degree of freedom degrades the uncertainty on S_8 by nearly a factor of two, such that the level of concordance with Planck improves to $T(S_8) = 1.6\sigma$ (an improvement by $|\Delta T(S_8)| = 0.8\sigma$). Moreover, the anti-correlation of S_8 with G_{matter} lowers the posterior mean by $\Delta S_8 = -0.030$ when the neutrinos are assumed massless and by $\Delta S_8 = -0.008$ when the sum of neutrino masses is varied. In other words, while a variation of $\sum m_\nu$ lowers the posterior mean of S_8 by approximately 0.01 in ΛCDM and in a restricted JBD model, the parameter correlations in the unrestricted JBD model drive the opposite behavior (i.e. a positive shift of $\Delta S_8 = 0.014$).

3. Model selection

As shown in Appendix C (specifically Table VII), and in agreement with earlier findings (e.g. [3, 171]), including baryonic feedback is marginally favored in a model selection sense ($\Delta\text{DIC} \approx -1$). For all of the cosmological extensions considered, there is no meaningful statistical preference for the extended model (considering both restricted and unrestricted

JBD gravity, with and without massive neutrinos) relative to Λ CDM, with $\Delta\text{DIC} \gtrsim 0$.

B. KiDS×2dFLenS + All-BOSS

As the BOSS dataset in Sec. [VIA](#) is restricted to the overlapping regions with KiDS, we also consider a scenario where the full BOSS dataset is included in our analysis. Here, we do not consider the galaxy-galaxy lensing signal between KiDS and BOSS given the marginal improvements in the cosmological constraining power that this would provide.¹⁵ Instead, we consider “3×2pt” measurements for KiDS and 2dFLenS (i.e. cosmic shear, galaxy-galaxy lensing, and overlapping redshift-space galaxy clustering) along with the BOSS DR12 growth rate, AP parameter, and BAO distance measurements (described in sections [IV A 2](#) and [IV A 3](#), respectively). We denote this setup “KiDS×2dFLenS + All-BOSS”.

1. Λ CDM comparisons: smaller overlapping spectroscopic area versus larger disconnected area

We first compare the Λ CDM results for KiDS×2dFLenS + All-BOSS against KiDS×{2dFLenS+BOSS}, finding a constraint on $S_8 = 0.745^{+0.029}_{-0.028}$ in our new setup as compared to $S_8 = 0.746^{+0.034}_{-0.035}$ when BOSS is restricted to the overlapping area with KiDS. This corresponds to a remarkable consistency in the posterior mean (less than 0.03σ shift) and a 20% improvement in the uncertainty. As a result, the S_8 tension with the Planck CMB is at the level of 2.8σ (an increase by 0.4σ). We further note that as compared to KiDS×2dFLenS alone, where $S_8 = 0.736^{+0.039}_{-0.038}$, the posterior mean increases by 0.3σ and the uncertainty decreases by 25%. Given the full BOSS dataset, we are moreover able to infer the Hubble constant, $H_0 = 70.6^{+5.8}_{-4.4} \text{ km s}^{-1} \text{ Mpc}^{-1}$, which reflects a strong (closer than 1σ) agreement with both the Planck CMB and Riess et al. (2019) [[77](#)] measurements of the Hubble constant.

We can also compare the constraints on the astrophysical systematics, focusing on the self-calibration of the baryonic feedback and intrinsic alignments. As the constraint on the baryonic feedback amplitude, B , is driven by the cosmic shear (given its sensitivity to nonlinear scales in the matter power spectrum along with the linear-scale restriction for the galaxy-galaxy lensing and multipole power spectra to avoid nonlinearities in the galaxy bias in KiDS×{2dFLenS+BOSS}), we find strong consistency in the upper bound on the baryonic feedback amplitude, such that $B < 3.3$ for KiDS×2dFLenS + All-BOSS as compared to $B < 3.2$ for KiDS×{2dFLenS+BOSS} and $B < 3.5$ for KiDS×2dFLenS alone (all at 95% CL).

The intrinsic alignment amplitude is constrained to $A_{\text{IA}} = 1.12^{+0.52}_{-0.46}$ for KiDS×2dFLenS + All-BOSS, which reflects an approximately 1σ downward shift as compared to the measurement from KiDS×{2dFLenS+BOSS} (where $A_{\text{IA}} = 1.71^{+0.48}_{-0.47}$). The downward shift in the amplitude brings it in greater agreement with the result from KiDS alone (where $A_{\text{IA}} = 1.16^{+0.77}_{-0.60}$ in Ref. [[3](#)]) and from KiDS×2dFLenS (where $A_{\text{IA}} = 1.23^{+0.69}_{-0.55}$). In spite of the overall weaker parameter constraints, we note that the constraint on A_{IA} is marginally stronger (by 3%) in the case of KiDS×{2dFLenS+BOSS} relative to KiDS×2dFLenS + All-BOSS, given the additional information from galaxy-galaxy lensing between KiDS and BOSS (this can be compared to the 30% improvement in the A_{IA} uncertainty that galaxy-galaxy lensing provides for KiDS×{2dFLenS+BOSS} as compared to KiDS alone [[3](#)]).

2. Moving beyond Λ CDM

As we turn to an extended cosmological model with unrestricted JBD gravity and massive neutrinos, we constrain $\sum m_\nu < 1.4 \text{ eV}$ (95% CL), $\omega_{\text{BD}} > 83$ (95% CL), and $G_{\text{matter}}/G = 1.05^{+0.18}_{-0.20}$, all in agreement with the fiducial model expectation. While the $\sum m_\nu$ and ω_{BD} bounds are marginally different to those obtained from the KiDS×{2dFLenS+BOSS} dataset (where the respective bounds are $\omega_{\text{BD}} > 78$ and $\sum m_\nu < 1.7 \text{ eV}$ at 95% CL), the constraint on G_{matter}/G is approximately 50% weaker as compared to that obtained from KiDS×{2dFLenS+BOSS}. In other words, in constraining modified gravity through the unrestricted JBD model, the self-consistent 3×2pt analysis in KiDS×{2dFLenS+BOSS} is here found to be more powerful than the alternative approach where growth rate and distance measurements from the full BOSS dataset are independently included in KiDS×2dFLenS + All-BOSS.

In the unrestricted JBD model with massive neutrinos, we continue to find a weak correlation for the baryonic feedback amplitude with the neutrino mass and modified gravity degrees of freedom (similarly for the intrinsic alignments). Concretely, $B < 3.2$ (95% CL), which agrees to within $|\Delta B| = 0.1$ with the corresponding bound in Λ CDM (and to that obtained from KiDS×{2dFLenS+BOSS}). Analogous to that found for the Planck CMB, mainly as a result of the positive correlation between G_{matter}/G and H_0 , the Hubble constant is shifted to larger values (by $\Delta H_0 = 3.3 \text{ km s}^{-1} \text{ Mpc}^{-1}$). As expected, in this extended cosmology, the uncertainty on the Hubble constant is larger than in Λ CDM (by 60%), and continues to be consistent with both the Planck CMB and Riess et al. (2019) [[77](#)] measurements to within 1σ .

Driven by the anti-correlation with G_{matter}/G , in the unrestricted JBD model with massive neutrinos we constrain $S_8 = 0.737^{+0.064}_{-0.085}$, which reflects a downward shift by $\Delta S_8 = -0.008$ (0.3σ relative to the Λ CDM uncertainty) and factor of 2.6 increase in the uncertainty relative to Λ CDM. The constraint on S_8 is weaker (by 10%) than that obtained from KiDS×{2dFLenS+BOSS}, which is consistent with the correspondingly weaker constraint on G_{matter}/G . Here, the constraint on S_8 agrees with the Planck CMB constraint at 1.0σ .

¹⁵ As discussed in Sec. [IV A 3](#), this is because the overlapping area between KiDS-450 and BOSS DR10 is more than a factor of 50 smaller than the full BOSS area, and does not increase for later BOSS data releases. As a result, the improvement in the BOSS galaxy bias constraints from including galaxy-galaxy lensing with KiDS is modest, as shown in e.g. Ref. [[3](#)].

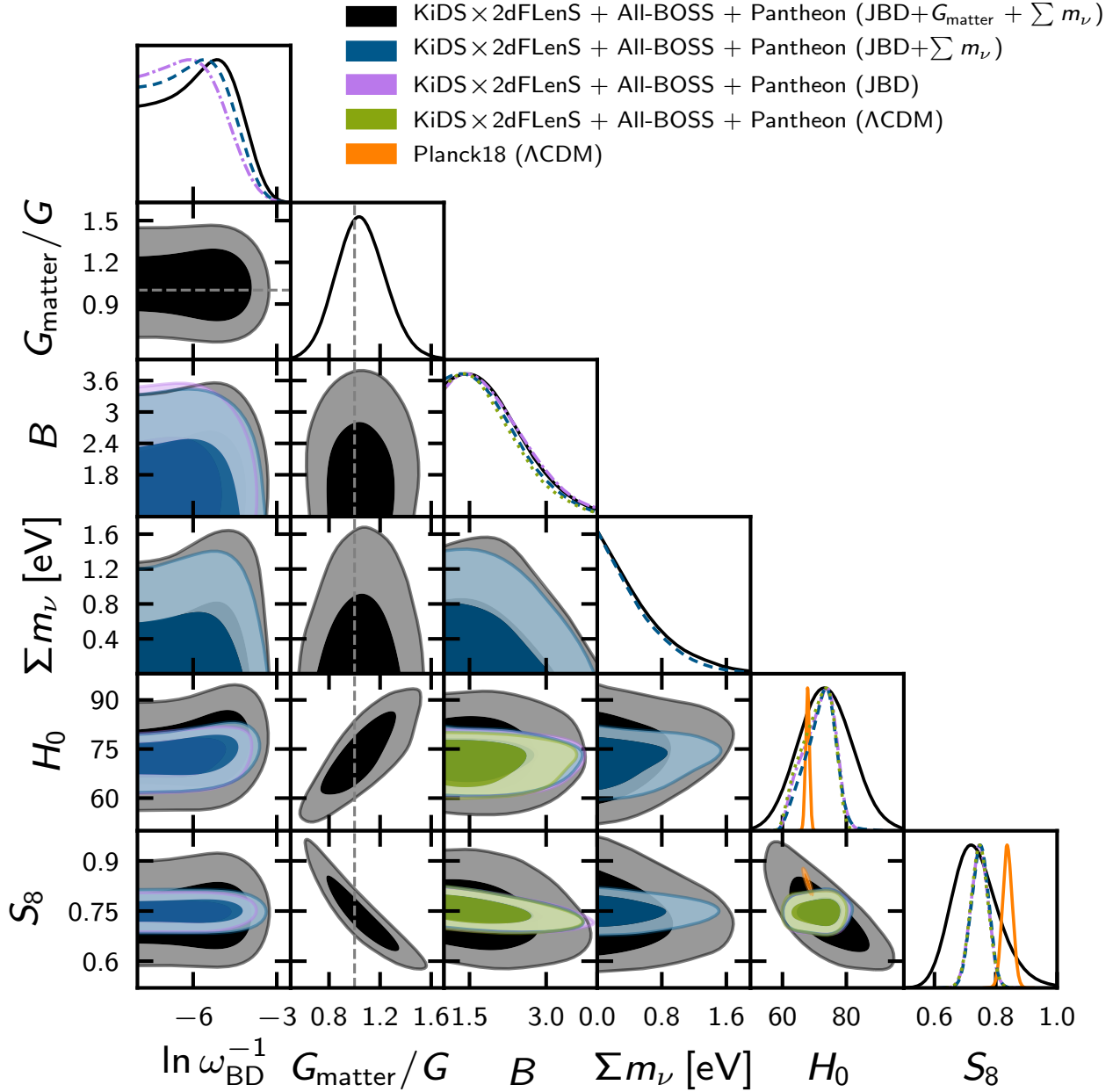


FIG. 10. Marginalized posterior distributions (inner 68% CL, outer 95% CL) of the JBD parameter, $\ln \omega_{\text{BD}}^{-1}$, the present effective gravitational constant, G_{matter}/G , the baryonic feedback amplitude, B , the sum of neutrino masses, Σm_ν , the Hubble constant, H_0 (in units of $\text{km s}^{-1} \text{Mpc}^{-1}$), and $S_8 = \sigma_8 \sqrt{\Omega_m}/0.3$ from the KiDS, 2dFLenS, BOSS, and Pantheon datasets. We also include the Planck18 ΛCDM constraints for comparison. All other standard cosmological and systematics parameters are simultaneously varied. For visual clarity, we have zoomed in on the $\ln \omega_{\text{BD}}^{-1}$ axis where the distributions begin to flatten, as they stay flat and unbounded in the direction of the GR limit (in practice towards $\ln \omega_{\text{BD}}^{-1} = -17$).

TABLE V. Marginalized posterior means and 68% confidence intervals for a subset of the cosmological parameters. For the JBD parameter, ω_{BD} , and the sum of neutrino masses, Σm_ν (in units of eV), we quote the 95% confidence lower and upper bounds, respectively. We also quote the 95% confidence upper bound for the feedback amplitude, B . The Hubble constant, H_0 , is in units of $\text{km s}^{-1} \text{Mpc}^{-1}$ and we define $S_8 = \sigma_8 \sqrt{\Omega_m}/0.3$. The tensions $T(H_0)$ and $T(S_8)$ are against Riess et al. (2019) [77] and Planck18, respectively. See Table II for further details.

Probe setup	ω_{BD}	G_{matter}/G	B	A_{IA}	Σm_ν	H_0	S_8	$T(H_0)$	$T(S_8)$
KiDS \times 2dFLenS + All-BOSS + Pantheon (ΛCDM)	3.1	$1.13^{+0.53}_{-0.46}$...	$70.8^{+6.0}_{-3.7}$	$0.746^{+0.028}_{-0.028}$	0.64	2.8
KiDS \times 2dFLenS + All-BOSS + Pantheon ($\Lambda\text{CDM} + \Sigma m_\nu$)	3.1	$1.34^{+0.49}_{-0.48}$	1.1	$71.0^{+3.7}_{-3.2}$	$0.748^{+0.028}_{-0.028}$	0.65	2.5
KiDS \times 2dFLenS + All-BOSS + Pantheon (JBD)	140	...	3.3	$1.12^{+0.51}_{-0.45}$...	$71.3^{+3.9}_{-4.0}$	$0.746^{+0.028}_{-0.028}$	0.53	2.8
KiDS \times 2dFLenS + All-BOSS + Pantheon (JBD + Σm_ν)	100	...	3.2	$1.36^{+0.51}_{-0.46}$	1.2	$71.7^{+5.4}_{-3.8}$	$0.748^{+0.028}_{-0.028}$	0.48	2.5
KiDS \times 2dFLenS + All-BOSS + Pantheon (JBD + G_{matter})	120	$1.10^{+0.19}_{-0.22}$	3.4	$1.13^{+0.51}_{-0.45}$...	$74.7^{+8.5}_{-9.3}$	$0.719^{+0.062}_{-0.085}$	0.08	1.5
KiDS \times 2dFLenS + All-BOSS + Pantheon (JBD + $G_{\text{matter}} + \Sigma m_\nu$)	79	$1.05^{+0.18}_{-0.20}$	3.3	$1.36^{+0.51}_{-0.47}$	1.3	$73.4^{+8.4}_{-8.3}$	$0.737^{+0.063}_{-0.085}$	0.07	1.4

Although the concordance between probes increases for this extended cosmology, and the best-fit χ^2_{eff} is marginally improved relative to ΛCDM (by $\Delta\chi^2_{\text{eff}} = -1.5$), the unrestricted JBD model is not found to be favored from the standpoint of model selection (given $\Delta\text{DIC} = 1.9$).

VII. RESULTS: DISTANCES AND GROWTH RATES IN COMBINED ANALYSES

A. All-Planck + All-BOSS + Pantheon

1. Constraining JBD gravity

We next turn to the combined analysis of the Planck 2018 CMB temperature, polarization, and lensing reconstruction (“All-Planck”), the BOSS BAO distances, AP parameters, and growth rates (“All-BOSS”), along with the Pantheon supernova distances. The combined analysis of these datasets allows for constraints on the coupling constant $\omega_{\text{BD}} > 1460$ (95% CL) in the restricted JBD model with massless neutrinos, and $\omega_{\text{BD}} > 970$ (95% CL) when including the sum of neutrino masses as an additional degree of freedom (see Table IV and Fig. 9).

These constraints can be contrasted with those found for the Planck CMB temperature and polarization alone (Sec. V), where $\omega_{\text{BD}} > 1150$ (95% CL) in the restricted JBD model and $\omega_{\text{BD}} > 1710$ (95% CL) when further allowing the sum of neutrino masses to vary in the analysis. In other words, as Planck (temperature and polarization) is combined with the lower redshift probes (BOSS, Pantheon, and Planck lensing reconstruction), the lower bound on the coupling constant increases in the massless neutrino scenario and decreases as the sum of neutrino masses is allowed to vary.

The lower bound on the coupling constant further sharpens as we consider an unrestricted JBD model. Here, $\omega_{\text{BD}} > 2040$ (95% CL) in a model with massless neutrinos, and $\omega_{\text{BD}} > 1420$ (95% CL) in a model where the sum of neutrino masses is further varied (which can be compared to the bound from the Planck temperature and polarization alone, where $\omega_{\text{BD}} > 1120$ at 95% CL). In the unrestricted JBD model with massless neutrinos, we constrain $G_{\text{matter}}/G = 0.989^{+0.030}_{-0.030}$ in concordance with the GR expectation to within 1σ . This constraint is robust to the corresponding setup where the sum of neutrino masses is varied, as $\Delta G_{\text{matter}}/G = +0.008$ with effectively the same uncertainty, and is driven by the Planck CMB temperature and polarization (as the uncertainty narrows by 6% with the inclusion of the additional datasets).

2. The sum of neutrino masses

The sum of neutrino masses is constrained to $\sum m_\nu < 0.11$ eV (95% CL) in ΛCDM , which remains robust as we consider a cosmology with JBD gravity (i.e. less than 0.01 eV degradation; both restricted and unrestricted models; up to factor of ~ 4 improvement compared to the Planck CMB temperature and polarization alone through the breaking of the geometric degeneracy). As seen in Fig. 9, there are only mild

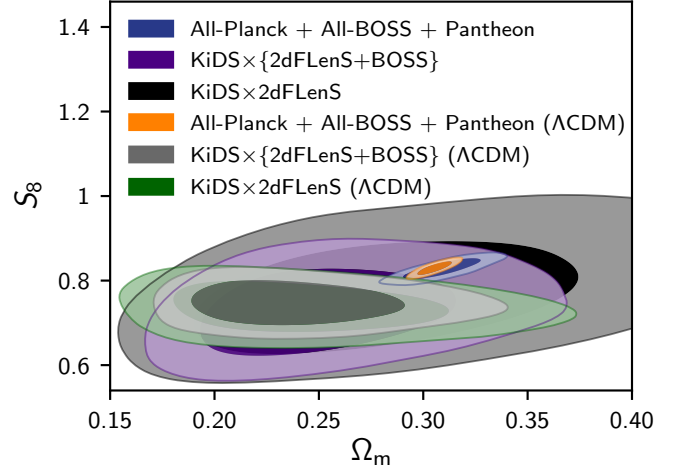


FIG. 11. Marginalized posterior distributions (inner 68% CL, outer 95% CL) in the S_8 – Ω_m plane for the dataset combinations All-Planck + All-BOSS + Pantheon, KiDS × {2dFLenS+BOSS}, and KiDS × 2dFLenS in the unrestricted JBD modified gravity model with massive neutrinos (JBD+ $G_{\text{matter}}+\sum m_\nu$) and in ΛCDM . Here, “All-Planck” refers to the Planck 2018 CMB temperature, polarization, and lensing reconstruction, and we simultaneously vary all standard cosmological and systematics parameters.

correlations between the extended cosmological parameters $\{\sum m_\nu, \omega_{\text{BD}}, G_{\text{matter}}\}$, which allows for largely decoupled constraints (with the exception of the ω_{BD} bound).

On closer inspection, as the strength of JBD gravity increases (i.e. as ω_{BD} decreases), there is a rise in the sum of neutrino masses, while G_{matter}/G appears marginally positively correlated with $\sum m_\nu$ and negatively correlated with $\ln \omega_{\text{BD}}^{-1}$, such that a stronger effective gravitational constant allows for larger neutrino masses and weaker coupling constant. However, as the data favors $G_{\text{matter}}/G \simeq 1$ (to within 1σ), these mild correlations are manifested in the posterior mean to lesser extent.

3. Impact on H_0 and S_8

The two derived parameters $H_0 = 68.15^{+0.42}_{-0.41}$ $\text{km s}^{-1}\text{Mpc}^{-1}$ and $S_8 = 0.830^{+0.010}_{-0.010}$ in ΛCDM degrade by 10% and mildly shift downwards (by 0.7σ in H_0 and 0.4σ in S_8) as we allow the sum of neutrino masses to vary (such that $H_0 = 67.86^{+0.51}_{-0.44}$ $\text{km s}^{-1}\text{Mpc}^{-1}$ and $S_8 = 0.826^{+0.011}_{-0.011}$). In the restricted JBD model, as in Sec. V A, the Hubble constant increases as the coupling constant decreases with the characteristic “hook-shape” upturn of the contour in the $\ln \omega_{\text{BD}}^{-1}$ – H_0 plane (which expectedly flattens towards the GR limit). However, the marginalized constraint on H_0 only changes mildly relative to that in ΛCDM (positive shift in the posterior mean 0.2σ and $\lesssim 10\%$ broadening of the uncertainty; negligible changes in the case of S_8), similar to that found for the Planck CMB temperature and polarization alone.

In the unrestricted JBD model, the contour in the plane of $\ln \omega_{\text{BD}}^{-1}$ and H_0 is substantially flattened (likewise for the contour in the ω_{BD} – S_8 plane), and the correlation between these

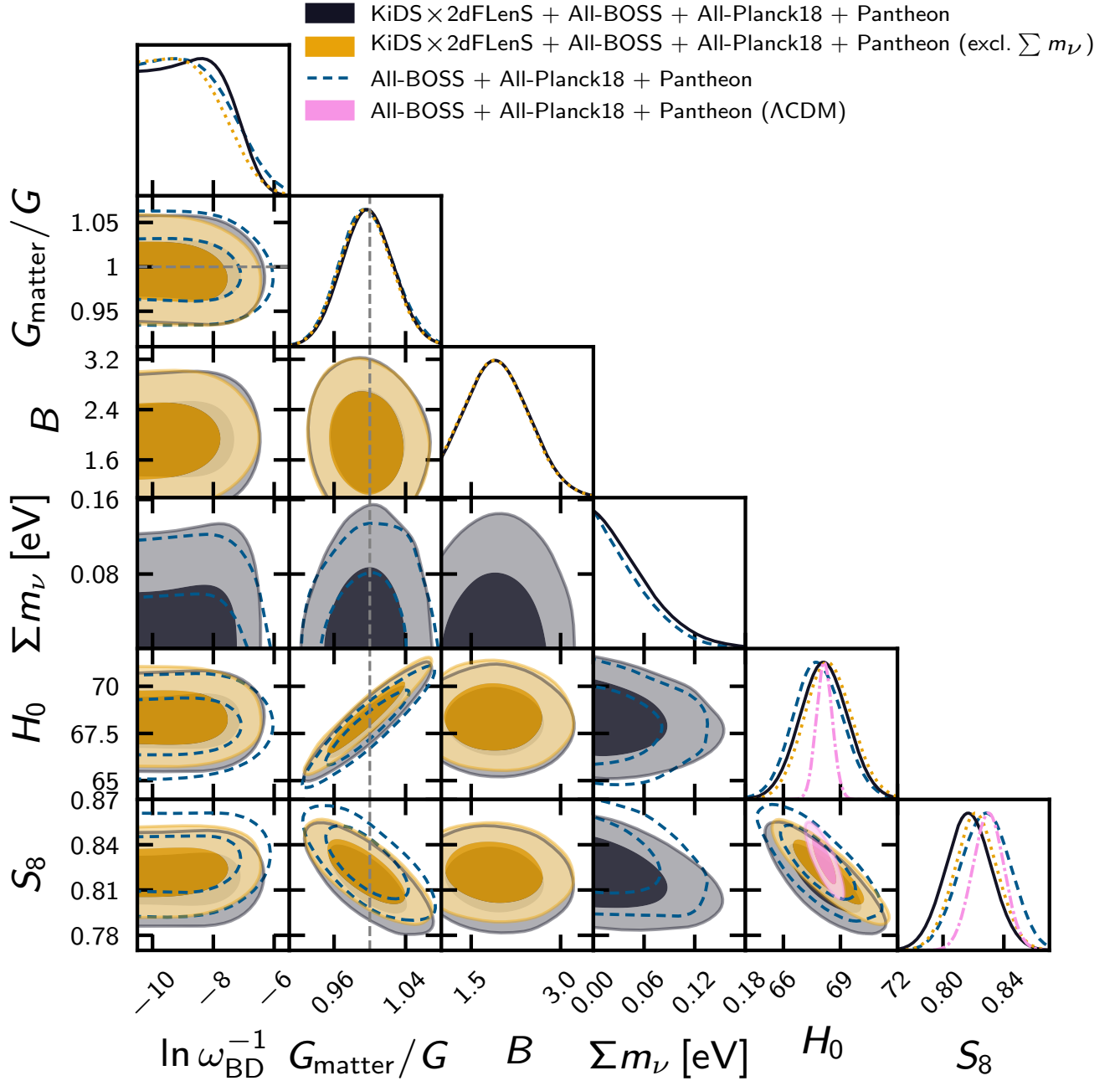


FIG. 12. Marginalized posterior distributions (inner 68% CL, outer 95% CL) of the JBD parameter, $\ln \omega_{\text{BD}}^{-1}$, the present effective gravitational constant, G_{matter}/G , the baryonic feedback amplitude, B , the sum of neutrino masses, Σm_ν , the Hubble constant, H_0 (in units of $\text{km s}^{-1} \text{Mpc}^{-1}$), and $S_8 = \sigma_8 \sqrt{\Omega_m}/0.3$ from different combinations of the KiDS, 2dFLenS, BOSS, Pantheon, and Planck datasets. All other standard cosmological and systematics parameters are simultaneously varied. For visual clarity, we have zoomed in on the $\ln \omega_{\text{BD}}^{-1}$ axis where the distributions flatten towards the GR limit at $-\infty$ (in practice towards the negative end of the prior range at $\ln \omega_{\text{BD}}^{-1} = -17$).

parameters becomes negligible. Instead, there is a strong correlation of H_0 and S_8 with the present effective gravitational constant (given its impact on the metric potentials along with the expansion and growth histories; see Figs. 1 and 2). Here, there is a factor of 3.1 and 1.5 increase in the uncertainties on H_0 and S_8 relative to ΛCDM , respectively, such that $H_0 = 67.80^{+1.28}_{-1.32} \text{ km s}^{-1} \text{Mpc}^{-1}$ and $S_8 = 0.835^{+0.015}_{-0.016}$. While the posterior means shift marginally relative to ΛCDM (by

$\Delta H_0 = -0.35 \text{ km s}^{-1} \text{Mpc}^{-1}$ and $\Delta S_8 = -0.005$), given the increase in the uncertainties, the concordances with the Riess et al. (2019) [77] and KiDS×2dFLenS datasets improve to 3.2σ (from 4.0σ in ΛCDM) and 0.7σ (from 2.3σ in ΛCDM), respectively. In the unrestricted JBD model with massive neutrinos, the additional degree of freedom in Σm_ν has only a marginal impact on H_0 and S_8 (the strongest impact is on S_8 which shifts downwards by 0.5σ compared to the unrestricted

TABLE VI. Marginalized posterior means and 68% confidence intervals for a subset of the cosmological parameters. For the JBD parameter, ω_{BD} , and the sum of neutrino masses, $\sum m_\nu$, we quote the 95% confidence lower and upper bounds, respectively. We also quote the 95% confidence upper bound for the baryonic feedback amplitude, B , and the tension, $T(H_0)$, with the Riess et al. (2019) [77] direct measurement of the Hubble constant. The sum of neutrino masses is in units of eV and the Hubble constant, H_0 , is in units of $\text{km s}^{-1} \text{Mpc}^{-1}$. See Table II for further details. There is a minor improvement in the H_0 (and A_{IA}) constraint when the sum of neutrino masses is varied in the Planck 2015 setup, as explained in Appendix D. For visual clarity, we do not show the constraints on $S_8 = \sigma_8 \sqrt{\Omega_m/0.3}$ in a separate column, but quote them here as $S_8 = [0.822^{+0.014}_{-0.014}, 0.817^{+0.015}_{-0.015}, 0.818^{+0.015}_{-0.015}, 0.809^{+0.016}_{-0.015}]$ from the first to the fourth row, respectively.

Probe setup	ω_{BD}	G_{matter}/G	B	A_{IA}	$\sum m_\nu$	H_0	$T(H_0)$
KiDS \times 2dFLenS + All-BOSS + All-Planck18 + Pantheon (JBD + G_{matter})	2230	$0.996^{+0.029}_{-0.029}$	2.8	$1.54^{+0.38}_{-0.39}$...	$68.37^{+1.24}_{-1.24}$	3.0
KiDS \times 2dFLenS + All-BOSS + All-Planck18 + Pantheon (JBD + G_{matter} + $\sum m_\nu$)	1540	$0.997^{+0.029}_{-0.029}$	2.8	$1.52^{+0.38}_{-0.38}$	0.12	$68.13^{+1.26}_{-1.25}$	3.1
KiDS \times 2dFLenS + All-BOSS + All-Planck15 + Pantheon (JBD + G_{matter})	2270	$1.010^{+0.030}_{-0.029}$	2.8	$1.49^{+0.38}_{-0.39}$...	$68.87^{+1.32}_{-1.32}$	2.7
KiDS \times 2dFLenS + All-BOSS + All-Planck15 + Pantheon (JBD + G_{matter} + $\sum m_\nu$)	1640	$1.017^{+0.029}_{-0.030}$	2.8	$1.52^{+0.36}_{-0.39}$	0.21	$68.71^{+1.27}_{-1.26}$	2.8

JBD model with fixed neutrino masses, such that the concordance with KiDS \times 2dFLenS improves to 0.6σ .

As compared to the corresponding constraints from the Planck CMB temperature and polarization alone (i.e. by adding BOSS, Pantheon, and Planck lensing), the constraints on H_0 and S_8 respectively strengthen by 30% and 40% in both ΛCDM and the restricted JBD model, which in the case of H_0 increases to a 60% improvement in ΛCDM and 50% improvement in the restricted JBD model when additionally including massive neutrinos (the improvement in S_8 remains at the 40% level in these cosmologies). In the unrestricted JBD model with massive neutrinos, there is a 35% improvement in the uncertainty on H_0 and 30% improvement in the uncertainty on S_8 . Across the different cosmologies, the posterior mean of H_0 “stabilizes” with the additional datasets, covering a range of $\Delta H_0 = 0.4 \text{ km s}^{-1} \text{Mpc}^{-1}$ in the “All-Planck18 + All-BOSS + Pantheon” setup, as compared to $\Delta H_0 = 1.6 \text{ km s}^{-1} \text{Mpc}^{-1}$ from the Planck CMB temperature and polarization alone, which reflects an increase in the agreement with the standard model (however, noting that the spread in $\Delta S_8 \lesssim 0.01$ is approximately the same between the two data setups).

4. Model selection

For an extended cosmological model to replace the standard model, we ideally require that it is able to simultaneously alleviate possible discordances between datasets, exhibit a statistically significant deviation (by $> 5\sigma$) in any extended parameters from the standard model expectation, and show a “decisive” improvement (e.g. according to Jeffreys’ scale [207]) in a model selection comparison with the standard model (employing statistical tools such as the deviance information criterion [190] or Bayesian evidence (e.g. [194])).

We have shown above that the first criterion is partly satisfied. However, in spite of the successes of the unrestricted JBD model in improving the concordance between datasets, we note that it is not favored in a model selection comparison with ΛCDM (given $\Delta\text{DIC} \gtrsim 0$). This also holds for all of the other extended cosmological models considered here (i.e. models involving restricted JBD and massive neutrinos). The extended cosmological parameters $\{\omega_{\text{BD}}, G_{\text{matter}}, \sum m_\nu\}$ moreover do not exhibit a statistically significant deviation

from the fiducial expectation, such that any increase in the concordance between datasets is driven by the increase in the parameter uncertainties rather than a change in the actual cosmology.

5. Comparing against the Planck 2015 dataset

In Fig. 9, we further compare the constraints from “All-Planck18 + All-BOSS + Pantheon” in the unrestricted JBD model with massive neutrinos to the corresponding constraints from “Planck15 + All-BOSS + Pantheon”, where only the baseline Planck 2015 CMB temperature and LFI low- ℓ polarization is considered instead of the full Planck 2018 dataset. Here, we find substantially weaker constraints on the subspace of parameters $\{\ln \omega_{\text{BD}}^{-1}, G_{\text{matter}}/G, \sum m_\nu, H_0, S_8\}$. In particular, the tension in H_0 with the measurement of Riess et al. (2019) [77] decreases by 1.0σ , down to 2.2σ . As seen in Sec. V, this is similar to the difference in the Hubble constant tension in the unrestricted JBD model when comparing the Planck 2018 temperature and polarization (where $T(H_0) \approx 3\sigma$) with the Planck 2015 temperature and LFI low- ℓ polarization (where $T(H_0) \lesssim 2\sigma$). In other words, it is predominantly the Planck 2018 polarization information that is driving the H_0 tension higher in this model.

We have also considered constraints on the restricted JBD models where the Planck 2018 and 2015 setups both include the respective high-multipole polarization and lensing measurements (i.e. comparing “All-Planck18 + All-BOSS + Pantheon” with “All-Planck15 + All-BOSS + Pantheon”). As shown in Appendix D (specifically Fig. 23, also see Table IX), we find no significant differences in the inferences in the subspace of $\{\ln \omega_{\text{BD}}^{-1}, \sum m_\nu, \tau, H_0, S_8\}$ aside from the constraint on $\sum m_\nu$, driven by the greater than factor-of-two improved 2018 constraint on the optical depth to reionization, τ (as $C_\ell \propto A_s e^{-2\tau}$, such that the constraint on the primordial scalar amplitude, A_s is comparably improved given the degeneracy with the optical depth [75]).

Combining All-BOSS and Pantheon with All-Planck15, we obtain the lower bound on $\omega_{\text{BD}} > 1050$ (95% CL) in a restricted JBD model with massless neutrinos, and $\omega_{\text{BD}} > 590$ (95% CL) in a restricted JBD model with massive neutrinos (which in both cases corresponds to a weakening of the bound

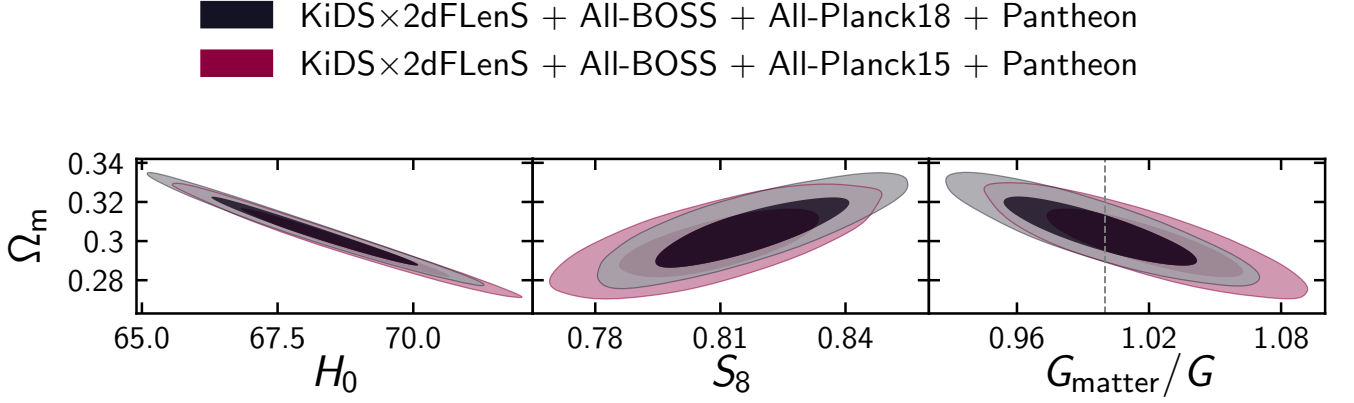


FIG. 13. Marginalized posterior distributions (inner 68% CL, outer 95% CL) of the matter density Ω_m against the present effective gravitational constant G_{matter}/G , Hubble constant H_0 (in units of $\text{km s}^{-1}\text{Mpc}^{-1}$), and $S_8 = \sigma_8 \sqrt{\Omega_m/0.3}$ from the KiDS, 2dFlenS, BOSS, Pantheon, and Planck datasets. We consider an unrestricted JBD cosmology with massive neutrinos (JBD+ G_{matter} + $\sum m_\nu$), where all standard cosmological and systematics parameters are simultaneously varied.

by $\Delta\omega_{\text{BD}} \approx -400$ as compared to the equivalent setup with Planck 2018). The sum of neutrino masses is constrained to $\sum m_\nu < 0.19$ eV (95% CL), which corresponds to a 70% weakening relative to the bound from the equivalent setup with Planck 2018.

Moreover, as shown in Appendix D (see Fig. 23 therein), the H_0 and S_8 constraints are marginally affected by the change between the Planck 2015 and 2018 datasets, and the respective tensions in these parameters with other datasets remain at a similar level ($< 0.1\sigma$ differences). For the restricted JBD model, we have also checked that we continue to find no meaningful model selection preference relative to ΛCDM for the Planck 2015 data combination (given $\Delta\text{DIC} \gtrsim 0$ for both neutrino setups).

B. KiDSx2dFlenS + All-BOSS + Pantheon

1. Impact of including Pantheon distances

In comparing the cosmological parameter constraints from KiDSx2dFlenS + All-BOSS + Pantheon with the earlier constraints from KiDSx2dFlenS + All-BOSS (Sec. VI B), we find that the addition of Pantheon supernova distance measurements has a marginal impact. In ΛCDM , we constrain $B > 3.1$ (95% CL), $A_{\text{IA}} = 1.13^{+0.53}_{-0.46}$, $H_0 = 70.8^{+6.0}_{-3.7} \text{ km s}^{-1}\text{Mpc}^{-1}$, and $S_8 = 0.746^{+0.028}_{-0.028}$. As compared to a setup that excludes the Pantheon dataset, this reflects a minor change in the upper bound of the baryonic feedback amplitude (by $\Delta B = -0.2$), along with marginal shifts in the posterior mean of the IA amplitude (by $\Delta A_{\text{IA}} = 0.01$, with sub-percent level change in the uncertainty), the Hubble constant (by $\Delta H_0 = 0.2 \text{ km s}^{-1}\text{Mpc}^{-1}$, with 5% decrease in the uncertainty), and S_8 (by 10^{-3} , with sub-percent level change in the uncertainty).

We find similarly small changes in these parameters for an extended cosmology that includes massive neutrinos and unrestricted JBD gravity. The extended cosmological parameters are constrained to $\sum m_\nu < 1.3$ eV (95% CL), $\omega_{\text{BD}} > 79$

(95% CL), and $G_{\text{matter}}/G = 1.05^{+0.18}_{-0.20}$, such that the lower and upper bounds differ by $\Delta\omega_{\text{BD}} = -4$ and $\Delta\sum m_\nu = -0.1$ eV, respectively, while the constraint on the effective gravitational constant agrees to within sub-percent level from that found when the Pantheon dataset is excluded.

2. Robustness in the cosmological constraints

In comparing the KiDSx2dFlenS + All-BOSS + Pantheon constraints in different JBD cosmologies with one another (restricted and unrestricted JBD cosmologies with and without neutrino mass), we find a robustness in the constraints to the extended cosmological degrees of freedom. In general, $\sum m_\nu \lesssim 1$ eV (95% CL), $\omega_{\text{BD}} \gtrsim 10^2$ (95% CL), and $G_{\text{matter}}/G \sim 1$ to within 68% CL where the uncertainty is at the $\Delta G_{\text{matter}}/G \approx 0.2$ level (the inequalities here respectively denote “less/greater than approximately”).

These constraints are substantially weaker than those found for All-Planck18 + All-BOSS + Pantheon (Sec. VII A), such that the respective bounds on ω_{BD} and $\sum m_\nu$ are approximately an order of magnitude weaker and the constraint on G_{matter} is a factor of six weaker. The weak correlations between the modified gravity parameters and the sum of neutrino masses (along with weak lensing systematics such as baryonic feedback) are shown in Fig. 10, and are consistent with the comparably weak correlations found for KiDSx{2dFlenS+BOSS} and KiDSx2dFlenS + All-BOSS (Secs. VI A and VI B).

3. H_0 and S_8 constraints

Turning to the constraints on the derived H_0 and S_8 parameters, correlations with G_{matter}/G continue to give rise to both a shift in the posterior mean and increase in the uncertainty. Concretely, for the unrestricted JBD model, $H_0 = 74.7^{+8.5}_{-9.3} \text{ km s}^{-1}\text{Mpc}^{-1}$ (while for the restricted JBD model, where G_{matter}/G is fixed to unity, $H_0 = 71.3^{+5.9}_{-4.0} \text{ km s}^{-1}\text{Mpc}^{-1}$).

In comparison with Λ CDM, these constraints correspond to a positive shift in the posterior mean by $\Delta H_0 = 0.5 \text{ km s}^{-1} \text{ Mpc}^{-1}$ (with percent-level increase in the uncertainty) when allowing ω_{BD} to vary (i.e. for the restricted JBD model), and an additional increase in the posterior mean by $\Delta H_0 = 3.4 \text{ km s}^{-1} \text{ Mpc}^{-1}$ (with an 80% increase in the uncertainty) when further allowing G_{matter}/G to vary (i.e. for the unrestricted JBD model).

For the S_8 parameter, the constraints are effectively at the sub-percent level between the restricted JBD model and Λ CDM, while $S_8 = 0.719^{+0.062}_{-0.085}$ in the unrestricted JBD model which corresponds to a decrease in the posterior mean by $\Delta S_8 = 0.027$ and a factor of 2.6 increase in the uncertainty (similar to that found when the Pantheon dataset is excluded from the analysis in Sec. VIB). While the increased uncertainty on S_8 is robust to varying $\sum m_\nu$, we note that allowing for this additional degree of freedom gives rise to an increase in the posterior mean by $\Delta S_8 = 0.018$ (such that $S_8 = 0.737^{+0.063}_{-0.085}$ in an unrestricted JBD model with massive neutrinos; similar to that found for KiDS \times {2dFLenS+BOSS}). As in the case of H_0 , this impact of the sum of neutrino masses on the S_8 posterior mean decreases as we fix G_{matter}/G to unity in the restricted JBD and Λ CDM models (shown in Table V).

4. H_0 and S_8 tensions

Given the increase in the S_8 uncertainty in the unrestricted JBD model, the concordance with the Planck CMB increases, such that the respective S_8 constraints differ by 1.5σ as compared to 2.8σ in both Λ CDM and the restricted JBD model (1.4σ and 2.5σ , respectively, as the sum of neutrino masses is further varied). In Λ CDM, the posterior mean of S_8 differs from that obtained by All-Planck18 + All-BOSS + Pantheon by $\Delta S_8 = 0.084$. This difference in S_8 is maximal for an unrestricted JBD model with fixed neutrino masses, where $\Delta S_8 = 0.116$. However, given the increase in the uncertainty on S_8 (as noted, by a factor of 2.6 for KiDS \times 2dFLenS + All-BOSS + Pantheon and a factor of 1.5 for All-Planck18 + All-BOSS + Pantheon, both relative to Λ CDM), this increase in ΔS_8 indeed corresponds to a decrease in the statistical significance of the tension between the datasets, as illustrated in Fig. 17.

While the constraint on the Hubble constant is consistent to within 68% CL with both the direct measurement from Riess et al. (2019) [77] and that inferred by the Planck CMB, we note that the posterior mean is generally in greater agreement with the direct measurement (both in Λ CDM and the extended cosmologies). In other words, the Hubble constant constraint from KiDS \times 2dFLenS + All-BOSS + Pantheon favors a $\Delta H_0 = 2.6 \text{ km s}^{-1} \text{ Mpc}^{-1}$ larger value as compared to All-Planck18 + All-BOSS + Pantheon in Λ CDM, and this difference increases to as much as $\Delta H_0 = 6.9 \text{ km s}^{-1} \text{ Mpc}^{-1}$ in an unrestricted JBD model with fixed neutrino masses (albeit with larger uncertainty). We show this difference in the H_0 constraints between KiDS \times 2dFLenS + All-BOSS + Pantheon and All-Planck18 + All-BOSS + Pantheon in Fig. 17.

5. Model selection

As shown in Appendix C (specifically Table VII), despite a decrease in the tension between datasets, we find no model selection preference for the extended cosmological models relative to Λ CDM (given $\Delta\text{DIC} \gtrsim 0$).

VIII. RESULTS: FULLY COMBINED DATA ANALYSIS OF THE JBD MODEL

We now proceed to constraining the JBD model with the full combination of datasets. This includes the cosmic shear, galaxy-galaxy lensing, and overlapping redshift-space galaxy clustering (KiDS \times 2dFLenS), BAO distances, AP distortions, and growth rates (All-BOSS), supernova distances (Pantheon), and the cosmic microwave background temperature, polarization, and lensing reconstruction (All-Planck).¹⁶ The KiDS, 2dFLenS, and BOSS datasets are combined as in Sec. VIB, where we avoid double-counting information by restricting the $3 \times 2\text{pt}$ dataset to KiDS \times 2dFLenS instead of KiDS \times {2dFLenS+BOSS}, in order to separately utilize the full BOSS dataset (i.e. All-BOSS).

1. Assessing concordance as a requirement for combining datasets

We have further taken care to only perform a combined analysis of concordant datasets. As shown in Fig. 11, the tension between KiDS \times {2dFLenS+BOSS} and All-Planck + All-BOSS + Pantheon in the $S_8 - \Omega_m$ plane diminishes as we transition from Λ CDM to the unrestricted JBD cosmology. This holds to even greater extent as we consider the concordance between KiDS \times 2dFLenS and All-Planck + All-BOSS + Pantheon (such that the 95% confidence level contours fully overlap and there is agreement in S_8 to within 1σ in the unrestricted JBD model). As observed in Fig. 10, in the unrestricted JBD model, Planck is also concordant in e.g. the $S_8 - H_0$ plane with KiDS \times 2dFLenS + All-BOSS + Pantheon.

In assessing the concordance between KiDS \times 2dFLenS + All-BOSS + Pantheon and All-Planck over the full parameter space, we find $\log \mathcal{I} = 0.93$ in the unrestricted JBD model with massless neutrinos and $\log \mathcal{I} = 0.37$ in the unrestricted JBD model where the sum of neutrino masses is varied, corresponding to substantial and weak concordance between the datasets, respectively. This concordance decreases by $\Delta \log \mathcal{I} \approx -1$ when instead assessing the concordance between All-Planck + All-BOSS + Pantheon and KiDS \times 2dFLenS. In other words, the “order” in which datasets are combined has an impact on the assessment of whether a fully combined analysis of the datasets is warranted. In our case, we take not only the concordance in the combination of All-Planck with the other

¹⁶ We do not include ACT DR4 in this final setup as its covariance with Planck is neglected in favor of further scale cuts, which has been validated to 5% precision for certain single-parameter extensions in addition to Λ CDM [97].

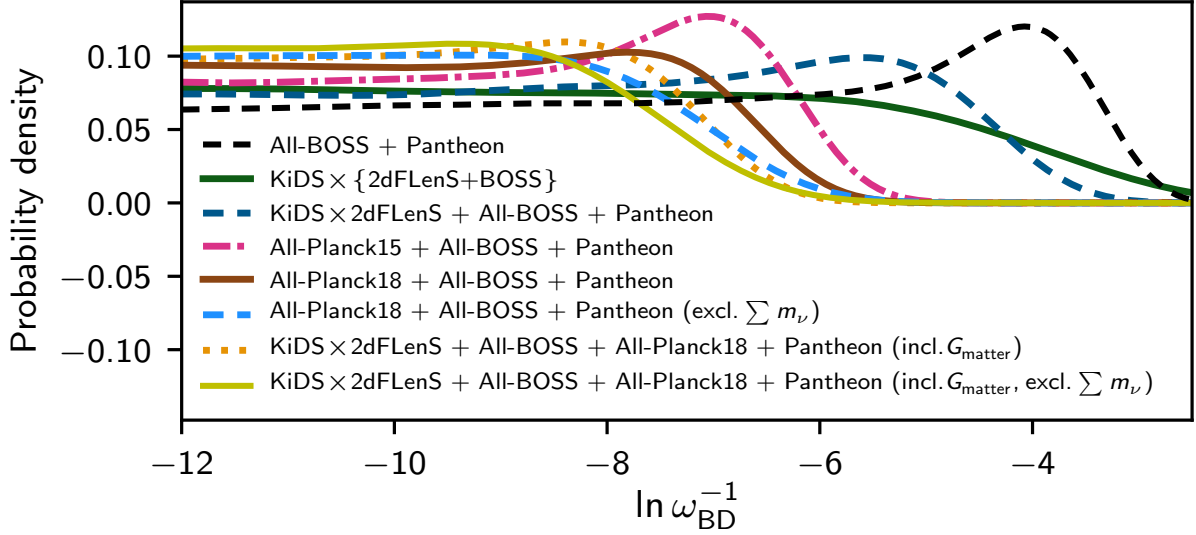


FIG. 14. Marginalized posterior distributions for the JBD parameter $\ln \omega_{\text{BD}}^{-1}$. We simultaneously vary all standard cosmological and systematics parameters, along with the sum of neutrino masses $\sum m_\nu$. We keep G_{matter}/G fixed unless indicated otherwise. In the MCMC analysis, $\ln \omega_{\text{BD}}^{-1}$ is allowed to vary down to -17 , zoomed in here for visual clarity (noting that the posteriors continue to stay flat below $\ln \omega_{\text{BD}}^{-1} = -12$).

datasets, but also the agreement in the parameters that lensing constrains most powerfully as motivation for performing a fully combined analysis of the datasets in the unrestricted JBD model. However, we do not quote constraints using the full combination of datasets in Λ CDM and the restricted JBD model where the datasets are evidently discordant.

A. KiDS×2dFLenS + All-BOSS + All-Planck + Pantheon

1. JBD gravity and massive neutrinos

We now consider “KiDS×2dFLenS + All-BOSS + All-Planck18 + Pantheon” in the unrestricted JBD model (see Fig. 12 and Table VI). We obtain our strongest bounds on $\omega_{\text{BD}} > 2230$ (95% CL) and $G_{\text{matter}}/G = 0.996^{+0.029}_{-0.029}$ as the sum of neutrino masses is fixed, and $\omega_{\text{BD}} > 1540$ (95% CL) and $G_{\text{matter}}/G = 0.997^{+0.029}_{-0.029}$ in the unrestricted JBD model as the sum of neutrino masses is varied (where $\sum m_\nu < 0.12$ eV at 95% CL). In both neutrino setups, the constraints are in agreement with the GR expectation. As compared to “All-Planck18 + All-BOSS + Pantheon”, where KiDS×2dFLenS is excluded, the ω_{BD} bounds are strengthened by $\Delta\omega_{\text{BD}} = \{190, 120\}$ in the {massless, massive} neutrino scenarios, respectively, while the uncertainties on G_{matter}/G are marginally narrowed (by 0.01 in both neutrino scenarios). Meanwhile, the bound on the sum of neutrino masses is robust (at the 0.01 eV level), as it is driven by the combination of Planck and BOSS.

2. Baryonic feedback and intrinsic alignments

In accordance with earlier results using subsets of the data, there are weak correlations between $\{\omega_{\text{BD}}, G_{\text{matter}}, \sum m_\nu\}$ in

this unrestricted JBD model. The parameters are also weakly correlated with the baryonic feedback amplitude, where $B < 2.8$ (95% CL) in both neutrino setups. This upper bound on the feedback amplitude is in agreement with the bounds from subsets of the data involving KiDS (Secs. VIA, VIB, VIB) and differs from the “no feedback” (or “dark matter only”) value of $B = 3.13$ at greater than 98% CL.

The constraints on the IA amplitude are improved by more than 20% relative to the equivalent data setup without Planck (i.e. as compared to KiDS×2dFLenS + All-BOSS + Pantheon). Concretely, we constrain $A_{\text{IA}} = 1.52^{+0.038}_{-0.038}$ in the unrestricted JBD model with massive neutrinos, which remains practically identical as we fix the sum of neutrino masses. The constraints are mildly shifted toward larger values (by $\Delta A_{\text{IA}} \sim 0.2\text{--}0.4$) with the addition of Planck, and are both positive at 4.0σ . However, we note that the large posterior mean favored here is likely driven (at least partly) by the uncertainties in the photometric redshift distributions (see e.g. Refs. [211–213]).

3. H_0 and S_8

In addition to the primary parameters, we constrain $H_0 = 68.37^{+1.24}_{-1.24}$ km s^{−1} Mpc^{−1} and $S_8 = 0.822^{+0.014}_{-0.014}$ in the unrestricted JBD model with fixed neutrino masses, which are modified to $H_0 = 68.13^{+1.26}_{-1.25}$ km s^{−1} Mpc^{−1} and $S_8 = 0.817^{+0.015}_{-0.015}$ in the unrestricted JBD model where the sum of neutrino masses is additionally varied. The H_0 constraints are consistent at the 0.2σ level and are marginally stronger (by $\sim 5\%$) than the respective constraints from All-Planck18 + All-BOSS + Pantheon. Given the positive shifts in the posterior mean as compared to All-Planck18 + All-BOSS + Pantheon, by $\Delta H_0 = \{0.57, 0.30\}$ km s^{−1} Mpc^{−1} in the {fixed, varying} neutrino mass scenarios, the discordance with the Riess et al. (2019) [77] measurement of the Hubble constant decreases

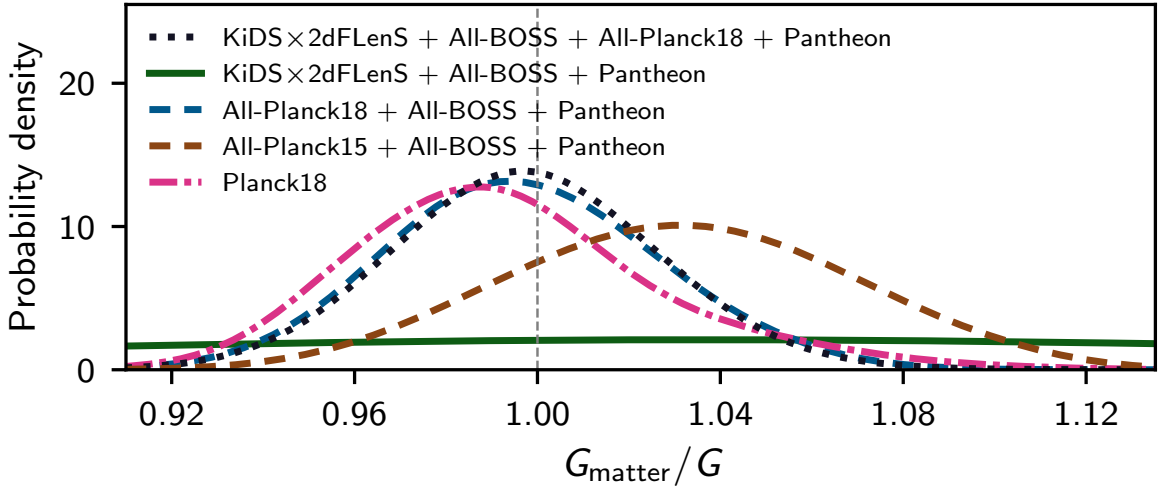


FIG. 15. Marginalized posterior distributions for the present effective gravitational constant (G_{matter}/G). We simultaneously vary all standard cosmological and systematics parameters, along with the JBD parameter $\ln \omega_{\text{BD}}^{-1}$ and the sum of neutrino masses $\sum m_\nu$. In the MCMC analysis, G_{matter}/G is allowed to vary between $-1/2$ to 2 (zoomed in here for visual clarity). The dashed grey vertical line indicates the GR expectation.

marginally to $T(H_0) = \{3.0\sigma, 3.1\sigma\}$, respectively (i.e. despite the narrower uncertainty).

By the inclusion of KiDSx2dFLenS, the S_8 constraints from the full combination of datasets are shifted by $\Delta S_8 = \{-0.8\sigma, -0.7\sigma\}$ as compared to All-Planck18 + All-BOSS + Pantheon alone, and are consistent at the 0.3σ level between the two neutrino mass setups. However, the constraints are closer to the posterior mean favored by Planck, rather than KiDSx2dFLenS, given its comparably higher constraining power.

4. Correlations with the matter density

In Fig. 13, given the full combination of datasets for both Planck 2018 and Planck 2015 (i.e. “KiDSx2dFLenS + All-BOSS + All-Planck18 + Pantheon” and “KiDSx2dFLenS + All-BOSS + All-Planck15 + Pantheon”), we show a subset of the correlations with the matter density (Ω_m). As expected, the matter density is negatively correlated with $\{H_0, G_{\text{matter}}\}$ and positively correlated with S_8 . Here, the correlation for the novel pair $\{\Omega_m, G_{\text{matter}}\}$ is negative as the parameters are to first order multiplicative in the Poisson equation, such that a positive shift in one parameter is counteracted by an equally negative shift in the other parameter to obtain the same fit to the data; a qualitatively similar relation holds for these two parameters in the Friedmann equation, where $H^2 \propto G_{\text{matter}}\rho$ (as shown in Sec. II).

We constrain $\Omega_m = 0.305^{+0.011}_{-0.012}$ in the unrestricted JBD model with massive neutrinos from the full combination of datasets, which is robust between the two Planck datasets (to within 0.5σ , as $\Omega_m = 0.298^{+0.011}_{-0.012}$ when Planck 2018 is replaced with Planck 2015), and is also robust to the exclusion of KiDSx2dFLenS (to within 0.3σ , as $\Omega_m = 0.309^{+0.012}_{-0.012}$ for All-Planck18 + All-BOSS + Pantheon).

5. Model selection

Although the unrestricted JBD model is able to alleviate dataset discordances, we find no model selection preference for this model, as $\Delta\text{DIC} = 2.0$ in our setup with fixed neutrino masses and $\Delta\text{DIC} = 4.6$ when allowing the sum of neutrino masses to vary.

6. Comparing against the Planck 2015 dataset

We can further compare the differences in the parameter constraints from KiDSx2dFLenS + All-BOSS + All-Planck + Pantheon between the 2018 and 2015 datasets of Planck. As shown in Appendix D (specifically Fig. 24), and similar to that found in the restricted JBD model (see Fig. 23), there is strong consistency in the parameter constraints between the two setups. The sum of neutrino masses constitutes the main exception (along with the primordial scalar amplitude) due to its strong correlation with the optical depth, τ , which is improved by 65% in the data combination with All-Planck18 (as compared to the data combination with All-Planck15).¹⁷ As a result, $\sum m_\nu < 0.12$ eV (95% CL) which reflects a 40% improvement in the upper bound (relative to the bound from the data combination with All-Planck15).

In combining KiDSx2dFLenS, All-BOSS, Pantheon, and All-Planck15, we constrain $\omega_{\text{BD}} > \{2270, 1640\}$ (95% CL) in the unrestricted JBD model with $\{\text{fixed, varying}\}$ sum of neutrino masses, respectively (corresponding to differences of $|\Delta\omega_{\text{BD}}| \lesssim 100$ with the equivalent bounds from the data combination with All-Planck18). The effective gravitational constant

¹⁷ We note that for the data combination with All-Planck18, the τ constraint is effectively unchanged between the restricted and unrestricted JBD models, while it is degraded by 30% for the data combination with All-Planck15 as we transition from the restricted to the unrestricted JBD model.

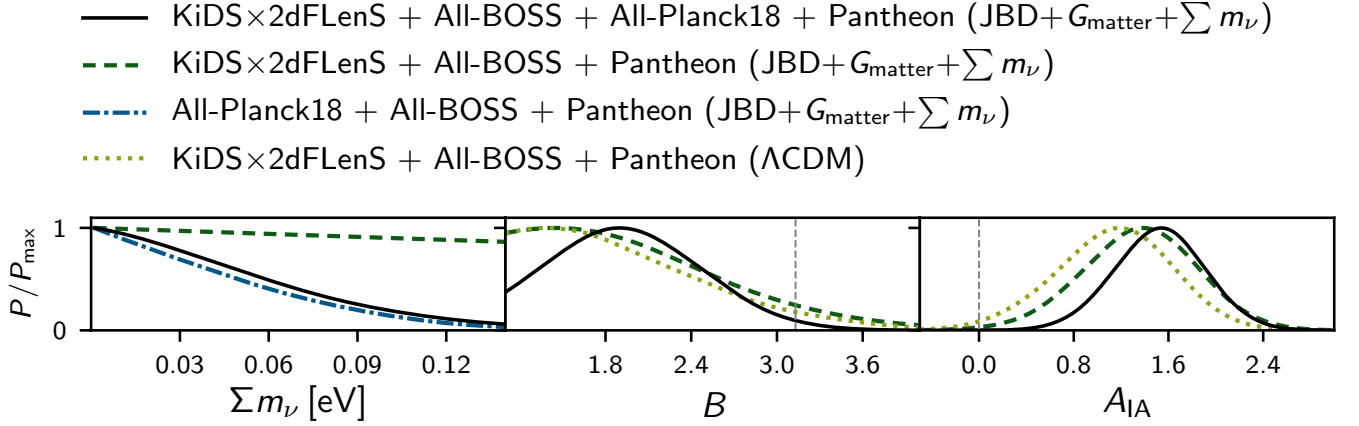


FIG. 16. Marginalized posterior distributions for the sum of neutrino masses, Σm_ν , the baryonic feedback amplitude, B , and the intrinsic alignment amplitude, A_{IA} . We simultaneously vary all standard cosmological and systematics parameters in an unrestricted JBD model with massive neutrinos (along with Λ CDM for comparison). The grey vertical line at $B = 3.13$ corresponds to the “no feedback” scenario.

remains in agreement with the GR expectation, as $G_{\text{matter}}/G = 1.017^{+0.029}_{-0.030}$, which corresponds to percent-level degradation in the uncertainty and shift of $|\Delta G_{\text{matter}}/G| = 0.021$ in the posterior mean relative to that from the data combination with All-Planck18.

Meanwhile, the constraint on the Hubble constant is positively shifted by 0.5σ (with effectively no change in the uncertainty), such that $H_0 = 68.71^{+1.27}_{-1.26} \text{ km s}^{-1} \text{ Mpc}^{-1}$ and $T(H_0) = 2.8$ (a decrease in the tension with Riess et al. 2019 by 0.3σ). As expected, the baryonic feedback and IA amplitude constraints are effectively unchanged (as these are driven by KiDS×2dFLenS); however, given the weaker neutrino mass bounds in the data combination with All-Planck15 (relative to All-Planck18), the cosmological parameter constraints are generally less robust, in an absolute sense, to allowing Σm_ν vary in the analysis (as shown in Table IX).

B. Take-away of JBD constraints, parameter degeneracies, model selection, and dataset concordances

1. JBD coupling constant and the effective gravitational constant

We summarize the constraints on the JBD coupling constant in Fig. 14, considering different combinations of datasets (consisting of KiDS, 2dFLenS, BOSS, Planck, and Pantheon) and different cosmological models (with a focus on the possible inclusion of Σm_ν and G_{matter}). As shown in this figure (and discussed in Secs. V–VIII A), the strongest bounds on ω_{BD} are from the Planck CMB, approximately an order of magnitude stronger than the bounds from KiDS, 2dFLenS, BOSS, and Pantheon (even when combined). The ω_{BD} bound favors the modified gravity solution more strongly as massive neutrinos are simultaneously considered, while the transition from a restricted to unrestricted JBD model (i.e. allowing for G_{matter} to vary) results in an ω_{BD} bound that is in greater agreement with the GR expectation.

We obtain the strongest bound on the JBD coupling constant in the unrestricted JBD model with fixed neutrino masses,

where $\omega_{\text{BD}} > 2230$ (95% CL) from the combination of all datasets. As described in Sec. VIII A, this bound weakens by approximately $\Delta\omega_{\text{BD}} \simeq -700$ as we allow for the sum of neutrino masses to vary, and by an additional $\Delta\omega_{\text{BD}} \simeq -600$ when we transition to a restricted JBD model (i.e. fix $G_{\text{matter}}/G = 1$; noting that we remove KiDS×2dFLenS to maintain dataset concordance in the restricted JBD model).

For the unrestricted JBD model, we summarize the constraints on the effective gravitational constant in Fig. 15, where $G_{\text{matter}}/G = \{0.996^{+0.029}_{-0.029}, 0.997^{+0.029}_{-0.029}\}$ as the sum of neutrino masses is {fixed, varying}, and which remains robust as we exclude any one of the datasets. These constraints on the JBD coupling constant and effective gravitational constant are also largely robust to whether the 2018 or 2015 datasets of Planck is considered (given the same observables). However, we note that the agreement with the GR expectation improves by 0.5σ with the 2018 dataset.

2. Comparison of JBD constraints to earlier work

We can compare our bounds on ω_{BD} to those obtained in earlier work. As discussed in the forthcoming section (Sec. VIII C), this is not straightforward given the different modeling choices. The most relevant comparison is to Avilez & Skordis (2014) [55] given the similar JBD modeling, where $\omega_{\text{BD}} > \{1901, 2441\}$ at 95% CL in the {restricted, unrestricted} JBD model with Planck 2013 (temperature and lensing), respectively. In addition to the comparable bounds on ω_{BD} to our analysis, these authors find a qualitatively similar difference in the ω_{BD} bounds between the restricted and unrestricted JBD models.

However, while the ω_{BD} bounds are comparable between the analyses, we note that these are one-sided parameter bounds and therefore not a reflection of the overall constraining power of the datasets considered. This can be seen by comparing the constraints on the effective gravitational constant in the unrestricted JBD model, where Avilez & Skordis (2014) [55] constrain this parameter to be in agreement with GR at the

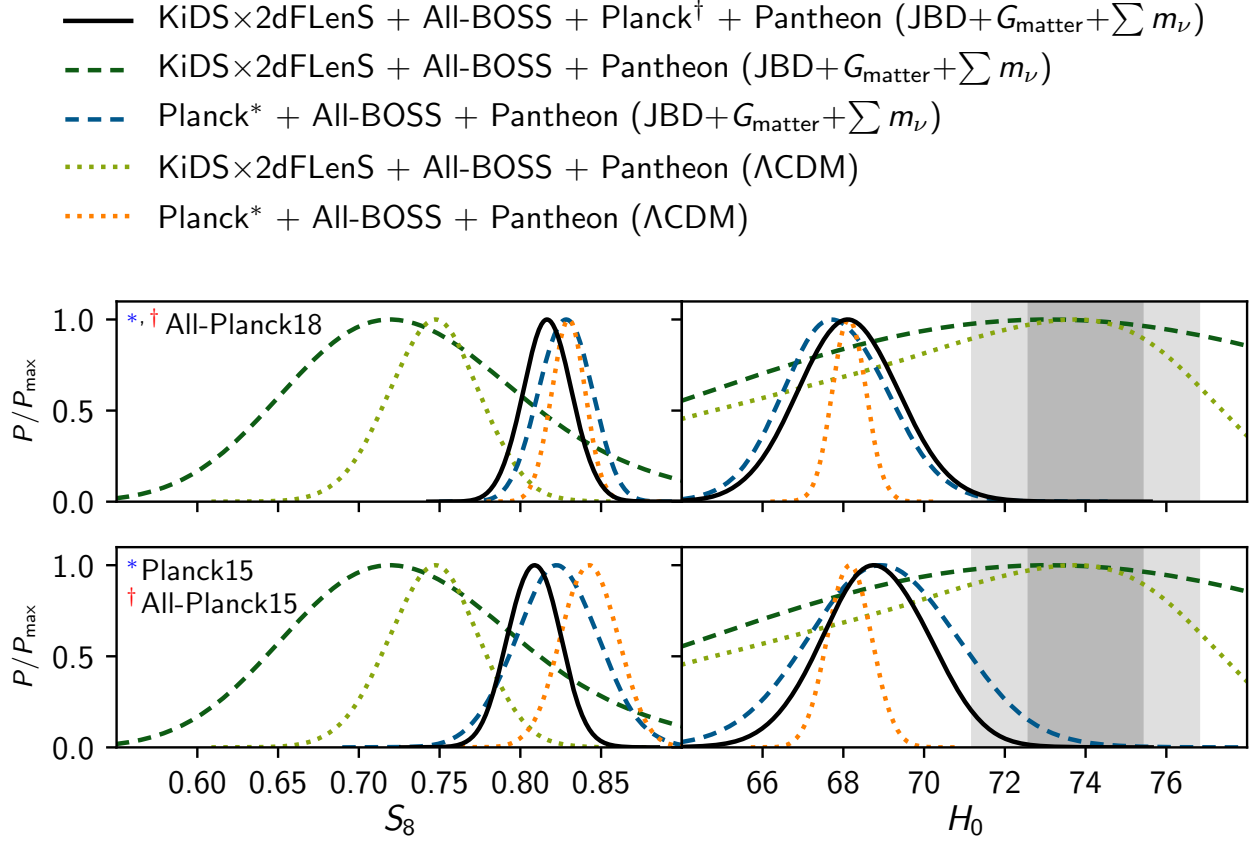


FIG. 17. Marginalized posterior distributions for $S_8 = \sigma_8 \sqrt{\Omega_m/0.3}$ (left) and the Hubble constant, H_0 (right), given in units of $\text{km s}^{-1} \text{Mpc}^{-1}$. We simultaneously vary all standard cosmological and systematics parameters in an unrestricted JBD model with massive neutrinos (along with ΛCDM for comparison). The grey vertical bars show the 68% CL (inner) and 95% CL (outer) constraints on H_0 from Riess et al. (2019) [77].

$\sigma(G_{\text{matter}}/G) \simeq 0.053$ level from Planck 2013 (temperature and lensing), ACT, and SPT, which we improve on by nearly a factor of two in our full analysis.

3. Consistency with Big Bang Nucleosynthesis

As we constrain the coupling constant, ω_{BD} , to be larger than $\sim 1 \times 10^3$ from the Planck CMB temperature and polarization alone and $\sim 2 \times 10^3$ when Planck is combined with other probes, the scalar field and thereby the effective gravitational constant, G_{matter}/G , is approximately constant with time, to within 0.5–1% from the present to the BBN epoch. As our G_{matter}/G constraint is effectively centered at unity (see Sec. VIII B 1), this implies that we approximately constrain the gravitational constant during BBN to $G_{\text{BBN}}/G = 0.99 \pm 0.03$.

This mild evolution of the gravitational constant and consistency with the standard model expectation is in agreement with the nucleosynthesis inference in Ref. [83], where the primordial helium and deuterium bounds are used to constrain $G_{\text{BBN}}/G = 0.98 \pm 0.03$ (i.e. similar precision, and evolution of the gravitational constant by 0.02 to reach the standard model expectation at present). Put differently, this implies that our JBD constraints respect the primordial abundances of light elements.

4. Neutrino mass, baryonic feedback, and intrinsic alignments

As summarized in Fig. 16, our strongest bound on the sum of neutrino masses is $\sum m_\nu < 0.11 \text{ eV}$ (95% CL) from Planck, BOSS, and Pantheon, which is not particularly affected by the assumptions of the JBD modeling or by the inclusion of the KiDSx2dFlenS dataset (at the 0.01 eV level). The baryon feedback amplitude is most strongly bounded in the unrestricted JBD model where all datasets are considered, such that $B < 2.8$ at 95% CL (as compared to the “no-feedback” scenario of $B = 3.13$). This bound is only weakly sensitive to the cosmological model and specific datasets considered in addition to KiDS (such that it weakens by at most $\Delta B \simeq 0.6$ as we consider an exclusion of Planck and fixed neutrino masses).

In Fig. 16, we also show that the IA amplitude is marginally larger in the JBD model relative to ΛCDM (by $\Delta A_{\text{IA}} \approx 0.2$) and we improve the constraint on the amplitude by more than 20% as Planck is considered alongside KiDS in the unrestricted JBD model. However, we emphasize that the large amplitude (positive by up to 4σ) might be partly explained by the systematic uncertainties in the photometric redshift distributions (as noted in Sec. VIII A).

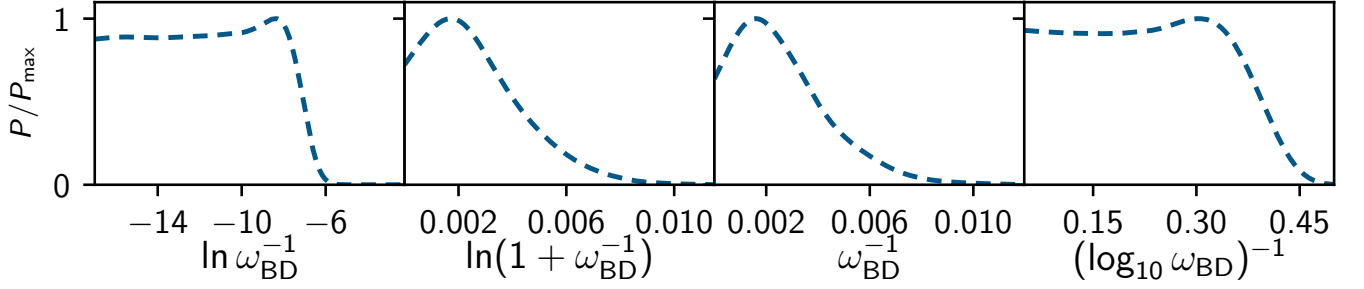


FIG. 18. Marginalized posterior distributions for the JBD coupling constant from the full combination of datasets (KiDS \times 2dFLenS + All-BOSS + All-Planck18 + Pantheon) considering four distinct parameterizations: $\ln \omega_{\text{BD}}^{-1}$, $\ln(1 + \omega_{\text{BD}}^{-1})$, ω_{BD}^{-1} , and $(\log_{10} \omega_{\text{BD}})^{-1}$. These are the effective primary parameters varied in the respective MCMC analysis (along with the other cosmological and systematics parameters).

5. H_0 and S_8

In Fig. 17, we illustrate the $\{H_0, S_8\}$ discordances (for S_8 between the CMB and weak lensing, and H_0 between the CMB and the direct measurement of Riess et al. 2019 [77]). The BOSS and Pantheon datasets can be combined with either KiDS or Planck, such that the S_8 tension between KiDS and Planck becomes more significant.

We show that the H_0 and S_8 tensions are ameliorated by the widening of the posteriors as we consider an unrestricted JBD model (i.e. a decrease in the H_0 tension down to approximately 3σ , and in the S_8 tension to below 1σ). We also show how the constraints improve in a combined analysis of all datasets in this extended model (which again increases the H_0 tension), and we contrast the results between the 2018 and 2015 datasets of Planck (notably finding that the H_0 tension decreases down to 2σ given the baseline Planck 2015 dataset which excludes the high-multipole polarization in particular). The fact that the H_0 and S_8 posteriors do not significantly shift, but are rather broadened, is further reflected in the agreement of ω_{BD} and G_{matter}/G with the respective GR expectations.

6. Ω_m versus Ω_m^* : impact on assessing the S_8 tension

In assessing the S_8 tension, we have used Ω_m for each dataset in the computation of the respective S_8 estimates, while in Sec. II (specifically Eq. 7) we showed that $\Omega_m^* = \Omega_m/\phi$ is the density for which the sum of all densities add to unity. As a result, there is a freedom in whether we evaluate the S_8 tensions using the respective Ω_m or Ω_m^* , which will increasingly differ as ω_{BD} decreases and G_{matter}/G increasingly deviates from unity.

As our constraints on the coupling constant are generally greater than 10^2 (for which the difference in the matter density is at the percent level; noting that $\Omega_m > \Omega_m^*$ as ω_{BD} decreases), the dominant cause of the difference in Ω_m and Ω_m^* is due to the effective gravitational constant where the difference scales linearly (i.e. $\Omega_m^* \propto G_{\text{matter}}/G$). The linear scaling of the density with the effective gravitational constant implies that $S_8^* \propto \sqrt{G_{\text{matter}}/G}$. In assessing the tension between KiDS and Planck, let us therefore consider a specific exam-

ple. In Table V, we find that G_{matter}/G is centered at 1.104 for KiDS \times 2dFLenS + All-BOSS + Pantheon (while $\omega_{\text{BD}} \gg 1$), which implies that the S_8 tension of 1.5σ is lowered by $\gtrsim 0.3\sigma$, such that the S_8^* tension is 1.2σ . However, as the constraints on JBD gravity tighten towards agreement with GR, as in the case of the fully combined datasets, where generally $\omega_{\text{BD}} > 10^3$ and $|\Delta G_{\text{matter}}/G| < 10^{-2}$, the difference between S_8 and S_8^* becomes negligible.

7. Model selection when including Riess et al. (2019)

Turning back to the Hubble constant, to assess whether the H_0 constraint from Planck (and data combinations with Planck) is more concordant with the direct measurement of Riess et al. (2019) [77] in an extended cosmological model, we have avoided a data analysis that includes both the Planck and Riess et al. (2019) measurements (i.e. our H_0 constraints have consistently excluded any “external” measurement from Riess et al. 2019). In this setup (which excludes Riess et al. 2019), both the restricted and unrestricted JBD models are at most weakly favored from a model selection standpoint relative to Λ CDM (see Table VII in Appendix C).

However, in assessing the model selection preference of the unrestricted JBD model, which does exhibit a smaller tension between Planck and Riess et al. (2019) [77], we also consider MCMC inferences that include the Riess et al. (2019) measurement. For a combined analysis of the 2018 dataset of Planck CMB temperature and polarization (i.e. excluding lensing reconstruction) and Riess et al. (2019), $\Delta\chi_{\text{eff}}^2 = -4.0$ and $\Delta\text{DIC} = -4.8$, reflecting weak-to-moderate preference in favor of the extended model relative to Λ CDM.

In a combined analysis of all datasets (KiDS \times 2dFLenS + All-BOSS + All-Planck + Pantheon, where Planck now further includes the 2018 lensing reconstruction) with Riess et al. (2019), $\Delta\chi_{\text{eff}}^2 = -4.7$ and $\Delta\text{DIC} = -2.7$, corresponding to weak preference in favor of the extended model. Hence, while the unrestricted JBD model is able to alleviate the H_0 and S_8 tensions, the extra parameters of the model are consistent with the GR expectation, and the extended model is only weakly favored in a model selection sense relative to Λ CDM.

C. Impact of JBD modeling choices

We next highlight two interrelated caveats to the modified gravity constraints presented, in the form of the prior range and parameterization of the JBD coupling constant. As the coupling constant favors GR in the limit $\omega_{\text{BD}} \rightarrow \infty$, we seek to parameterize it in a way that allows for both weak and strong levels of modified gravity to be well sampled. Our fiducial parameterization is taken to be $\mathcal{P}(\omega_{\text{BD}}) = \ln \omega_{\text{BD}}^{-1}$ in accordance with the choice in Avilez & Skordis (2014) [55],¹⁸ and we have uniformly varied $\ln \omega_{\text{BD}}^{-1}$ as a primary parameter in the range $[-17, -2.3]$ in our fiducial MCMC analyses (as described in Sec. IV C).

1. Impact of the JBD prior range on the ω_{BD} bounds

In Appendix B (specifically Fig. 22), we explore the impact of extending the lower prior bound such that $\ln \omega_{\text{BD}}^{-1}$ is uniformly sampled in the range $[-47, -2.3]$ (we do not extend the upper prior bound as it is already ruled out by the data). As increasingly negative values of $\ln \omega_{\text{BD}}^{-1}$ continue to be favored by the data, given its consistency with GR, we find that the $\ln \omega_{\text{BD}}^{-1}$ constraint (and by extension the constraint on ω_{BD}) is sensitive to the prior range. In other words, the $\ln \omega_{\text{BD}}^{-1}$ posterior has a relatively sharp transition and eventually flattens given the inability of the data to distinguish between lower values of $\ln \omega_{\text{BD}}^{-1}$ (between e.g. $\ln \omega_{\text{BD}}^{-1}$ of -10 and -15). As a result, the 95% confidence region of $\ln \omega_{\text{BD}}^{-1}$ is pushed to increasingly negative values as the prior range is widened (and by extension the lower boundary of ω_{BD} is increasingly positive). This is an inescapable feature of any logarithmic parameter that is uniformly sampled without a well-motivated or constrained finite boundary.

In the appendix, as an example, we have considered the data combination KiDS \times 2dFLenS + All-BOSS + All-Planck18 + Pantheon, where for our fiducial prior range of $\ln \omega_{\text{BD}}^{-1}$ we obtain $\omega_{\text{BD}} > 1540$ (95% CL), and for our extended prior range we obtain $\omega_{\text{BD}} > 17600$ (95% CL). In other words, the ω_{BD} bounds from cosmology need to be interpreted with caution. However, given the weak correlation of $\ln \omega_{\text{BD}}^{-1}$ with the other cosmological and systematics parameters (including with G_{matter}/G), as shown in the appendix, the constraints on these other parameters are robust.

2. Impact of the JBD parameterization on the ω_{BD} bounds

In Fig. 18, we moreover explore how the constraint on the JBD coupling constant changes as a result of how we parameterize it. In addition to the fiducial parameterization ($\mathcal{P} = \ln \omega_{\text{BD}}^{-1}$), designed to allow for a wide range of JBD gravity to be well sampled [55], we consider the parameterization

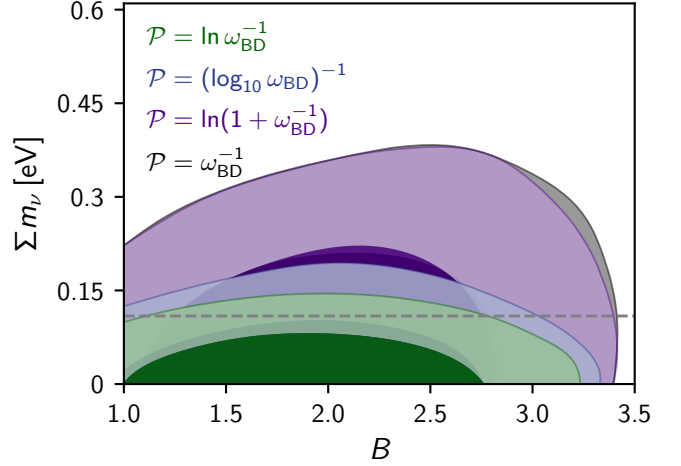


FIG. 19. Marginalized posterior distributions (inner 68% CL, outer 95% CL) in the plane of the sum of neutrino masses, Σm_ν , and the baryonic feedback amplitude, B , from the full combination of datasets (KiDS \times 2dFLenS + All-BOSS + All-Planck18 + Pantheon). The different contours correspond to four distinct parameterizations \mathcal{P} of the JBD coupling constant ($\ln \omega_{\text{BD}}^{-1}$, $(\log_{10} \omega_{\text{BD}})^{-1}$, $\ln(1 + \omega_{\text{BD}}^{-1})$, ω_{BD}^{-1}). For comparison, the horizontal dashed line shows the 95% upper bound on Σm_ν from All-Planck18 + All-BOSS + Pantheon in ΛCDM .

of Wu & Chen (2009) [62], where $\mathcal{P} = \ln(1 + \omega_{\text{BD}}^{-1})$, along with a simple $\mathcal{P} = \omega_{\text{BD}}^{-1}$ parameterization. We expect these last two parameterizations to be effectively identical in the limit of large ω_{BD} given the Mercator series (where to first order $\ln(1 + \omega_{\text{BD}}^{-1}) \approx \omega_{\text{BD}}^{-1}$ for $|\omega_{\text{BD}}^{-1}| \leq 1$ and $\omega_{\text{BD}}^{-1} \neq -1$). A benefit of these two parameterizations is that the GR limit is obtained at zero instead of infinity (negative infinity in the fiducial parameterization). However, in an MCMC analysis with a uniform prior on \mathcal{P} , they tend to penalize weaker JBD gravity scenarios by not adequately sampling large ω_{BD} .¹⁹

We moreover consider a parameterization of the form $\mathcal{P} = (\log_{10} \omega_{\text{BD}})^{-1}$, created to allow for a wide range of ω_{BD} to be sampled more uniformly (as compared to for instance $\mathcal{P} = \omega_{\text{BD}}^{-1}$ or $\mathcal{P} = \ln(1 + \omega_{\text{BD}}^{-1})$), while at the same time having the GR-limit at $\mathcal{P} = 0$ (thus avoiding a GR-limit at infinity). Given an example prior range of $\mathcal{P} \in [0.05, 0.5]$, ω_{BD} is sampled in the range $[10^2, 10^{20}]$, where a non-negligible region of \mathcal{P} probes each decade in ω_{BD} . Here, concrete values of $\omega_{\text{BD}} = \{10^2, 10^4, 10^{10}, 10^{20}\}$ correspond to $\mathcal{P} = \{0.5, 0.25, 0.1, 0.05\}$, while in the case of the ω_{BD}^{-1} or $\ln(1 + \omega_{\text{BD}}^{-1})$ parameterizations $\mathcal{P} \approx \{10^{-2}, 10^{-4}, 10^{-10}, 10^{-20}\}$. Hence, with the new parameterization, we expect to adequately sample a wider range of JBD gravity strengths.

For each parameterization, we can translate the constraints on \mathcal{P} (posteriors shown in Fig. 18) into constraints on ω_{BD} .

¹⁸ We note that this parameterization is qualitatively similar to an earlier $\ln[(4\omega_{\text{BD}})^{-1}]$ parameterization advocated by Acquaviva et al. (2004) [61].

¹⁹ As a concrete example, translating the prior range for $\ln \omega_{\text{BD}}^{-1}$ to $\ln(1 + \omega_{\text{BD}}^{-1})$, the latter is sampled in the range $[4.1 \times 10^{-8}, 0.095]$. Hence, $10 \leq \omega_{\text{BD}} < 100$ covers 90% of the prior space of $\ln(1 + \omega_{\text{BD}}^{-1})$, while $\omega_{\text{BD}} > 100$ is restricted to 10% of the space, $\omega_{\text{BD}} > 1000$ is restricted to 1% of the space, and so on. This hinders the ability of the MCMC to adequately sample parts of the $\ln(1 + \omega_{\text{BD}}^{-1})$ space that corresponds to large ω_{BD} .

As a concrete example, for the same dataset combination of KiDS \times 2dFLenS + All-BOSS + All-Planck + Pantheon, in the case of the four parameterizations $\mathcal{P} = \{\ln \omega_{\text{BD}}^{-1}, \ln(1 + \omega_{\text{BD}}^{-1}), \omega_{\text{BD}}^{-1}, (\log_{10} \omega_{\text{BD}})^{-1}\}$, the coupling constant is respectively constrained to $\omega_{\text{BD}} > \{1540, 160, 160, 350\}$ (95% CL). As expected, the JBD constraints are approximately the same for the $\ln(1 + \omega_{\text{BD}}^{-1})$ and ω_{BD}^{-1} parameterizations. We also note that the constraints using the latter three parameterizations do not suffer from the same dependence on the prior interval of ω_{BD} as the fiducial parameterization, given their GR limit at $\mathcal{P} \rightarrow 0$ (for completeness, however, we have maintained the same prior interval as for the fiducial parameterization in the case of the $\ln(1 + \omega_{\text{BD}}^{-1})$ and ω_{BD}^{-1} parameterizations).

3. Impact of the JBD parameterization on the effective gravitational constant, neutrino mass, and baryonic feedback

The constraint on the effective gravitational constant is $G_{\text{matter}}/G = 0.997^{+0.029}_{-0.029}$ in the fiducial parameterization, and deviates by at most to $G_{\text{matter}}/G = 0.970^{+0.033}_{-0.033}$ for both the $\ln(1 + \omega_{\text{BD}}^{-1})$ and ω_{BD}^{-1} parameterizations, which corresponds to a 15% increase in the uncertainty and 0.9σ shift away from the GR expectation. While the other cosmological and systematics parameters are largely robust to the choice of JBD parameterization, in Fig. 19 we highlight an exception to this for the constraints in the plane of the sum of neutrino masses and the baryonic feedback amplitude. These constraints demonstrate the interplay of modified gravity, neutrino mass, and baryonic feedback, where the contours expectedly expand in the $\sum m_\nu$ – B plane for the parameterizations that allow for stronger JBD gravity.

Considering the four different JBD parameterizations, we find 95% upper bounds on B in the range 2.8 to 3.1 and on $\sum m_\nu$ in the range 0.12 eV to 0.32 eV. In other words, notably, the bound on the sum of neutrino masses degrades by up to a factor of three as we consider a JBD parameterization that favors a stronger coupling constant. This exploration of the effects of the prior and parameterization of the JBD coupling constant on the parameter constraints underscores the need for clarity of the assumptions that enter the cosmological analysis, and illustrates the more complete inference that is possible from a broader consideration of these assumptions.

IX. CONCLUSIONS

As the precision and accuracy of cosmological datasets continue to improve, we will increasingly be able to test extensions to the standard cosmological model. One such extension consists of a modification of the gravitational theory, General Relativity, underpinning the expansion and the growth of structure in the Universe. To this end, we have performed a robust exploration of “modified gravity” with current cosmological data, capturing its impact on nonlinear scales with numerical simulations, and focusing on possible degeneracies with other cosmological and astrophysical degrees of freedom, such as

the sum of neutrino masses and baryonic feedback, which we simultaneously constrain.

We specifically consider the scalar-tensor theory of Jordan-Brans-Dicke (JBD) [39], where Newton’s constant is promoted to a dynamical field as the scalar curvature becomes coupled to a hypothesized scalar field. We consider this model as a testbed for cosmological analyses of modified gravity (and extended cosmologies more broadly), given its rich history and the role it plays in some of the fundamentally motivated extensions to the standard model of particle physics: in particular in string theory, extra-dimensional theories, and the decoupling limit of theories with higher spin fields [34]. While JBD gravity can be considered the simplest modified gravity theory, it approximates a wider range of scalar-tensor theories (within Horndeski) on cosmological scales where gradients are suppressed [55]. JBD gravity is also one of the remaining viable theories after the LIGO-Virgo measurement of the speed of gravitational waves [40–43].

We provide an analytical and numerical description of JBD gravity in the linear regime, detailing its impact on the background evolution and linear perturbations (through modifications of the EFTCAMB Einstein-Boltzmann solver). We extend this modeling of JBD gravity to nonlinear scales by performing a hybrid suite of N -body simulations to calibrate the `HMCODE` fitting function for the matter power spectrum to within 5–10% precision. As `HMCODE` is further calibrated to simulations that separately include baryonic feedback and massive neutrinos [101, 102], we use this single fitting function to describe the nonlinear matter power spectrum in a Universe with cold dark matter, baryons, massive neutrinos, and modified gravity (neglecting the sub-dominant differences with an approach where all are simultaneously included in a single simulation suite [154–161]).

We methodically constrain the JBD model (via MCMC computations using our extended CosmoLSS analysis package), mainly considering the CMB temperature, polarization, and lensing reconstruction from Planck 2018 [75], the “ $3 \times 2\text{pt}$ ” combined dataset of cosmic shear, galaxy-galaxy lensing, and overlapping redshift-space galaxy clustering from KiDS \times 2dFLenS (restricted to 450 deg²) [3], the Pantheon supernova distances [95], along with the BOSS DR12 measurements of BAO distances, Alcock-Paczynski effect, and the growth rate [76]. We consider both a restricted JBD model with the coupling constant, ω_{BD} , as a new degree of freedom, along with an unrestricted JBD model where the effective gravitational constant at present, G_{matter}/G , is additionally varied. In GR, $\omega_{\text{BD}} \rightarrow \infty$ and $G_{\text{matter}}/G = 1$. For both types of JBD gravity (and GR), we consider setups where the sum of neutrino masses, $\sum m_\nu$, is either fixed or allowed to vary. The baryonic feedback amplitude moreover varies when we probe nonlinear scales.

In the restricted JBD model, the Planck CMB temperature and polarization anisotropies constrain $\omega_{\text{BD}} > 1150$, which improves to $\omega_{\text{BD}} > 1380$ when combined with the anisotropy measurements of the Atacama Cosmology Telescope (ACT DR4; both at 95% CL). For both datasets, the Hubble constant, H_0 , rises as the strength of JBD gravity increases, with a “hook shape” in the ω_{BD} – H_0 plane. However, the uncertainties in

our marginalized H_0 and $S_8 = \sigma_8 \sqrt{\Omega_m/0.3}$ increase by $\lesssim 10\%$ and the parameters shift by $\lesssim 0.3\sigma$ due to modified gravity alone, and so the discordances in these parameters persist; the former at the level of $\sim 4\sigma$ with the direct measurement of the Hubble constant from Riess et al. (2019) [77], and the latter at $\sim 2.5\sigma$ with weak lensing (e.g. CFHTLenS [162], KiDS [177, 178], DES [214], HSC [215], and combinations thereof [179, 216]; however also see [217, 218]).

The full Planck dataset (temperature, polarization, lensing reconstruction) in combination with the lower redshift datasets of BOSS and Pantheon constrain $\omega_{\text{BD}} > 1460$ (95% CL) as the sum of neutrino masses is kept fixed, and $\omega_{\text{BD}} > 970$ (95% CL) as the sum of neutrino masses is additionally varied (where $\sum m_\nu < 0.11$ eV at 95% CL). We further combine the joint datasets of Planck, BOSS, and Pantheon with the 3×2 pt dataset of KiDS \times 2dFLenS in the unrestricted JBD cosmology, where the 2.3σ S_8 discrepancy in Λ CDM is reduced to 0.7σ (0.6σ as the sum of neutrino masses is varied), and where there is weak-to-substantial concordance between the datasets over the full parameter space as estimated by the log \mathcal{I} statistic.

The Planck, BOSS, and Pantheon joint constraint on H_0 is also weakened in the unrestricted JBD cosmology, such that the tension with Riess et al. (2019) decreases to 3.0σ for the full combination of datasets (3.1σ as the sum of neutrino masses is varied). In this model, we constrain $\omega_{\text{BD}} > 2230$ (95% CL) and $G_{\text{matter}}/G = 0.996^{+0.029}_{-0.029}$ given fixed neutrino masses, along with $\omega_{\text{BD}} > 1540$ (95% CL) and $G_{\text{matter}}/G = 0.997^{+0.029}_{-0.029}$ as the sum of neutrino masses is simultaneously varied, both in excellent agreement with GR. These constraints on the coupling constant and present effective gravitational constant are driven by the Planck CMB and are the strongest to date, where in particular the G_{matter}/G constraints are improved by nearly a factor of two relative to comparable past analyses (e.g. Ref. [55]). The 3% constraint on G_{matter}/G is also comparable to the precision of the BBN constraint in Ref. [83].

In the unrestricted JBD model, the neutrino mass bound is marginally weakened to $\sum m_\nu < 0.12$ eV (95% CL). The combined datasets improve the constraint on the intrinsic alignment amplitude by 40% relative to KiDS \times 2dFLenS alone (by 20% relative to KiDS \times {2dFLenS+BOSS}), such that $A_{\text{IA}} = 1.52^{+0.38}_{-0.38}$ is positive at 4.0σ . However, we note that this large amplitude is not found favored in direct measurements of A_{IA} [211] and is likely driven by the photometric redshift uncertainties (e.g. [212, 213]). We also constrain the baryonic feedback amplitude to $B < 2.8$ (95% CL), which corresponds to a shift of $\Delta B = -0.7$ in the upper bound relative to the Λ CDM constraint of KiDS \times 2dFLenS ($\Delta B = -0.4$ relative to KiDS \times {2dFLenS+BOSS}), and mildly favors a deviation from the “no feedback” scenario of $B = 3.13$.

Employing the deviance information criterion, we find no meaningful model selection preference for JBD gravity (relative to Λ CDM) for the different dataset combinations and specific cosmologies considered. Given the alleviation of the $\{H_0, S_8\}$ discordances in the unrestricted JBD model, we additionally performed a model selection assessment with the Riess et al. (2019) measurement of the Hubble constant included in the analysis. For Planck 2018 combined with Riess et al. (2019), we find $\Delta\text{DIC} = -4.8$, which corresponds to weak-

to-moderate preference in favor of the extended model. However, for the full combination of datasets (which here includes Riess et al. 2019), this decreases to $\Delta\text{DIC} = -2.7$, corresponding to weak preference in favor of the extended model.

In addition to our fiducial cosmological constraints, we have examined their sensitivity to the modeling choices. In particular, we have illustrated how the choice of parameterization of the coupling constant can affect the constraints on the present effective gravitational constant, the baryonic feedback amplitude, and the sum of neutrino masses, in the latter case degrading the upper bound by up to a factor of three. We have further highlighted the possible degeneracy of the effective gravitational constant with other physics that affect the CMB damping tail. As the effective gravitational constant gives rise to a response in the CMB temperature and polarization power spectra that coherently strengthens towards smaller scales, it is correlated with physics such as the primordial helium abundance, the effective number of neutrinos, and the running of the spectral index, targeted by CMB surveys such as AdvACT [129], SPT-3G [130], and the Simons Observatory [131].

We note that our bounds on the JBD coupling constant are approximately an order of magnitude weaker than the bounds from astrophysical probes (i.e. $\omega_{\text{BD}} \gtrsim 10^3$ from cosmology as compared to $\omega_{\text{BD}} \gtrsim 10^4$ from astrophysics). Concretely, our strongest bound on the coupling constant is a factor of 16 weaker than that obtained from Shapiro time delay measurements by the Cassini satellite [57] and a factor of 5 weaker than the lower bound from the analysis of the pulsar–white dwarf binary PSR J1738+0333 [58]. However, we emphasize the usefulness of constraining modified gravity through multiple pathways. In the case of JBD theory, as it can be considered an approximation to a wider class of Horndeski scalar-tensor theories on cosmological scales [55], which may be endowed with screening mechanisms on astrophysical scales, these stronger astrophysical bounds might not be representative of the true strength of its corrections on the cosmological observables.

We expect approximately an order of magnitude improvement in the constraints on JBD gravity with next-generation (Stage-IV) surveys of the CMB, the large-scale structure, and the radio sky [92], which can be further improved in a combined analysis with a future set of gravitational wave standard siren events (e.g. [219]). This will allow for cosmological constraints on JBD gravity that are at a similar precision to the most powerful astrophysical probes.

For the expected improvements in cosmological inferences to be realized, a series of conditions need to be met, in particular: continued progress in the nonlinear modeling of the modified gravity, the disentanglement of possible degeneracies with other cosmological and systematics degrees of freedom, and concordance between distinct cosmological datasets (required for multi-probe analyses; noting that the concordance might only emerge in the extended cosmology, as we have shown). The impact of modeling choices, for instance concerning the choice of modified gravity parameterization and prior ranges, also needs to be highlighted in a robust cosmological analysis. We have illustrated these different ingredients for JBD gravity, and anticipate the advent of more powerful datasets which will either signpost deviations to or confirm the standard

cosmological model to ever higher precision.

ACKNOWLEDGEMENTS

We thank S. Alam, D. Alonso, A. Avilez, D. Bartlett, E. Bellini, E. Calabrese, H. Desmond, B. Hu, K. Kuijken, E. M. Mueller, T. Nanayakkara, V. Niro, D. Parkinson, M. Raveri, A. Silvestri, C. Skordis, and M. Zumalacarregui for useful discussions. We thank Shadab Alam for providing the BOSS DR12 final consensus likelihood, and Nora Elisa Chisari for performing an internal KiDS Collaboration review of the manuscript. We also thank Jonathan Patterson and

Jon Wakelin for HPC support. We acknowledge the use of the CAMB [163], CosmoMC [164], and GetDist [220] packages. SJ and PGF acknowledge support from the Beecroft Trust, the Science and Technology Facilities Council (STFC), and the European Research Council under grant agreement No. 693024. We acknowledge the use of the Oxford computing cluster Glamdring. Part of this work was performed using the DiRAC Data Intensive service at Leicester operated by the University of Leicester IT Services, and DiRAC@Durham managed by the Institute for Computational Cosmology, which form part of the STFC DiRAC HPC Facility acknowledging BEIS and STFC grants STK0003731, STR0023631, STR0010141, STP0022931, STR0023711, STR0008321.

-
- [1] F. Simpson *et al.*, *MNRAS* **429**, 2249 (2013), arXiv:1212.3339 [astro-ph.CO].
 - [2] E.-M. Mueller, W. Percival, E. Linder, S. Alam, G.-B. Zhao, A. G. Sánchez, F. Beutler, and J. Brinkmann, *MNRAS* **475**, 2122 (2018), arXiv:1612.00812 [astro-ph.CO].
 - [3] S. Joudaki *et al.*, *Mon. Not. Roy. Astron. Soc.* **474**, 4894 (2018), arXiv:1707.06627 [astro-ph.CO].
 - [4] T. M. C. Abbott *et al.*, arXiv e-prints, arXiv:1810.02499 (2018), arXiv:1810.02499 [astro-ph.CO].
 - [5] C. Blake *et al.*, arXiv e-prints, arXiv:2005.14351 (2020), arXiv:2005.14351 [astro-ph.CO].
 - [6] R. Bean and M. Tangmatitham, *Phys. Rev. D* **81**, 083534 (2010), arXiv:1002.4197 [astro-ph.CO].
 - [7] C.-P. Ma and E. Bertschinger, *Astrophys. J.* **455**, 7 (1995), astro-ph/9506072.
 - [8] S. Tsujikawa, *Phys. Rev. D* **76**, 023514 (2007), arXiv:0705.1032 [astro-ph].
 - [9] B. Jain and P. Zhang, *Phys. Rev. D* **78**, 063503 (2008), arXiv:0709.2375.
 - [10] L. Pogosian and A. Silvestri, *Phys. Rev. D* **94**, 104014 (2016), arXiv:1606.05339.
 - [11] L. Amendola, C. Quercellini, and E. Giallongo, *MNRAS* **357**, 429 (2005), arXiv:astro-ph/0404599 [astro-ph].
 - [12] E. V. Linder, *Phys. Rev. D* **72**, 043529 (2005), arXiv:astro-ph/0507263 [astro-ph].
 - [13] P. Zhang, M. Liguori, R. Bean, and S. Dodelson, *Physical Review Letters* **99**, 141302 (2007), arXiv:0704.1932.
 - [14] R. Reyes, R. Mandelbaum, U. Seljak, T. Baldauf, J. E. Gunn, L. Lombriser, and R. E. Smith, *Nature (London)* **464**, 256 (2010), arXiv:1003.2185 [astro-ph.CO].
 - [15] G. W. Horndeski, *Int. J. Theor. Phys.* **10**, 363 (1974).
 - [16] C. Cheung, A. L. Fitzpatrick, J. Kaplan, L. Senatore, and P. Creminelli, *Journal of High Energy Physics* **2008**, 014-014 (2008), arXiv:0709.0293 [hep-th].
 - [17] G. Gubitosi, F. Piazza, and F. Vernizzi, *JCAP* **2013**, 032 (2013), arXiv:1210.0201 [hep-th].
 - [18] E. Bellini and I. Sawicki, *JCAP* **2014** (7), 050, arXiv:1404.3713 [astro-ph.CO].
 - [19] S. F. Daniel *et al.*, *Phys. Rev. D* **81**, 123508 (2010), arXiv:1002.1962 [astro-ph.CO].
 - [20] S. Joudaki *et al.*, *MNRAS* **471**, 1259 (2017), arXiv:1610.04606 [astro-ph.CO].
 - [21] P. A. R. Ade *et al.*, *A&A* **594**, A14 (2016), arXiv:1502.01590.
 - [22] C. Blake *et al.*, *MNRAS* **456**, 2806 (2016), arXiv:1507.03086 [astro-ph.CO].
 - [23] A. Amon *et al.*, *MNRAS* **479**, 3422 (2018), arXiv:1711.10999 [astro-ph.CO].
 - [24] R. Caldwell, A. Cooray, and A. Melchiorri, *Phys. Rev. D* **76**, 023507 (2007), arXiv:astro-ph/0703375 [astro-ph].
 - [25] C. Blake *et al.*, *MNRAS* **415**, 2876 (2011), arXiv:1104.2948 [astro-ph.CO].
 - [26] L. Samushia, W. J. Percival, and A. Raccanelli, *MNRAS* **420**, 2102 (2012), arXiv:1102.1014 [astro-ph.CO].
 - [27] A. Johnson, C. Blake, J. Dossett, J. Koda, D. Parkinson, and S. Joudaki, *Mon. Not. Roy. Astron. Soc.* **458**, 2725 (2016), arXiv:1504.06885 [astro-ph.CO].
 - [28] T. Okumura *et al.*, *Publ. Astron. Soc. Jap.* **68**, 38 (2016), arXiv:1511.08083 [astro-ph.CO].
 - [29] A. Spurio Mancini *et al.*, *MNRAS* **490**, 2155 (2019), arXiv:1901.03686 [astro-ph.CO].
 - [30] A. Ferté, D. Kirk, A. R. Liddle, and J. Zuntz, *Phys. Rev. D* **99**, 083512 (2019), arXiv:1712.01846 [astro-ph.CO].
 - [31] J. Noller and A. Nicola, *Phys. Rev. D* **99**, 103502 (2019), arXiv:1811.12928 [astro-ph.CO].
 - [32] D. Traykova, E. Bellini, and P. G. Ferreira, *JCAP* **2019**, 035 (2019), arXiv:1902.10687 [astro-ph.CO].
 - [33] A. Zucca, L. Pogosian, A. Silvestri, and G. B. Zhao, *JCAP* **2019**, 001 (2019), arXiv:1901.05956 [astro-ph.CO].
 - [34] T. Clifton, P. G. Ferreira, A. Padilla, and C. Skordis, *Phys. Rept.* **513**, 1 (2012), arXiv:1106.2476 [astro-ph.CO].
 - [35] R. Laureijs *et al.*, arXiv e-prints, arXiv:1110.3193 (2011), arXiv:1110.3193 [astro-ph.CO].
 - [36] P. A. Abell *et al.*, arXiv e-prints, arXiv:0912.0201 (2009), arXiv:0912.0201 [astro-ph.IM].
 - [37] A. Aghamousa *et al.*, arXiv e-prints, arXiv:1611.00036 (2016), arXiv:1611.00036 [astro-ph.IM].
 - [38] D. Spergel *et al.*, arXiv e-prints, arXiv:1503.03757 (2015), arXiv:1503.03757 [astro-ph.IM].
 - [39] C. Brans and R. H. Dicke, *Phys. Rev.* **124**, 925 (1961).
 - [40] B. P. Abbott *et al.*, *Phys. Rev. Lett.* **119**, 161101 (2017), arXiv:1710.05832 [gr-qc].
 - [41] T. Baker, E. Bellini, P. G. Ferreira, M. Lagos, J. Noller, and I. Sawicki, *Phys. Rev. Lett.* **119**, 251301 (2017), arXiv:1710.06394 [astro-ph.CO].
 - [42] P. Creminelli and F. Vernizzi, *Phys. Rev. Lett.* **119**, 251302 (2017), arXiv:1710.05877 [astro-ph.CO].
 - [43] J. M. Ezquiaga and M. Zumalacarregui, *Phys. Rev. Lett.* **119**, 251304 (2017), arXiv:1710.05901 [astro-ph.CO].
 - [44] N. A. Lima and P. G. Ferreira, *JCAP* **2016** (1), 010, arXiv:1506.07771 [astro-ph.CO].

- [45] L. Amendola, *Phys. Rev. D* **62**, 043511 (2000), arXiv:astro-ph/9908023 [astro-ph].
- [46] A. De Felice and S. Tsujikawa, *Living Reviews in Relativity* **13**, 3 (2010), arXiv:1002.4928 [gr-qc].
- [47] C. Deffayet, G. Esposito-Farese, and A. Vikman, *Phys. Rev. D* **79**, 084003 (2009), arXiv:0901.1314 [hep-th].
- [48] C. Deffayet, X. Gao, D. A. Steer, and G. Zahariade, *Phys. Rev. D* **84**, 064039 (2011), arXiv:1103.3260 [hep-th].
- [49] J. Gleyzes, D. Langlois, F. Piazza, and F. Vernizzi, *Phys. Rev. Lett.* **114**, 211101 (2015), arXiv:1404.6495 [hep-th].
- [50] J. Gleyzes, D. Langlois, F. Piazza, and F. Vernizzi, *JCAP* **2015** (2), 018, arXiv:1408.1952 [astro-ph.CO].
- [51] M. Crisostomi, K. Koyama, and G. Tasinato, *JCAP* **1604** (04), 044, arXiv:1602.03119 [hep-th].
- [52] J. Ben Achour, M. Crisostomi, K. Koyama, D. Langlois, K. Noui, and G. Tasinato, arXiv e-prints , arXiv:1608.08135 (2016), arXiv:1608.08135 [hep-th].
- [53] M. Zumalacarregui and J. Garcia-Bellido, *Phys.Rev.* **D89**, 064046 (2014), arXiv:1308.4685 [gr-qc].
- [54] D. Langlois, M. Mancarella, K. Noui, and F. Vernizzi, *JCAP* **1705** (05), 033, arXiv:1703.03797 [hep-th].
- [55] A. Avilez and C. Skordis, *Phys. Rev. Lett.* **113**, 011101 (2014), arXiv:1303.4330 [astro-ph.CO].
- [56] E. Berti *et al.*, *Class. Quant. Grav.* **32**, 243001 (2015), arXiv:1501.07274 [gr-qc].
- [57] B. Bertotti, L. Iess, and P. Tortora, *Nature* **425**, 374 (2003).
- [58] P. C. C. Freire *et al.*, *M.N.R.A.S.* **423**, 3328 (2012), arXiv:1205.1450 [astro-ph.GA].
- [59] X. Chen and M. Kamionkowski, *Phys. Rev. D* **60**, 104036 (1999), arXiv:astro-ph/9905368 [astro-ph].
- [60] R. Nagata, T. Chiba, and N. Sugiyama, *Phys. Rev. D* **69**, 083512 (2004), arXiv:astro-ph/0311274 [astro-ph].
- [61] V. Acquaviva, C. Baccigalupi, S. M. Leach, A. R. Liddle, and F. Perrotta, *Phys. Rev. D* **71**, 104025 (2005), arXiv:astro-ph/0412052 [astro-ph].
- [62] F. Wu and X. Chen, *Phys. Rev. D* **82**, 083003 (2010), arXiv:0903.0385 [astro-ph.CO].
- [63] C. Umiltà, M. Ballardini, F. Finelli, and D. Paoletti, *JCAP* **2015**, 017 (2015), arXiv:1507.00718 [astro-ph.CO].
- [64] M. Ballardini, F. Finelli, C. Umiltà, and D. Paoletti, *JCAP* **2016** (5), 067, arXiv:1601.03387 [astro-ph.CO].
- [65] J. Ooba, K. Ichiki, T. Chiba, and N. Sugiyama, *Phys. Rev. D* **93**, 122002 (2016), arXiv:1602.00809 [astro-ph.CO].
- [66] J. Ooba, K. Ichiki, T. Chiba, and N. Sugiyama, *PTEP* **2017**, 043E03 (2017), arXiv:1702.00742 [astro-ph.CO].
- [67] J. Solà Peracaula, A. Gómez-Valent, J. de Cruz Pérez, and C. Moreno-Pulido, *ApJ* **886**, L6 (2019), arXiv:1909.02554 [astro-ph.CO].
- [68] M. Ballardini *et al.*, arXiv e-prints , arXiv:2004.14349 (2020), arXiv:2004.14349 [astro-ph.CO].
- [69] J. Sola, A. Gomez-Valent, J. de Cruz Perez, and C. Moreno-Pulido, arXiv e-prints , arXiv:2006.04273 (2020), arXiv:2006.04273 [astro-ph.CO].
- [70] P. A. R. Ade *et al.*, *A&A* **571**, A16 (2014), arXiv:1303.5076 [astro-ph.CO].
- [71] P. A. R. Ade *et al.* (Planck), *Astron. Astrophys.* **594**, A13 (2016), arXiv:1502.01589 [astro-ph.CO].
- [72] F. Beutler, C. Blake, M. Colless, D. H. Jones, L. Staveley-Smith, L. Campbell, Q. Parker, W. Saunders, and F. Watson, *MNRAS* **416**, 3017 (2011), arXiv:1106.3366.
- [73] A. J. Ross, L. Samushia, C. Howlett, W. J. Percival, A. Burden, and M. Manera, *MNRAS* **449**, 835 (2015), arXiv:1409.3242.
- [74] L. Anderson *et al.*, *MNRAS* **441**, 24 (2014), arXiv:1312.4877.
- [75] N. Aghanim *et al.*, arXiv e-prints , arXiv:1807.06209 (2018), arXiv:1807.06209 [astro-ph.CO].
- [76] S. Alam *et al.*, *Monthly Notices of the Royal Astronomical Society* **470**, 2617 (2017), arXiv:1607.03155 [astro-ph.CO].
- [77] A. G. Riess, S. Casertano, W. Yuan, L. M. Macri, and D. Scolnic, *Astrophys. J.* **876**, 85 (2019), arXiv:1903.07603 [astro-ph.CO].
- [78] J. Casas, J. Garcia-Bellido, and M. Quiros, *Mod. Phys. Lett. A* **7**, 447 (1992).
- [79] C. J. Copi, A. N. Davis, and L. M. Krauss, *Phys. Rev. Lett.* **92**, 171301 (2004), arXiv:astro-ph/0311334 [astro-ph].
- [80] V. Pettorino, C. Baccigalupi, and G. Mangano, *JCAP* **2005**, 014 (2005), arXiv:astro-ph/0412334 [astro-ph].
- [81] T. Clifton, J. D. Barrow, and R. J. Scherrer, *Phys. Rev. D* **71**, 123526 (2005), arXiv:astro-ph/0504418 [astro-ph].
- [82] F. Iocco, G. Mangano, G. Miele, O. Pisanti, and P. D. Serpico, *Phys. Rept.* **472**, 1 (2009), arXiv:0809.0631 [astro-ph].
- [83] J. Alvey, N. Sabti, M. Escudero, and M. Fairbairn, *European Physical Journal C* **80**, 148 (2020), arXiv:1910.10730 [astro-ph.CO].
- [84] J.-P. Uzan, *Living Reviews in Relativity* **14**, 2 (2011), arXiv:1009.5514 [astro-ph.CO].
- [85] A. I. Vainshtein, *Physics Letters B* **39**, 393 (1972).
- [86] E. Babichev and C. Deffayet, *Class. Quant. Grav.* **30**, 184001 (2013), arXiv:1304.7240 [gr-qc].
- [87] J. Khoury and A. Weltman, *Physical Review Letters* **93**, 171104 (2004), astro-ph/0309300.
- [88] J. Khoury and A. Weltman, *PRD* **69**, 044026 (2004), astro-ph/0309411.
- [89] K. Hinterbichler and J. Khoury, *Physical Review Letters* **104**, 231301 (2010), arXiv:1001.4525 [hep-th].
- [90] P. Ade *et al.*, *JCAP* **2019**, 056 (2019), arXiv:1808.07445 [astro-ph.CO].
- [91] L. Amendola *et al.*, *Living Reviews in Relativity* **16**, 6 (2013), arXiv:1206.1225 [astro-ph.CO].
- [92] D. Alonso, E. Bellini, P. G. Ferreira, and M. Zumalacarregui, *Phys. Rev. D* **95**, 063502 (2017), arXiv:1610.09290 [astro-ph.CO].
- [93] M. Ballardini, D. Sapone, C. Umiltà, F. Finelli, and D. Paoletti, *JCAP* **2019**, 049 (2019), arXiv:1902.01407 [astro-ph.CO].
- [94] C. Heinrich and O. Doré, arXiv e-prints , arXiv:2006.03138 (2020), arXiv:2006.03138 [astro-ph.CO].
- [95] D. M. Scolnic *et al.*, *Astrophys. J.* **859**, 101 (2018), arXiv:1710.00845 [astro-ph.CO].
- [96] T. Louis *et al.*, *JCAP* **2017**, 031 (2017), arXiv:1610.02360 [astro-ph.CO].
- [97] S. Aiola *et al.*, arXiv e-prints , arXiv:2007.07288 (2020), arXiv:2007.07288 [astro-ph.CO].
- [98] S. Tassev, M. Zaldarriaga, and D. J. Eisenstein, *JCAP* **2013** (6), 036, arXiv:1301.0322 [astro-ph.CO].
- [99] H. A. Winther, K. Koyama, M. Manera, B. S. Wright, and G.-B. Zhao, *JCAP* **1708** (08), 006, arXiv:1703.00879 [astro-ph.CO].
- [100] R. Teyssier, *Astron. Astrophys.* **385**, 337 (2002), arXiv:astro-ph/0111367 [astro-ph].
- [101] A. Mead, J. Peacock, C. Heymans, S. Joudaki, and A. Heavens, *Mon. Not. Roy. Astron. Soc.* **454**, 1958 (2015), arXiv:1505.07833 [astro-ph.CO].
- [102] A. J. Mead, C. Heymans, L. Lombriser, J. A. Peacock, O. I. Steele, and H. A. Winther, *MNRAS* **459**, 1468 (2016), arXiv:1602.02154.
- [103] H. Nariai, *Progress of Theoretical Physics* **40**, 49 (1968).
- [104] L. E. Gurevich, A. M. Finkelstein, and V. A. Ruban, *Astrophysics and Space Science* **22**, 231 (1973).
- [105] C. Mathiazhagan and V. B. Johri, *Classical and Quantum Gravity* **1**, L29 (1984).

- [106] D. La and P. J. Steinhardt, *Phys. Rev. Lett.* **62**, 376 (1989).
- [107] A. De Felice, T. Kobayashi, and S. Tsujikawa, *Phys. Lett.* **B706**, 123 (2011), [arXiv:1108.4242 \[gr-qc\]](#).
- [108] T. Baker, P. G. Ferreira, and C. Skordis, *Phys. Rev.* **D89**, 024026 (2014), [arXiv:1310.1086 \[astro-ph.CO\]](#).
- [109] S. F. Daniel, R. R. Caldwell, A. Cooray, P. Serra, and A. Melchiorri, *Phys. Rev. D* **80**, 023532 (2009), [arXiv:0901.0919 \[astro-ph.CO\]](#).
- [110] L. Amendola, S. Fogli, A. Guarnizo, M. Kunz, and A. Vollmer, *Phys. Rev. D* **89**, 063538 (2014), [arXiv:1311.4765 \[astro-ph.CO\]](#).
- [111] M. Aparicio Resco *et al.*, *MNRAS* **493**, 3616 (2020), [arXiv:1910.02694 \[astro-ph.CO\]](#).
- [112] E. Bellini *et al.*, *Phys. Rev.* **D97**, 023520 (2018), [arXiv:1709.09135 \[astro-ph.CO\]](#).
- [113] J. Schaye *et al.*, *MNRAS* **402**, 1536 (2010), [arXiv:0909.5196 \[astro-ph.CO\]](#).
- [114] M. P. van Daalen *et al.*, *MNRAS* **415**, 3649 (2011), [arXiv:1104.1174 \[astro-ph.CO\]](#).
- [115] E. Semboloni, H. Hoekstra, J. Schaye, M. P. van Daalen, and I. G. McCarthy, *MNRAS* **417**, 2020 (2011), [arXiv:1105.1075](#).
- [116] J. R. Bond, G. Efstathiou, and J. Silk, *Phys. Rev. Lett.* **45**, 1980 (1980).
- [117] J. Lesgourgues and S. Pastor, *arXiv e-prints*, [arXiv:1212.6154](#) (2012), [arXiv:1212.6154 \[hep-ph\]](#).
- [118] R. Jimenez, T. Kitching, C. Peña-Garay, and L. Verde, *JCAP* **2010**, 035 (2010), [arXiv:1003.5918 \[astro-ph.CO\]](#).
- [119] Z. Hou, R. Keisler, L. Knox, M. Millea, and C. Reichardt, *Phys. Rev. D* **87**, 083008 (2013), [arXiv:1104.2333 \[astro-ph.CO\]](#).
- [120] W. Hu and N. Sugiyama, *Astrophys. J.* **444**, 489 (1995), [arXiv:astro-ph/9407093 \[astro-ph\]](#).
- [121] G. Mangano, G. Miele, S. Pastor, and M. Peloso, *Physics Letters B* **534**, 8 (2002), [arXiv:astro-ph/0111408 \[astro-ph\]](#).
- [122] W. Hu, D. Scott, N. Sugiyama, and M. White, *Phys. Rev. D* **52**, 5498 (1995), [arXiv:astro-ph/9505043 \[astro-ph\]](#).
- [123] O. Zahn and M. Zaldarriaga, *Phys. Rev. D* **67**, 063002 (2003), [arXiv:astro-ph/0212360 \[astro-ph\]](#).
- [124] E. Komatsu *et al.*, *ApJS* **192**, 18 (2011), [arXiv:1001.4538 \[astro-ph.CO\]](#).
- [125] S. Bashinsky and U. Seljak, *Phys. Rev. D* **69**, 083002 (2004), [arXiv:astro-ph/0310198 \[astro-ph\]](#).
- [126] C. Bambi, M. Giannotti, and F. L. Villante, *Phys. Rev. D* **71**, 123524 (2005), [arXiv:astro-ph/0503502 \[astro-ph\]](#).
- [127] B. D. Fields, K. A. Olive, T.-H. Yeh, and C. Young, *JCAP* **2020**, 010 (2020), [arXiv:1912.01132 \[astro-ph.CO\]](#).
- [128] R. J. Scherrer, *Phys. Rev. D* **69**, 107302 (2004), [arXiv:astro-ph/0310699 \[astro-ph\]](#).
- [129] S. Henderson *et al.*, *J. Low Temp. Phys.* **184**, 772 (2016), [arXiv:1510.02809 \[astro-ph.IM\]](#).
- [130] B. Benson *et al.* (SPT-3G), *Proc. SPIE Int. Soc. Opt. Eng.* **9153**, 91531P (2014), [arXiv:1407.2973 \[astro-ph.IM\]](#).
- [131] P. Ade *et al.*, *JCAP* **2019**, 056 (2019), [arXiv:1808.07445 \[astro-ph.CO\]](#).
- [132] E. Aver, K. A. Olive, and E. D. Skillman, *JCAP* **2015**, 011 (2015), [arXiv:1503.08146 \[astro-ph.CO\]](#).
- [133] A. Peimbert, M. Peimbert, and V. Luridiana, *Rev. Mex. Astron. Astrofis.* **52**, 419 (2016), [arXiv:1608.02062 \[astro-ph.CO\]](#).
- [134] B. Hu, M. Raveri, N. Frusciante, and A. Silvestri, *Phys. Rev. D* **89**, 103530 (2014), [arXiv:1312.5742 \[astro-ph.CO\]](#).
- [135] F. R. Bouchet, in *Dark Matter in the Universe*, edited by S. Bonometto, J. R. Primack, and A. Provenzale (1996) p. 565, [arXiv:astro-ph/9603013 \[astro-ph\]](#).
- [136] C. Howlett, M. Manera, and W. J. Percival, *Astronomy and Computing* **12**, 109 (2015), [arXiv:1506.03737 \[astro-ph.CO\]](#).
- [137] F. R. Bouchet, S. Colombi, E. Hivon, and R. Juszkiewicz, *A&A* **296**, 575 (1995), [arXiv:astro-ph/9406013 \[astro-ph\]](#).
- [138] A. Schneider *et al.*, *JCAP* **2016**, 047 (2016), [arXiv:1503.05920 \[astro-ph.CO\]](#).
- [139] A. Mead, S. Brieden, T. Tröster, and C. Heymans, *arXiv e-prints*, [arXiv:2009.01858](#) (2020), [arXiv:2009.01858 \[astro-ph.CO\]](#).
- [140] A. J. Mead *et al.*, *arXiv e-prints*, [arXiv:2005.00009](#) (2020), [arXiv:2005.00009 \[astro-ph.CO\]](#).
- [141] A. Cooray and R. K. Sheth, *Phys. Rept.* **372**, 1 (2002), [arXiv:astro-ph/0206508 \[astro-ph\]](#).
- [142] K. Heitmann, E. Lawrence, J. Kwan, S. Habib, and D. Higdon, *Astrophys. J.* **780**, 111 (2014), [arXiv:1304.7849](#).
- [143] R. E. Smith, J. A. Peacock, A. Jenkins, S. D. M. White, C. S. Frenk, F. R. Pearce, P. A. Thomas, G. Efstathiou, and H. M. P. Couchman, *MNRAS* **341**, 1311 (2003), [astro-ph/0207664](#).
- [144] R. Takahashi *et al.*, *Astrophys. J.* **761**, 152 (2012), [arXiv:1208.2701](#).
- [145] E. Massara, F. Villaescusa-Navarro, and M. Viel, *JCAP* **2014**, 053 (2014), [arXiv:1410.6813 \[astro-ph.CO\]](#).
- [146] E. Lawrence *et al.*, *Astrophys. J.* **713**, 1322 (2010), [arXiv:0912.4490 \[astro-ph.CO\]](#).
- [147] M. Knabenhans *et al.*, *MNRAS* **484**, 5509 (2019), [arXiv:1809.04695 \[astro-ph.CO\]](#).
- [148] R. E. Angulo *et al.*, *arXiv e-prints*, [arXiv:2004.06245](#) (2020), [arXiv:2004.06245 \[astro-ph.CO\]](#).
- [149] M. Cataneo *et al.*, *MNRAS* **488**, 2121 (2019), [arXiv:1812.05594 \[astro-ph.CO\]](#).
- [150] B. Bose *et al.*, *arXiv e-prints*, [arXiv:2005.12184](#) (2020), [arXiv:2005.12184 \[astro-ph.CO\]](#).
- [151] A. Schneider *et al.*, *JCAP* **2019**, 020 (2019), [arXiv:1810.08629 \[astro-ph.CO\]](#).
- [152] A. Schneider *et al.*, *JCAP* **2020**, 019 (2020), [arXiv:1910.11357 \[astro-ph.CO\]](#).
- [153] A. Schneider *et al.*, *JCAP* **2020**, 020 (2020), [arXiv:1911.08494 \[astro-ph.CO\]](#).
- [154] E. Puchwein, M. Baldi, and V. Springel, *MNRAS* **436**, 348 (2013), [arXiv:1305.2418 \[astro-ph.CO\]](#).
- [155] C. Arnold and B. Li, *MNRAS* **490**, 2507 (2019), [arXiv:1907.02980 \[astro-ph.CO\]](#).
- [156] C. Hernández-Aguayo, C. Arnold, B. Li, and C. M. Baugh, *arXiv e-prints*, [arXiv:2006.15467](#) (2020), [arXiv:2006.15467 \[astro-ph.CO\]](#).
- [157] B. O. Mummery, I. G. McCarthy, S. Bird, and J. Schaye, *MNRAS* **471**, 227 (2017), [arXiv:1702.02064 \[astro-ph.CO\]](#).
- [158] I. G. McCarthy, S. Bird, J. Schaye, J. Harnois-Deraps, A. S. Font, and L. van Waerbeke, *MNRAS* **476**, 2999 (2018), [arXiv:1712.02411 \[astro-ph.CO\]](#).
- [159] M. Baldi, F. Villaescusa-Navarro, M. Viel, E. Puchwein, V. Springel, and L. Moscardini, *MNRAS* **440**, 75 (2014), [arXiv:1311.2588 \[astro-ph.CO\]](#).
- [160] C. Giocoli, M. Baldi, and L. Moscardini, *MNRAS* **481**, 2813 (2018), [arXiv:1806.04681 \[astro-ph.CO\]](#).
- [161] B. S. Wright, K. Koyama, H. A. Winther, and G.-B. Zhao, *JCAP* **2019**, 040 (2019), [arXiv:1902.10692 \[astro-ph.CO\]](#).
- [162] S. Joudaki *et al.*, *Mon. Not. Roy. Astron. Soc.* **465**, 2033 (2017), [arXiv:1601.05786 \[astro-ph.CO\]](#).
- [163] A. Lewis, A. Challinor, and A. Lasenby, *Astrophys. J.* **538**, 473 (2000), [astro-ph/9911177](#).
- [164] A. Lewis and S. Bridle, *Phys. Rev. D* **66**, 103511 (2002), [astro-ph/0205436](#).
- [165] A. Gelman and D. Rubin, *Statistical Science* **7**, 457 (1992).
- [166] A. R. Liddle, A. Mazumdar, and J. D. Barrow, *Phys. Rev. D* **58**, 027302 (1998), [arXiv:astro-ph/9802133 \[astro-ph\]](#).

- [167] R. K. Sachs and A. M. Wolfe, *Astrophys. J.* **147**, 73 (1967).
- [168] P. A. R. Ade *et al.*, *A&A* **594**, A15 (2016), arXiv:1502.01591 [astro-ph.CO].
- [169] N. Aghanim *et al.*, arXiv e-prints, arXiv:1807.06210 (2018), arXiv:1807.06210 [astro-ph.CO].
- [170] K. Kuijken *et al.*, *MNRAS* **454**, 3500 (2015), arXiv:1507.00738.
- [171] H. Hildebrandt, M. Viola, C. Heymans, S. Joudaki, K. Kuijken, *et al.*, *MNRAS* **465**, 1454 (2017), arXiv:1606.05338.
- [172] C. Blake *et al.*, *MNRAS* **462**, 4240 (2016), arXiv:1608.02668.
- [173] A. J. Ross *et al.*, arXiv e-prints, arXiv:2007.09000 (2020), arXiv:2007.09000 [astro-ph.CO].
- [174] K. S. Dawson *et al.* (BOSS), *Astron. J.* **145**, 10 (2013), arXiv:1208.0022 [astro-ph.CO].
- [175] N. Benítez, *Astrophys. J.* **536**, 571 (2000), astro-ph/9811189.
- [176] D. Kodwani, D. Alonso, and P. Ferreira, *The Open Journal of Astrophysics* **2**, 3 (2019), arXiv:1811.11584 [astro-ph.CO].
- [177] H. Hildebrandt *et al.*, *A&A* **633**, A69 (2020), arXiv:1812.06076 [astro-ph.CO].
- [178] M. Asgari *et al.*, arXiv e-prints, arXiv:2007.15633 (2020), arXiv:2007.15633 [astro-ph.CO].
- [179] S. Joudaki *et al.*, *A&A* **638**, L1 (2020), arXiv:1906.09262 [astro-ph.CO].
- [180] S. Alam *et al.*, arXiv e-prints, arXiv:2007.08991 (2020), arXiv:2007.08991 [astro-ph.CO].
- [181] N. Aghanim *et al.*, arXiv e-prints, arXiv:1907.12875 (2019), arXiv:1907.12875 [astro-ph.CO].
- [182] N. Aghanim *et al.*, *A&A* **594**, A11 (2016), arXiv:1507.02704 [astro-ph.CO].
- [183] C. M. Hirata and U. Seljak, *Phys. Rev. D* **70**, 063526 (2004), [Erratum: *Phys. Rev. D* **82**, 049901 (2010)], arXiv:astro-ph/0406275 [astro-ph].
- [184] S. Bridle and L. King, *New J. Phys.* **9**, 444 (2007), arXiv:0705.0166 [astro-ph].
- [185] N. E. Chisari, A. J. Mead, S. Joudaki, *et al.*, *The Open Journal of Astrophysics* **2**, 4 (2019), arXiv:1905.06082 [astro-ph.CO].
- [186] H.-J. Huang, T. Eifler, R. Mandelbaum, and S. Dodelson, *MNRAS* **488**, 1652 (2019), arXiv:1809.01146 [astro-ph.CO].
- [187] M. Vargas-Magaña *et al.*, *MNRAS* **477**, 1153 (2018), arXiv:1610.03506 [astro-ph.CO].
- [188] R. H. Cyburt, B. D. Fields, K. A. Olive, and T.-H. Yeh, *Reviews of Modern Physics* **88**, 015004 (2016), arXiv:1505.01076 [astro-ph.CO].
- [189] M. Tanabashi *et al.* (Particle Data Group), *Phys. Rev. D* **98**, 030001 (2018).
- [190] D. Spiegelhalter, N. G. Best, and B. P. Carlin, *J. Royal. Stat. Soc. B* **64**, 583 (2002).
- [191] P. Marshall, N. Rajguru, and A. Slosar, *Phys. Rev. D* **73**, 067302 (2006), astro-ph/0412535.
- [192] M. Kunz, R. Trotta, and D. R. Parkinson, *Phys. Rev. D* **74**, 023503 (2006), astro-ph/0602378.
- [193] A. R. Liddle, *MNRAS* **377**, L74 (2007), astro-ph/0701113.
- [194] R. Trotta, *Contemporary Physics* **49**, 71 (2008).
- [195] D. Spiegelhalter, N. G. Best, B. P. Carlin, and A. van der Linde, *J. Royal. Stat. Soc. B* **76**, 485 (2014).
- [196] M. Raveri, *Phys. Rev. D* **93**, 043522 (2016), arXiv:1510.00688 [astro-ph.CO].
- [197] S. Grandis, S. Seehars, A. Refregier, A. Amara, and A. Nicola, arXiv e-prints, 1510.06422 (2015), arXiv:1510.06422.
- [198] S. Seehars, S. Grandis, A. Amara, and A. Refregier, arXiv e-prints, 1510.08483 (2015), arXiv:1510.08483.
- [199] W. Lin and M. Ishak, *Phys. Rev. D* **96**, 023532 (2017), arXiv:1705.05303 [astro-ph.CO].
- [200] M. Raveri and W. Hu, *Phys. Rev. D* **99**, 043506 (2019), arXiv:1806.04649 [astro-ph.CO].
- [201] W. Handley and P. Lemos, *Phys. Rev. D* **100**, 043504 (2019), arXiv:1902.04029 [astro-ph.CO].
- [202] P. Lemos, F. Köhlinger, W. Handley, B. Joachimi, L. White-way, and O. Lahav, arXiv e-prints, arXiv:1910.07820 (2019), arXiv:1910.07820 [astro-ph.CO].
- [203] S. M. Feeney, H. V. Peiris, A. R. Williamson, S. M. Nissanke, D. J. Mortlock, J. Alsing, and D. Scolnic, *Phys. Rev. Lett.* **122**, 061105 (2019), arXiv:1802.03404 [astro-ph.CO].
- [204] F. Köhlinger, B. Joachimi, M. Asgari, M. Viola, S. Joudaki, and T. Tröster, *MNRAS* **484**, 3126 (2019), arXiv:1809.01406 [astro-ph.CO].
- [205] S. Adhikari and D. Huterer, *JCAP* **2019**, 036 (2019), arXiv:1806.04292 [astro-ph.CO].
- [206] A. Nicola, A. Amara, and A. Refregier, *JCAP* **2019**, 011 (2019), arXiv:1809.07333 [astro-ph.CO].
- [207] H. Jeffreys, *Theory of probability*, 3rd edn, OUP, Oxford, UK (1961).
- [208] R. E. Kass and A. E. Raftery, *J. Am. Stat. Ass.* **90**, 773 (1995).
- [209] C. Heymans *et al.*, arXiv e-prints, arXiv:2007.15632 (2020), arXiv:2007.15632 [astro-ph.CO].
- [210] Y.-C. Li, F.-Q. Wu, and X. Chen, *Phys. Rev. D* **88**, 084053 (2013), arXiv:1305.0055 [astro-ph.CO].
- [211] H. Johnston *et al.*, *A&A* **624**, A30 (2019), arXiv:1811.09598 [astro-ph.CO].
- [212] A. H. Wright *et al.*, arXiv e-prints, arXiv:2005.04207 (2020), arXiv:2005.04207 [astro-ph.CO].
- [213] M. C. Fortuna *et al.*, arXiv e-prints, arXiv:2003.02700 (2020), arXiv:2003.02700 [astro-ph.CO].
- [214] M. A. Troxel *et al.*, *Phys. Rev. D* **98**, 043528 (2018), arXiv:1708.01538 [astro-ph.CO].
- [215] C. Hikage *et al.* (HSC), *Publ. Astron. Soc. Jap.* **71**, Publ. Astron. Soc. Jap., Volume 71, Issue 2, April 2019, 43 (2019), arXiv:1809.09148 [astro-ph.CO].
- [216] M. Asgari *et al.*, *A&A* **634**, A127 (2020), arXiv:1910.05336 [astro-ph.CO].
- [217] M. J. Jee *et al.*, *Astrophys. J.* **824**, 77 (2016), arXiv:1510.03962 [astro-ph.CO].
- [218] T. Hamana *et al.*, *Publ. Astron. Soc. Jap.* **72**, Publ. Astron. Soc. Jap., Volume 72, Issue 1, February 2020, 16 (2020), arXiv:1906.06041 [astro-ph.CO].
- [219] T. Baker and I. Harrison, arXiv e-prints, arXiv:2007.13791 (2020), arXiv:2007.13791 [astro-ph.CO].
- [220] A. Lewis, arXiv e-prints, arXiv:1910.13970 (2019), arXiv:1910.13970 [astro-ph.IM].
- [221] M. Zumalacárregui, E. Bellini, I. Sawicki, J. Lesgourgues, and P. G. Ferreira, *JCAP* **2017**, 019 (2017), arXiv:1605.06102 [astro-ph.CO].

Appendix A: Impact of JBD gravity on the CMB polarization

In addition to showing the impact of JBD gravity on the CMB temperature power spectrum in Figs. 2 and 3, we illustrate the impact of JBD gravity on the CMB polarization power spectrum and polarization-temperature cross-spectrum in Fig. 20 (along with the CMB temperature power spectrum again for comparison). Similar to the CMB temperature power spectrum, the peaks of the polarization power spectrum are primarily shifted by the coupling constant, ω_{BD} , while the damping tail is coherently suppressed (enhanced) as the present effective gravitational constant $(G_{\text{matter}}/G)|_{a=1}$ is

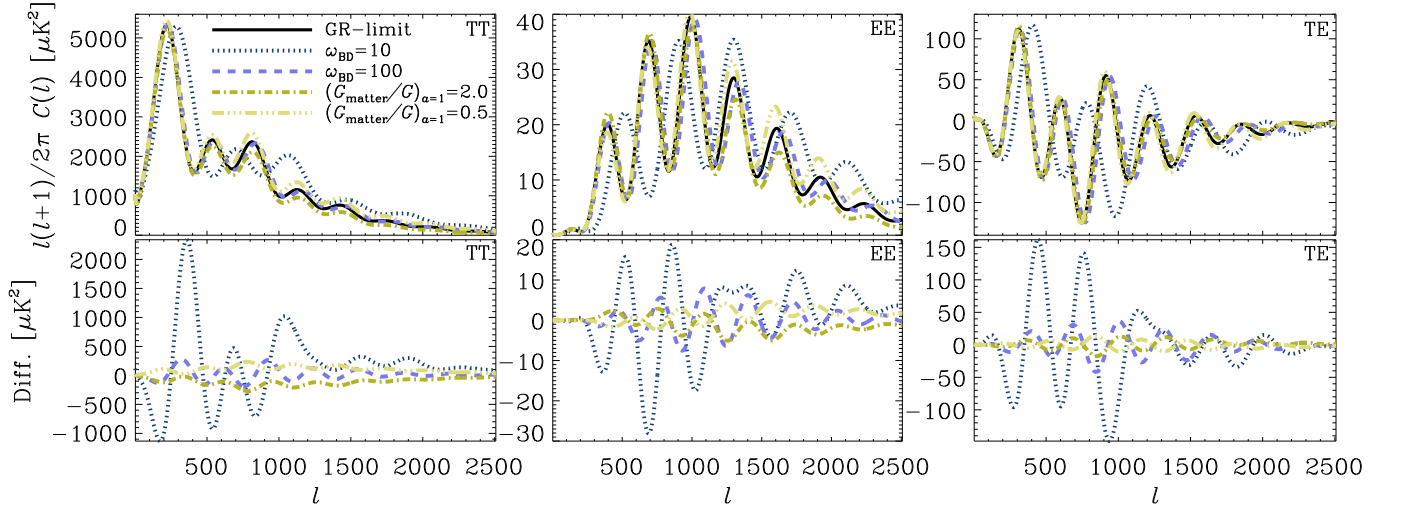


FIG. 20. CMB temperature (T) and polarization (E) power spectra in a cosmology with JBD gravity along with their respective differences relative to GR, defined as $A_{\text{JBD}} - A_{\text{GR}}$, where $A \in \{TT, EE, TE\}$ (noting that TT here is the same as in Fig. 2 and shown for comparison with EE and TE). For our GR limit, we have effectively imposed $\omega_{\text{BD}} \rightarrow \infty$ and $G_{\text{matter}}/G = 1$. For the JBD model, we show the four cases $\omega_{\text{BD}} = 10$, $\omega_{\text{BD}} = 100$, $G_{\text{matter}}/G = 0.5$, and $G_{\text{matter}}/G = 2.0$ (such that $\omega_{\text{BD}} \rightarrow \infty$ when $G_{\text{matter}}/G \neq 1$, and $G_{\text{matter}}/G = 1$ when $\omega_{\text{BD}} \neq \infty$). We emphasize that our use of “ G_{matter}/G ” here is shorthand for $(G_{\text{matter}}/G)|_{a=1}$ (as defined in Eq. 18).

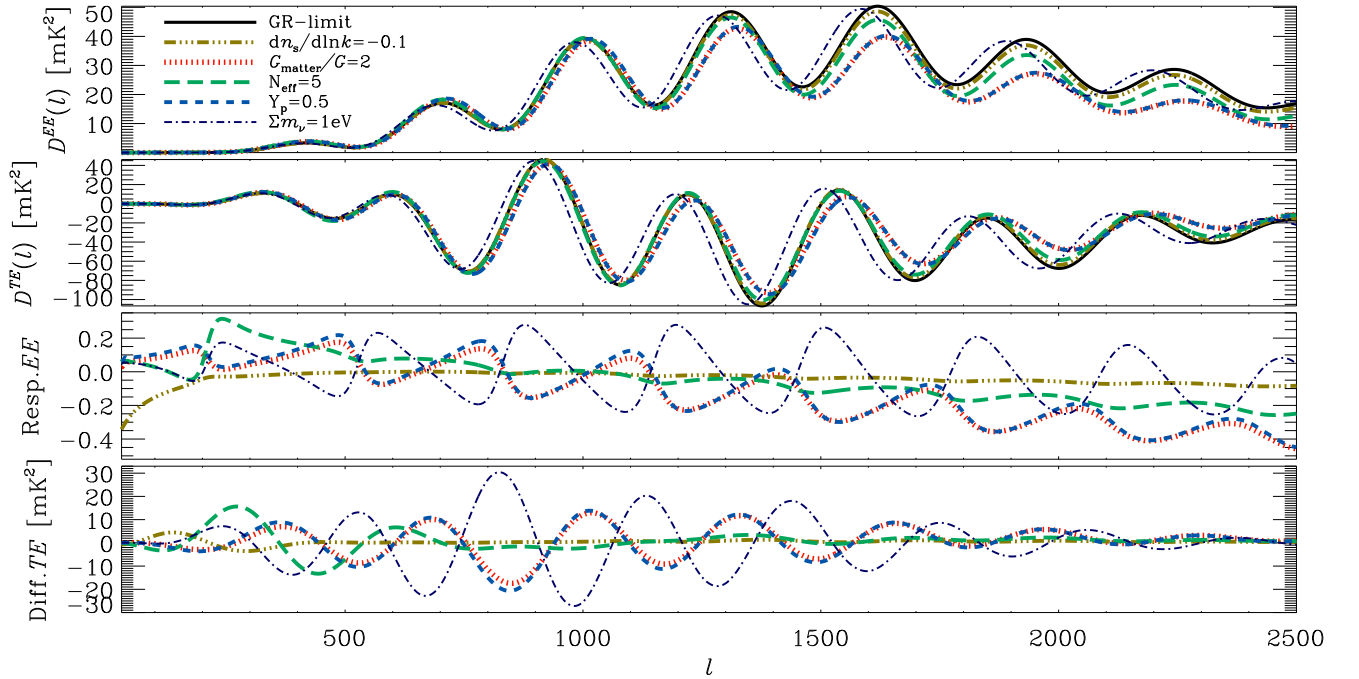


FIG. 21. CMB polarization power spectra (EE) and temperature-polarization cross-spectra (TE) in extended cosmological parameter spaces, where $D(\ell) = \ell^3(\ell+1)/2\pi C(\ell)$, along with the EE responses, defined as $C^{\text{extended}}(\ell)/C^{\Lambda\text{CDM}}(\ell) - 1$, and the TE differences, defined as $C^{\text{extended}}(\ell) - C^{\Lambda\text{CDM}}(\ell)$. We consider deviations in the running of the spectral index, $dn_s/d\ln k$, the effective number of neutrinos, N_{eff} , the sum of neutrino masses, Σm_ν , the primordial helium abundance, Y_p , and the present effective gravitational constant, G_{matter}/G .

greater (smaller) than unity. However, while a positive shift in the effective gravitational constant induces a suppression in the temperature power spectrum across scales, the polarization power spectrum primarily exhibits an enhancement for $\ell \lesssim 10^3$ (as also pointed out in Ref. [123]). For the CMB temperature-polarization cross-spectrum, the peaks oscillate about zero, such that a positive ω_{BD} and $(G_{\text{matter}}/G)|_{a=1} < 1$ counteract

one another. The different signatures in the CMB temperature and polarization power spectra can thereby be used to place stringent constraints on JBD gravity, as shown in Sec. V.

While we are showing the differences between the JBD and GR (technically GR-limit) power spectra in Fig. 20, the absolute value of the response $|\mathcal{R}_\ell| = |C_\ell^{\text{JBD}}/C_\ell^{\text{GR}} - 1|$ coherently increases with ℓ in the damping tail for both the temperature

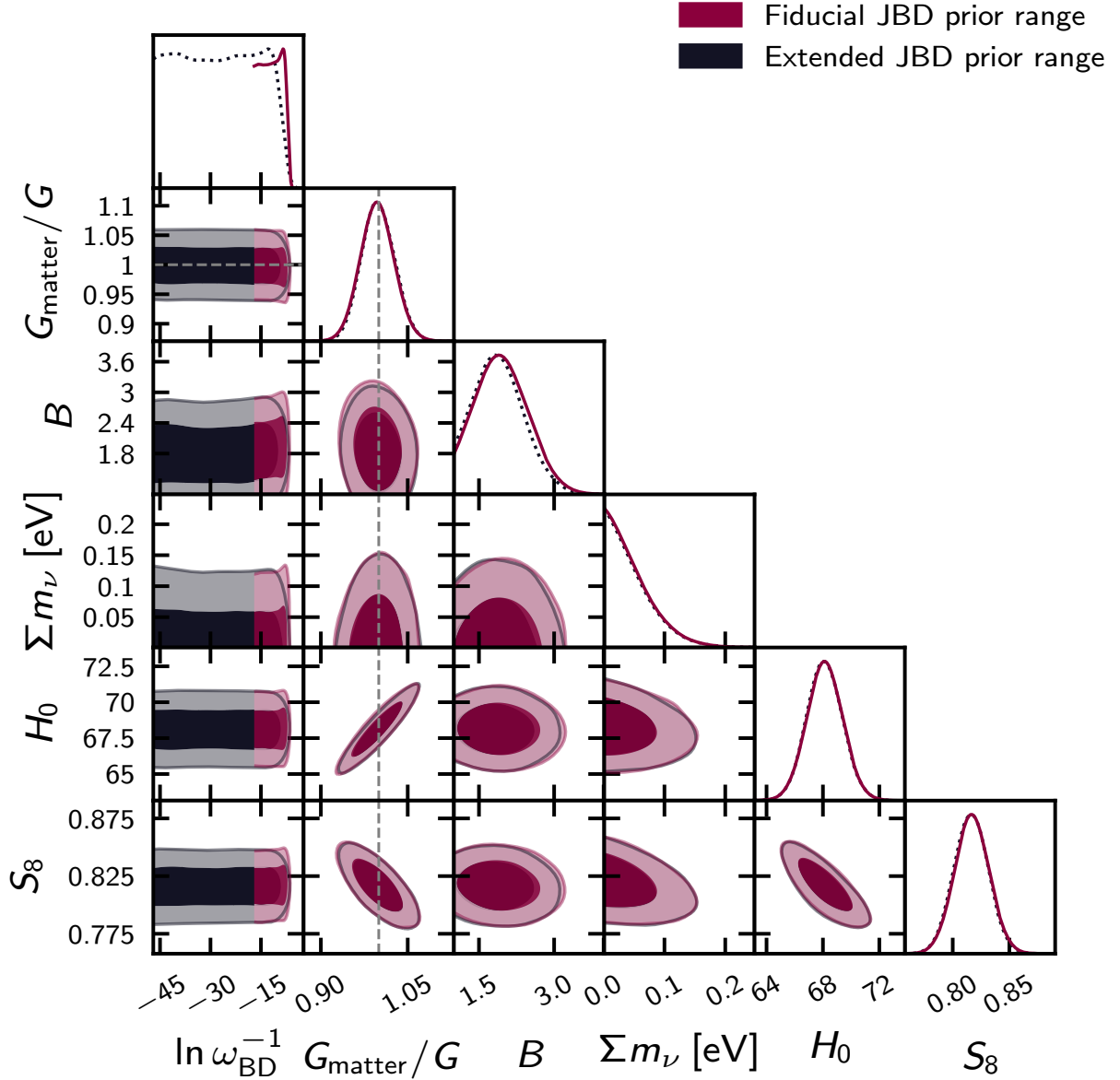


FIG. 22. Marginalized posterior distributions (inner 68% CL, outer 95% CL) of the JBD parameter, $\ln \omega_{\text{BD}}^{-1}$, the present effective gravitational constant, G_{matter}/G , the baryonic feedback amplitude, B , the sum of neutrino masses, Σm_ν , the Hubble constant, H_0 (in units of $\text{km s}^{-1} \text{Mpc}^{-1}$), and $S_8 = \sigma_8 \sqrt{\Omega_m/0.3}$, considering two different choices of the prior range of the primary parameter $\ln \omega_{\text{BD}}^{-1}$. In the fiducial setup, $-17 \leq \ln \omega_{\text{BD}}^{-1} \leq -2.3$, while in the extended setup, $-47 \leq \ln \omega_{\text{BD}}^{-1} \leq -2.3$. All other standard cosmological and systematics parameters are simultaneously varied.

and polarization auto spectra as $(G_{\text{matter}}/G)|_{a=1}$ deviates from unity. This is shown explicitly for the polarization in Fig. 21 (and for the temperature in Figs. 2 and 3), and implies that the impact of the present effective gravitational constant will be correlated in both the temperature and polarization power spectra with that of other physics affecting the small-scale CMB, such as the primordial helium abundance in particular (discussed in Sec. IIH), but also the effective number of neutrinos, mass of the neutrinos, and running of the spectral index (targeted by surveys such as AdvACT [129], SPT-3G [130], and Simons Observatory [131]).

Appendix B: Impact of the JBD prior range

In Fig. 22, we show the impact of the uniform prior range of the primary parameter $\ln \omega_{\text{BD}}^{-1}$, where ω_{BD} is the JBD coupling constant, on the cosmological parameter constraints in an unrestricted JBD model (considering the KiDS, 2dFLenS, BOSS, Planck, and Pantheon datasets combined). While the constraints are shown for only a subset of the parameters (where H_0 and S_8 are derived parameters), the agreement in the constraints between the fiducial and extended prior cases is strong for the other cosmological and systematics parameters simultaneously varied in the analysis (see Table I for a list of additional

TABLE VII. The changes in the best-fit χ^2_{eff} and deviance information criterion (DIC) relative to Λ CDM for different data combinations and parameter extensions. A negative change indicates preference in favor of the extended model. For completeness, the absolute numbers for the best-fit χ^2_{eff} and DIC of the two most central runs are: All-Planck18 + All-BOSS + Pantheon (JBD + $\sum m_\nu$), where $\chi^2_{\text{eff}} = 3820.4$ and DIC = 3865.1, and KiDS \times 2dFLenS + All-BOSS + All-Planck18 + Pantheon (JBD + G_{matter} + $\sum m_\nu$), where $\chi^2_{\text{eff}} = 4019.7$ and DIC = 4072.7.

Probe setup	$\Delta\chi^2_{\text{eff}}$	ΔDIC
Planck18 (Λ CDM + $\sum m_\nu$)	1.1	3.9
Planck18 (JBD)	-0.41	1.0
Planck18 (JBD + $\sum m_\nu$)	1.6	3.3
Planck18 (JBD + G_{matter} + $\sum m_\nu$)	2.7	4.0
ACT DR4 (JBD)	-0.10	0.22
Planck18 + ACT DR4 (JBD)	-0.04	0.34
All-Planck18 (Λ CDM + $\sum m_\nu$)	0.83	3.0
All-Planck18 (JBD)	-0.84	1.3
KiDS \times 2dFLenS (Λ CDM + $\sum m_\nu$)	0.097	0.030
KiDS \times 2dFLenS (JBD)	0.15	-0.41
KiDS \times 2dFLenS (JBD + $\sum m_\nu$)	-0.32	0.62
KiDS \times 2dFLenS (JBD + G_{matter})	0.12	1.2
KiDS \times 2dFLenS (JBD + G_{matter} + $\sum m_\nu$)	-0.41	2.3
All-BOSS + Pantheon (Λ CDM + $\sum m_\nu$)	0.0044	-0.072
All-BOSS + Pantheon (JBD)	-0.0038	-0.033
All-BOSS + Pantheon (JBD + $\sum m_\nu$)	0.0012	-0.10
All-BOSS + Pantheon (JBD + G_{matter})	-0.061	-0.060
All-BOSS + Pantheon (JBD + G_{matter} + $\sum m_\nu$)	-1.4	1.3
KiDS \times {2dFLenS + BOSS} (Λ CDM + $\sum m_\nu$)	0.34	0.55
KiDS \times {2dFLenS + BOSS} (JBD)	0.46	-0.098
KiDS \times {2dFLenS + BOSS} (JBD, no feedback)	3.2	1.4
KiDS \times {2dFLenS + BOSS} (JBD + $\sum m_\nu$)	-1.3	2.1
KiDS \times {2dFLenS + BOSS} (JBD + $\sum m_\nu$, no feedback)	3.9	2.8
KiDS \times {2dFLenS + BOSS} (JBD + G_{matter})	3.3	1.4
KiDS \times {2dFLenS + BOSS} (JBD + G_{matter} + $\sum m_\nu$)	0.62	2.2
KiDS \times 2dFLenS + All-BOSS + Pantheon (Λ CDM + $\sum m_\nu$)	-1.2	-0.48
KiDS \times 2dFLenS + All-BOSS + Pantheon (JBD)	0.43	-0.60
KiDS \times 2dFLenS + All-BOSS + Pantheon (JBD + $\sum m_\nu$)	-1.8	0.0055
KiDS \times 2dFLenS + All-BOSS + Pantheon (JBD + G_{matter})	0.50	1.5
KiDS \times 2dFLenS + All-BOSS + Pantheon (JBD + G_{matter} + $\sum m_\nu$)	-1.8	1.9
All-Planck18 + All-BOSS + Pantheon (Λ CDM + $\sum m_\nu$)	2.1	0.53
All-Planck18 + All-BOSS + Pantheon (JBD)	0.14	-0.22
All-Planck18 + All-BOSS + Pantheon (JBD + $\sum m_\nu$)	0.076	2.4
All-Planck18 + All-BOSS + Pantheon (JBD + G_{matter})	1.6	3.3
All-Planck18 + All-BOSS + Pantheon (JBD + G_{matter} + $\sum m_\nu$)	1.5	4.1
KiDS \times 2dFLenS + All-BOSS + All-Planck18 + Pantheon (JBD + G_{matter})	0.45	1.7
KiDS \times 2dFLenS + All-BOSS + All-Planck18 + Pantheon (JBD + G_{matter} + $\sum m_\nu$)	-2.0	4.6
Planck18 + Riess 2019 (JBD + G_{matter} + $\sum m_\nu$)	-4.0	-4.8
KiDS \times 2dFLenS + All-BOSS + All-Planck18 + Pantheon + Riess 2019 (JBD + G_{matter} + $\sum m_\nu$)	-4.7	-2.7

primary parameters). We discuss these results in Sec. VIII C.

Appendix C: Model selection and additional parameter constraints

In Table VIII, we provide parameter constraints and assess dataset tensions for a subset of additional combinations of probes (namely KiDS \times 2dFLenS alone, and All-BOSS + Pantheon alone). In Table VII, we provide the changes in the best-fit χ^2_{eff} and deviance information criterion (DIC) relative to Λ CDM for a range of different combinations of probes and parameter extensions. The datasets consist of KiDS, 2dFLenS, Planck, BOSS, Pantheon, and ACT, and the parameter extensions consist of Λ CDM + $\sum m_\nu$, JBD, JBD + $\sum m_\nu$, JBD + G_{matter} , and JBD + G_{matter} + $\sum m_\nu$. Here, a negative DIC

(and χ^2_{eff}) implies a model selection preference in favor of the extended model (the significance of which is described in Sec. IV D). We find that none of the cases favor an extended model beyond $\Delta\text{DIC} \simeq -5$ which is the threshold of moderate preference in favor of the extended model.

Appendix D: Multi-probe parameter constraints including either Planck 2015 or Planck 2018

For completeness, we consider a comparison of the cosmological constraints for dataset combinations that respectively include Planck 2015 and Planck 2018. The datasets that we combine are BOSS and Pantheon together with Planck which includes the CMB temperature, polarization, and lensing reconstruction from either the 2015 [71]

TABLE VIII. Marginalized posterior means and 68% confidence intervals for the Hubble constant, H_0 , in units of $\text{km s}^{-1} \text{Mpc}^{-1}$, and $S_8 = \sigma_8 \sqrt{\Omega_m}/0.3$. The symbol “ \diamond ” implies that the parameter is effectively unconstrained by the data, and the symbol “ \circ ” implies that the tension T is not meaningful to quote (i.e. $T \sim 0$).

Probe setup	H_0	S_8	$T(H_0)_{\text{Riess19}}$	$T(S_8)_{\text{Planck18}}$
KiDS \times 2dFLenS (Λ CDM)	\diamond	$0.736^{+0.039}_{-0.038}$	\circ	2.4
KiDS \times 2dFLenS (Λ CDM + $\sum m_\nu$)	\diamond	$0.723^{+0.037}_{-0.037}$	\circ	2.6
KiDS \times 2dFLenS (JBD)	\diamond	$0.738^{+0.039}_{-0.039}$	\circ	2.4
KiDS \times 2dFLenS (JBD + $\sum m_\nu$)	\diamond	$0.725^{+0.035}_{-0.035}$	\circ	2.5
KiDS \times 2dFLenS (JBD + G_{matter})	\diamond	$0.768^{+0.083}_{-0.105}$	\circ	0.8
KiDS \times 2dFLenS (JBD + G_{matter} + $\sum m_\nu$)	\diamond	$0.772^{+0.080}_{-0.095}$	\circ	0.7

	H_0	S_8	$T(H_0)_{\text{Riess19}}$	$T(S_8)_{\text{Planck18}}$	$T(S_8)_{\text{KiDS}\times\text{2dFLenS}}$
All-BOSS + Pantheon (Λ CDM)	$71.1^{+6.3}_{-4.3}$	$0.805^{+0.051}_{-0.052}$	0.54	0.6	1.1
All-BOSS + Pantheon (Λ CDM + $\sum m_\nu$)	$69.7^{+6.2}_{-4.3}$	$0.812^{+0.051}_{-0.051}$	0.79	0.3	1.4
All-BOSS + Pantheon (JBD)	$73.7^{+4.9}_{-7.9}$	$0.802^{+0.051}_{-0.051}$	0.04	0.7	1.0
All-BOSS + Pantheon (JBD + $\sum m_\nu$)	$72.3^{+5.2}_{-7.5}$	$0.810^{+0.051}_{-0.051}$	0.26	0.4	1.3
All-BOSS + Pantheon (JBD + G_{matter})	\diamond	\diamond	\circ	\circ	\circ
All-BOSS + Pantheon (JBD + G_{matter} + $\sum m_\nu$)	\diamond	\diamond	\circ	\circ	\circ

TABLE IX. Marginalized posterior means and 68% confidence intervals for a subset of the cosmological parameters when analyzing the Planck 2015 dataset (instead of Planck 2018). For the JBD parameter, ω_{BD} , and the sum of neutrino masses, $\sum m_\nu$, we quote the 95% confidence lower and upper bounds, respectively. The sum of neutrino masses, $\sum m_\nu$, is in units of eV, the Hubble constant, H_0 , is in $\text{km s}^{-1} \text{Mpc}^{-1}$, and $S_8 = \sigma_8 \sqrt{\Omega_m}/0.3$. A table element with “...” implies that the parameter is not varied in the analysis. There is a minor improvement in the H_0 (and A_{IA}) constraint as we allow the sum of neutrino masses to vary in KiDS \times 2dFLenS + All-BOSS + All-Planck15 + Pantheon, as the fiducial $\sum m_\nu$ is located at the boundary of the posterior when varied, such that the widest range in H_0 is favored at this boundary, and due to the weak correlation between the parameters (see Fig. 24). The tensions $T(H_0)$ and $T(S_8)$ are against Riess et al. 2019 [77] and KiDS \times {2dFLenS+BOSS}, respectively (in the latter case only against KiDS \times 2dFLenS when Planck is combined with BOSS). See the caption of Table II for further details.

Probe setup	ω_{BD}	G_{matter}/G	$\sum m_\nu$	H_0	S_8	$T(H_0)$	$T(S_8)$	
Planck15 (Λ CDM)	$67.94^{+1.00}_{-0.98}$	$0.853^{+0.025}_{-0.025}$	3.5	2.5	
Planck15 (Λ CDM + $\sum m_\nu$)	0.64	$65.59^{+1.63}_{-2.43}$	$0.843^{+0.026}_{-0.026}$	3.4	2.5	
Planck15 (JBD)	530	$68.27^{+0.93}_{-1.29}$	$0.850^{+0.025}_{-0.025}$	3.2	2.4	
Planck15 (JBD + $\sum m_\nu$)	860	...	0.62	$65.95^{+2.49}_{-1.92}$	$0.842^{+0.026}_{-0.025}$	3.3	2.4	
Planck15 (JBD + G_{matter})	850	$1.024^{+0.046}_{-0.053}$...	$69.86^{+2.57}_{-2.88}$	$0.842^{+0.034}_{-0.034}$	1.6	1.6	
Planck15 + ACT DR3 (Λ CDM)	$67.76^{+0.94}_{-0.95}$	$0.853^{+0.024}_{-0.024}$	3.7	2.5	
Planck15 + ACT DR3 (JBD)	900	$67.97^{+0.92}_{-1.10}$	$0.851^{+0.023}_{-0.024}$	3.5	2.5	
All-Planck15 (Λ CDM)	$68.02^{+0.64}_{-0.64}$	$0.834^{+0.012}_{-0.013}$	3.9	2.4	
All-Planck15 (JBD)	1110	$68.18^{+0.65}_{-0.74}$	$0.835^{+0.013}_{-0.013}$	3.7	2.3	
Planck15 + All-BOSS + Pantheon (Λ CDM)	$68.16^{+0.54}_{-0.54}$	$0.843^{+0.018}_{-0.017}$	3.9	2.5	
Planck15 + All-BOSS + Pantheon (Λ CDM + $\sum m_\nu$)	0.20	$67.85^{+0.59}_{-0.60}$	$0.832^{+0.020}_{-0.020}$	4.0	2.5	
Planck15 + All-BOSS + Pantheon (JBD)	840	$68.26^{+0.53}_{-0.63}$	$0.844^{+0.018}_{-0.018}$	3.8	2.5	
Planck15 + All-BOSS + Pantheon (JBD + $\sum m_\nu$)	480	...	0.22	$68.02^{+0.60}_{-0.71}$	$0.832^{+0.020}_{-0.020}$	3.8	2.5	
Planck15 + All-BOSS + Pantheon (JBD + G_{matter})	1460	$1.014^{+0.045}_{-0.045}$...	$68.79^{+1.89}_{-1.90}$	$0.839^{+0.023}_{-0.025}$	2.2	0.7	
Planck15 + All-BOSS + Pantheon (JBD + G_{matter} + $\sum m_\nu$)	1140	$1.029^{+0.045}_{-0.044}$	0.22	$69.03^{+1.80}_{-1.83}$	$0.822^{+0.026}_{-0.026}$	2.2	0.6	
All-Planck15 + All-BOSS + Pantheon (Λ CDM)	$68.11^{+0.45}_{-0.45}$	$0.832^{+0.011}_{-0.011}$	4.0	2.4	
All-Planck15 + All-BOSS + Pantheon (JBD)	1050	$68.22^{+0.46}_{-0.52}$	$0.833^{+0.011}_{-0.011}$	3.9	2.3	
All-Planck15 + All-BOSS + Pantheon (JBD + $\sum m_\nu$)	590	...	0.19	$67.88^{+0.59}_{-0.61}$	$0.828^{+0.012}_{-0.012}$	4.0	2.6	
	ω_{BD}	G_{matter}/G	B	A_{IA}	$\sum m_\nu$	H_0	S_8	$T(H_0)$
KiDS \times 2dFLenS + All-BOSS + Planck15 (JBD + G_{matter} + $\sum m_\nu$)	840	$1.034^{+0.042}_{-0.046}$	3.0	$1.50^{+0.41}_{-0.41}$	0.30	$69.51^{+1.80}_{-1.79}$	$0.790^{+0.025}_{-0.025}$	2.0
KiDS \times 2dFLenS + All-BOSS + All-Planck15 + Pantheon (JBD + G_{matter})	2270	$1.010^{+0.030}_{-0.029}$	2.8	$1.49^{+0.38}_{-0.39}$...	$68.87^{+1.32}_{-1.32}$	$0.818^{+0.015}_{-0.015}$	2.7
KiDS \times 2dFLenS + All-BOSS + All-Planck15 + Pantheon (JBD + G_{matter} + $\sum m_\nu$)	1640	$1.017^{+0.029}_{-0.030}$	2.8	$1.52^{+0.36}_{-0.39}$	0.21	$68.71^{+1.27}_{-1.26}$	$0.809^{+0.016}_{-0.015}$	2.8

or 2018 [75] dataset (i.e. “TT,TE,EE+lowP+lensing” and “TT,TE,EE+lowE+lensing” for Planck 2015 and 2018, respectively). In constraining the unrestricted JBD model, we further consider the KiDS \times 2dFLenS $3 \times 2\text{pt}$ dataset.

We show a comparison of the constraints on a subset of the parameter space $\{\ln \omega_{\text{BD}}^{-1}, \sum m_\nu, \tau, H_0, S_8\}$ for the restricted JBD model in Fig. 23 and an expanded subset $\{\ln \omega_{\text{BD}}^{-1}, G_{\text{matter}}/G, \sum m_\nu, \tau, B, H_0, S_8\}$ for the unrestricted

JBD model in Fig. 24. A range of Planck 2015 constraints are also summarized in Table IX. As expected, we find substantial improvements in the constraints on the optical depth (and scalar amplitude) and thereby the sum of neutrino masses when the Planck 2018 dataset is considered (instead of Planck 2015). However, the constraints on the other parts of the sub-space, in particular the constraints on JBD gravity, baryonic feedback, the Hubble constant, and S_8 seem largely robust be-

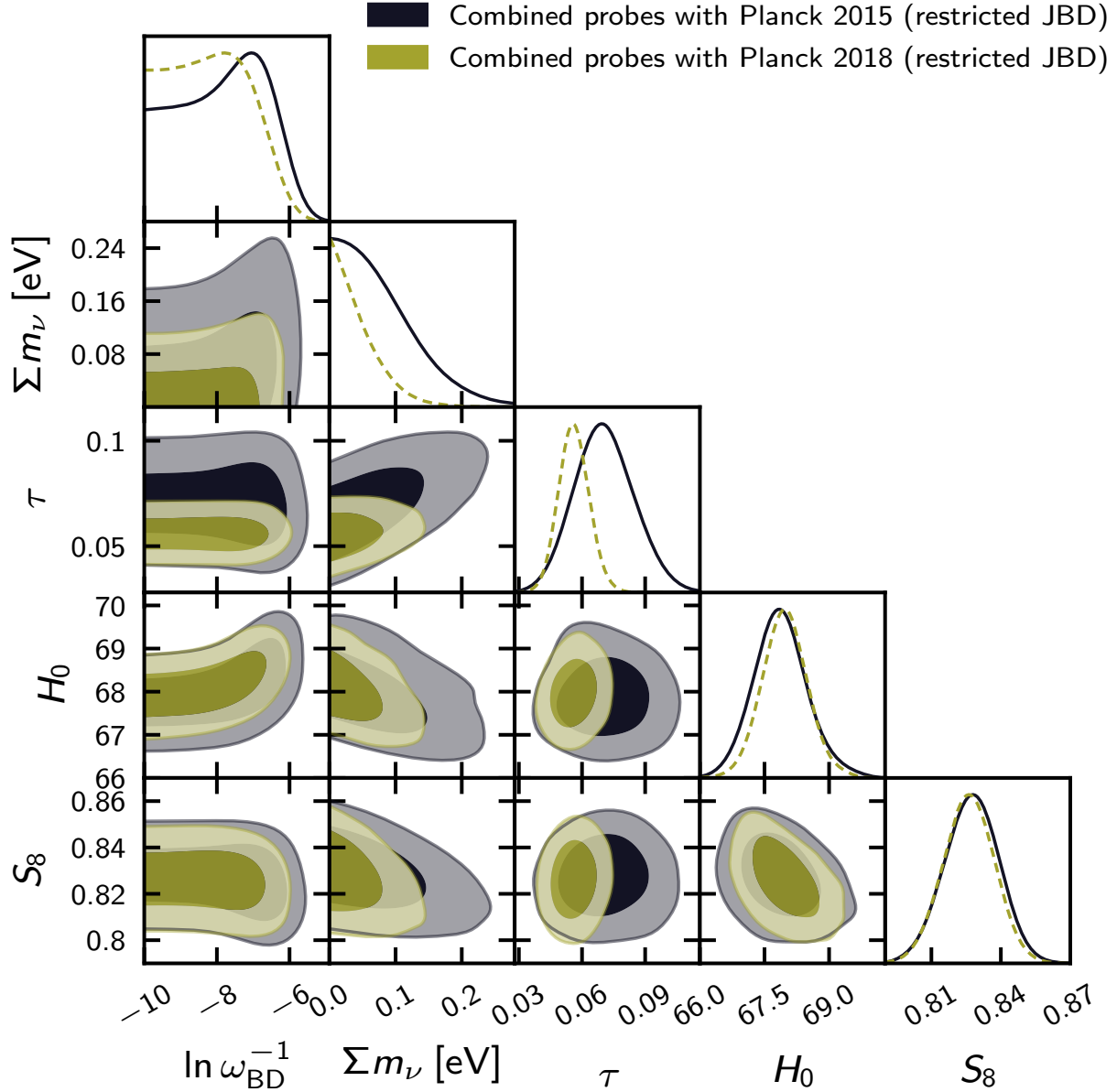


FIG. 23. Marginalized posterior distributions (inner 68% CL, outer 95% CL) of the JBD parameter, $\ln \omega_{\text{BD}}^{-1}$, the sum of neutrino masses, Σm_ν , the optical depth, τ , the Hubble constant, H_0 (in units of $\text{km s}^{-1} \text{Mpc}^{-1}$), and $S_8 = \sigma_8 \sqrt{\Omega_m/0.3}$ from All-Planck + All-BOSS + Pantheon, where for “All-Planck” we consider either Planck 2015 (TT+TE+EE+lowTEB+lensing) or Planck 2018 (TT+TE+EE+lowl+lowE+lensing). All other standard cosmological and systematics parameters are simultaneously varied in this restricted JBD model. For visual clarity, we have zoomed in on the $\ln \omega_{\text{BD}}^{-1}$ axis where the distributions flatten towards the GR limit at $-\infty$ (in practice towards the end of the prior range at $\ln \omega_{\text{BD}}^{-1} = -17$).

tween the two dataset combinations. This also seems to hold for the correlations and degeneracies between the parameters over the full subspace.

For the dataset combination KiDS×2dFLenS + All-BOSS + All-Planck15 + Pantheon, we note that there is a minor unexpected improvement in the H_0 (and A_{IA}) constraint when the sum of neutrino masses is varied in the unrestricted JBD model, as the fiducial Σm_ν is located at the boundary of the posterior when varied, where the widest range in H_0 is favored, and due to the weak correlation between the parameters (quoted in Table IX and shown in Fig. 24). We obtain the ex-

pected change in the uncertainty on the Hubble constant with the inclusion of massive neutrinos as Planck 2018 is considered instead of Planck 2015.

In Table IX, we can also compare the parameter constraints from KiDS×2dFLenS + All-BOSS + All-Planck15 + Pantheon to those from the data combination KiDS×2dFLenS + All-BOSS + Planck15 in the unrestricted JBD model. As expected, we find weaker parameter constraints for the latter data combination, as $\omega_{\text{BD}} > 840$ (95% CL) and $G_{\text{matter}}/G = 1.034^{+0.042}_{-0.046}$ in the unrestricted JBD model with massive neutrinos (where $\Sigma m_\nu < 0.30$ eV at 95% CL). These weaker constraints (no-

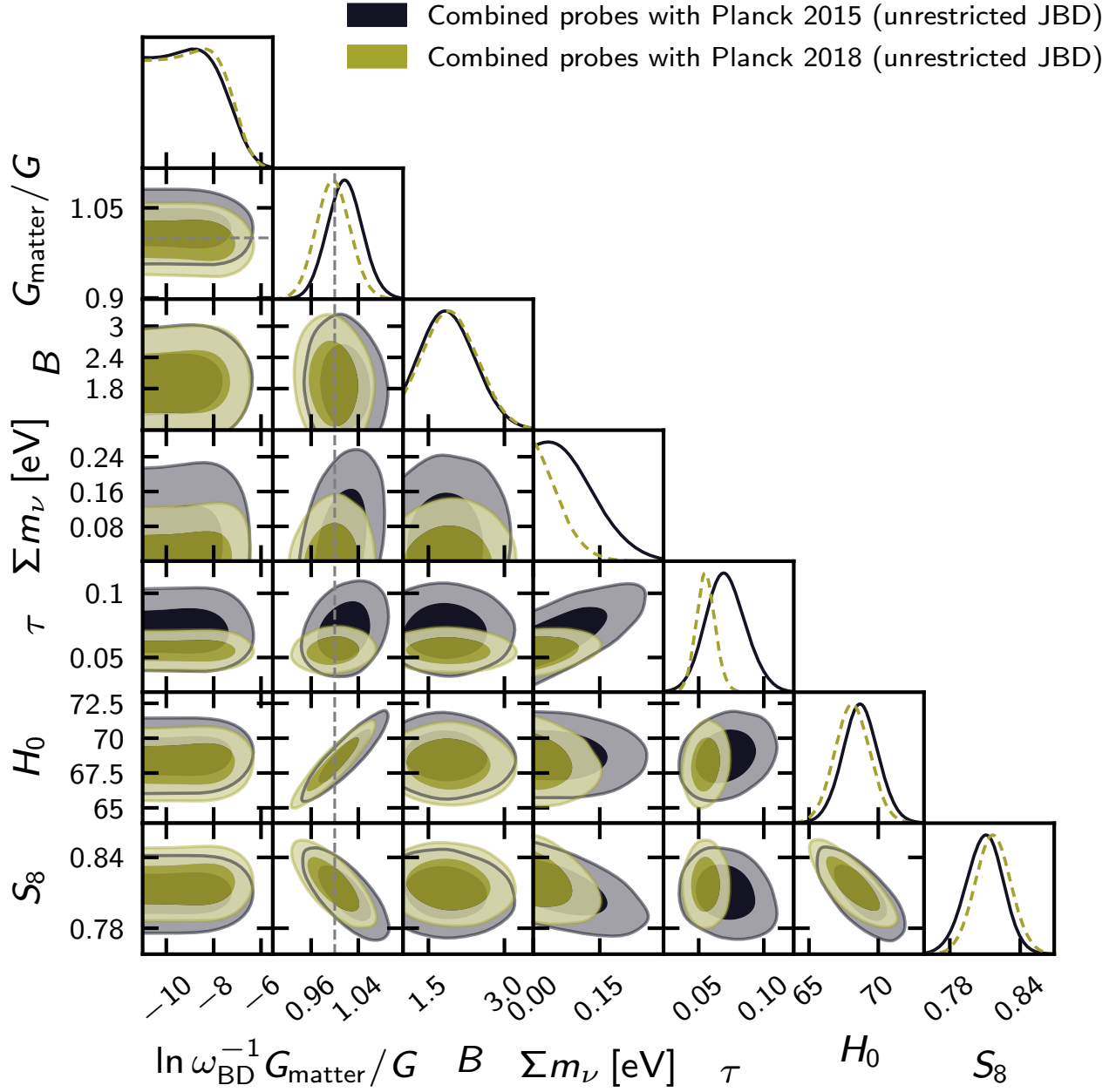


FIG. 24. Marginalized posterior distributions (inner 68% CL, outer 95% CL) of the JBD parameter, $\ln \omega_{\text{BD}}^{-1}$, the present effective gravitational constant, G_{matter}/G , the baryonic feedback amplitude, B , the sum of neutrino masses, Σm_ν , the optical depth, τ , the Hubble constant, H_0 (in units of $\text{km s}^{-1} \text{Mpc}^{-1}$), and $S_8 = \sigma_8 \sqrt{\Omega_m/0.3}$ from the full dataset combination KiDS×2dFLenS + All-BOSS + All-Planck + Pantheon, where for “All-Planck” we consider either Planck 2015 (TT+TE+EE+lowTEB+lensing) or Planck 2018 (TT+TE+EE+lowl+lowE+lensing). All other standard cosmological and systematics parameters are simultaneously varied. For visual clarity, we have zoomed in on the $\ln \omega_{\text{BD}}^{-1}$ axis where the distributions flatten towards the GR limit at $-\infty$ (in practice towards the negative end of the prior range at $\ln \omega_{\text{BD}}^{-1} = -17$).

tably by 50% for G_{matter}) are driven by the absence of the CMB polarization and lensing reconstruction (i.e. Planck instead of All-Planck, rather than the Pantheon SNe). The constraints on H_0 and S_8 are also weakened (by 40% and 60%, respectively), as $H_0 = 69.5^{+1.8}_{-1.8} \text{ km s}^{-1} \text{Mpc}^{-1}$ and $S_8 = 0.790^{+0.025}_{-0.025}$. This highlights the significance of the additional CMB observables in both strengthening the parameter constraints in the unrestricted JBD model and increasing the agreement with the GR expectation.

Appendix E: JBD theory in EFTCAMB

Since the scalar field is expected to remain frozen during radiation domination at early times due to the Hubble friction term in its equation of motion (Eq. 5), we set its initial velocity, $\dot{\phi}_i$, to zero and find its initial value, ϕ_i , by means of a binary search enforcing $\phi(a=1)$ to be the desired value. The background evolution is commenced at $a_i = 10^{-10}$, and

we ensure that the flatness condition is respected and verified up to a tolerance of $\sim 10^{-4}$, which is important for the overall soundness and stability of the model. In the language of EFTCAMB [134], the effective field theory functions that describe the background dynamics and linear perturbations of

JBD gravity are given by (e.g. [112])

$$\begin{aligned}\Omega^{\text{EFT}}(t) &= \phi - 1 \\ \gamma_{i \in \{1,2,3\}}^{\text{EFT}} &= 0 \\ \Lambda^{\text{EFT}}(t) &= \frac{1}{2} \frac{\omega_{\text{BD}}}{\phi} \dot{\phi}^2 - V(\phi) \\ c^{\text{EFT}}(t) &= \frac{1}{2} \frac{\omega_{\text{BD}}}{\phi} \dot{\phi}^2,\end{aligned}\tag{E1}$$

where the potential $V(\phi)$ is fixed to the cosmological constant as discussed in Sec. II, and we have added the superscripts “EFT” to avoid confusion with Ω , γ , Λ , and c defined elsewhere. We note that $\Lambda^{\text{EFT}}(t)$ and $c^{\text{EFT}}(t)$ are not independent functions, but can be expressed in terms of $\Omega^{\text{EFT}}(t)$ (encapsulating the scalar field coupling to gravity and matter in the Jordan and Einstein frames, respectively), the Hubble parameter, and the matter density and pressure (e.g. [17, 134]), and that a direct one-to-one correspondence can be established between the EFT functions and the α_i parameterization (e.g. [21, 92, 112, 221]).